



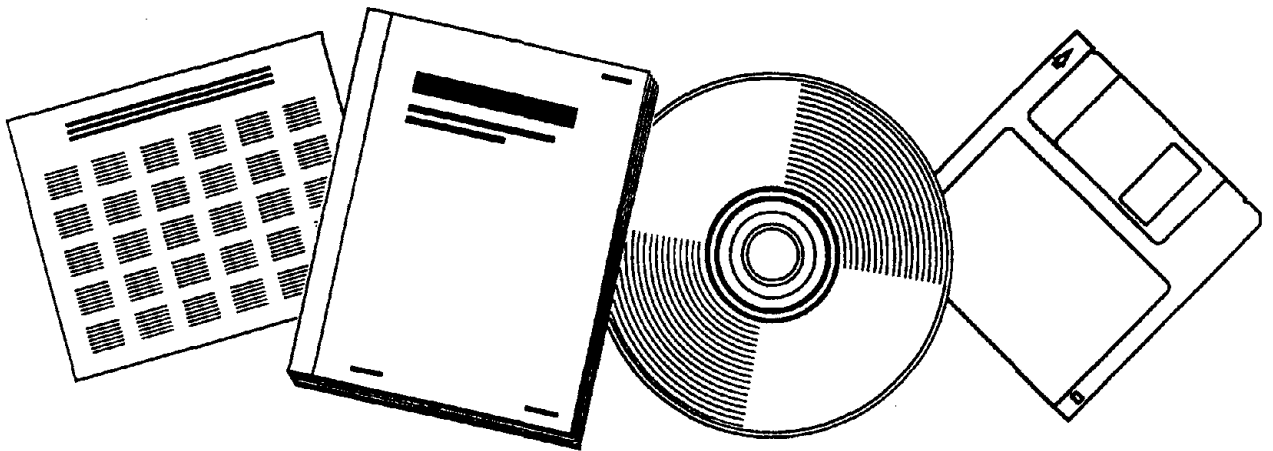
PB93-221711

NTIS[®]
Information is our business.

EVALUATION OF AN ACTIVE VARIABLE-DAMPING- STRUCTURE

EARTHQUAKE ENGINEERING RESEARCH CENTER
RICHMOND, CA

FEB 93



U.S. DEPARTMENT OF COMMERCE
National Technical Information Service



PB93-221711

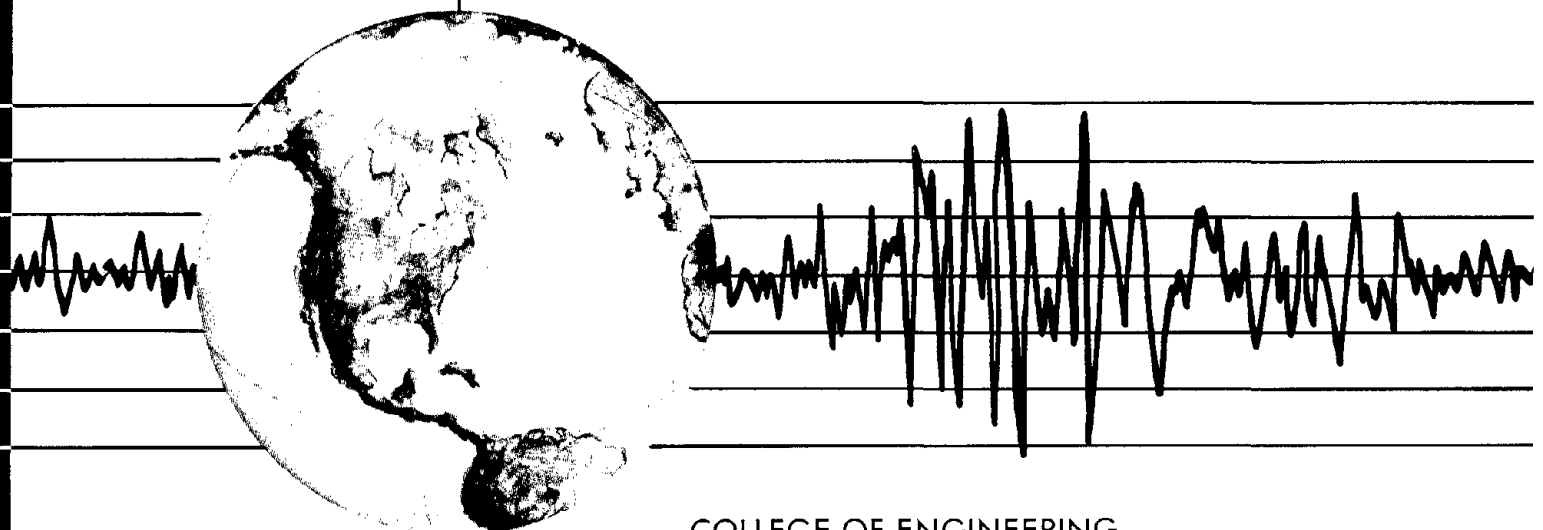
REPORT NO.
UCB/EERC-93/02
FEBRUARY 1993

EARTHQUAKE ENGINEERING RESEARCH CENTER

EVALUATION OF AN ACTIVE VARIABLE-DAMPING-STRUCTURE

by

E. POLAK
G. MEEKER
K. YAMADA
N. KURATA



COLLEGE OF ENGINEERING

UNIVERSITY OF CALIFORNIA AT BERKELEY

REPRODUCED BY
U.S. DEPARTMENT OF COMMERCE
NATIONAL TECHNICAL INFORMATION SERVICE

For sale by the National Technical Information Service, U.S. Department of Commerce, Springfield, Virginia 22161

See back of report for up to date listing of EERC reports.

DISCLAIMER

Any opinions, findings, and conclusions or recommendations expressed in this publication are those of the authors and do not necessarily reflect the views of the Sponsors or the Earthquake Engineering Research Center, University of California at Berkeley.



PB93-221711

EVALUATION OF AN ACTIVE VARIABLE-DAMPING-STRUCTURE[†]

by

E. Polak and G. Meeker

Department of Electrical Engineering
and Computer Sciences
University of California
Berkeley, CA 94720
USA

K. Yamada and N. Kurata


Kobori Research Complex
Kajima Corporation
KI Building, 6-5-30
Akasaka, Minato-ku
Tokyo 107
JAPAN

Report No. UCB/EERC-93/02
Earthquake Engineering Research Center
College of Engineering
University of California at Berkeley

February 1993

[†] The research reported herein was sponsored by the Kajima Corporation, the Air Force Office of Scientific Research contract AFOSR-90-0068, and the National Science Foundation grant ECS-8916168.



REPORT DOCUMENTATION PAGE	1. REPORT NO. NSF/ENG-93002	2.	3.  PB93-221711
4. Title and Subtitle "Evaluation of an Active Variable-Damping-Structure"			5. Report Date February 1993
7. Author(s) E. Polak, G. Meeker, K. Yamada, and N. Kurata			6. 8. Performing Organization Rept. No. UCB/EERC-93/02
9. Performing Organization Name and Address Earthquake Engineering Research Center University of California, Berkeley 1301 So. 46th Street Richmond, Calif. 94804			10. Project/Task/Work Unit No.
12. Sponsoring Organization Name and Address National Science Foundation 1800 G Street, N.W. Washington, D.C. 20550			11. Contract(C) or Grant(G) No. (C) (G) ECS-8916168
15. Supplementary Notes			13. Type of Report & Period Covered
16. Abstract (Limit: 200 words) We present an evaluation of the potential improvements in seismic disturbance rejection obtained by using active variable damping control in a structure. Using the response to seismic excitation of an optimally controlled variable structure and of a minimax optimally designed fixed structure, we obtain an upper bound on the achievable performance and a lower bound on the acceptability of a control system for a variable damping structure. Our numerical experiments suggest three conclusions. (1) A minimax optimal designed structure gives very good seismic disturbance suppression, not only for the earthquakes used in its design, but also for other earthquakes of similar intensity. (2) The use of variable structure control is not likely to result in smaller maximum interstory drifts than exhibited by a fixed minimax designed structure. (3) The gap between the upper and lower bounds is rather small, which makes designing a feedback law that results in performance superior to that of a minimax designed structure very difficult. The best choice appears to be in the form of a continuous moving horizon control law, using a horizon of under 0.2 seconds. This requires determination of whether local ground motion can be predicted up to 0.2 sec. ahead, using ground motion monitoring sensors located a small distance away from the site.			14.
17. Document Analysis a. Descriptors b. Identifiers/Open-Ended Terms c. COSATI Field/Group			
18. Availability Statement: Release Unlimited		19. Security Class (This Report) unclassified	21. No. of Pages 75
		20. Security Class (This Page) unclassified	22. Price

Abstract

We present an evaluation of the potential improvements in seismic disturbance rejection to be obtained by using active variable damping control in a structure. Using the responses to seismic excitation of an optimally controlled variable structure and of a minimax optimally designed fixed structure, we obtain an upper bound on the achievable performance and a lower bound on the acceptability of a control system for a variable damping structure.

Our numerical experiments suggest the following three conclusions:

- (i)* A minimax optimal designed structure gives very good seismic disturbance suppression, not only for the earthquakes used in its design, but also, for other earthquakes of similar intensity.
- (ii)* The use of variable structure control is not likely to result in smaller maximum interstory drifts than exhibited by a fixed minimax designed structure. However, the use of variable structure control may be somewhat more effective in the reduction of peak and average accelerations. Overall, controlled variable structures are likely to perform best when the earthquakes are moderate to severe, and at sites, such as landfills and dry lake beds, where resonances can be expected, but the resonance frequency cannot be estimated in advance.
- (iii)* The gap between the upper and lower bounds is rather small, which makes designing a feedback law that results in performance superior to that of a minimax designed structure, very difficult. The best choice appears to be in the form of a continuous moving horizon control law, using a horizon of under 0.2 seconds. An implementation of such a control law will require determination whether local ground motion can be predicted up to 0.2 sec. ahead, using ground motion monitoring sensors located a small distance away from the site.



Table of Contents

Abstract	i
Table of Contents	iii
List of Tables	iv
List of Figures	v
1. Introduction	1
2. System Models for Numerical Experimentation	3
2.1. Variable Structure System Model	3
2.2. Simplified Variable Structure System Model I	6
2.3. Simplified Variable Structure System Model II	10
3. Estimation of Performance Bounds	14
3.1. Development of a Performance Criterion	14
3.2. Upper Performance Bounds: Optimal Controls	17
3.3. Lower Performance Bounds: Minimax-Optimal Fixed Structure	22
4. Moving Horizon Feedback Control Laws	24
5. Evaluation of Numerical Results	26
6. Conclusion	38
7. References	39
Appendix: Discretized Gradient Computation	42
Figures	46

List of Tables

Table	Description	Page
2.1.1	Parameter Values for Variable Structure	5
2.3.1	Effect of α on Peak and Average Acceleration	12
2.3.2	Comparison of Peak Interstory Drifts	13
2.3.3	Comparison of Peak Accelerations	13
2.3.4	Comparison of Average Accelerations	14
3.1.1	Design Performance Specifications	15
3.1.2	Peak Interstory Drifts vs. Weighting Factor	16
3.1.3	Ground Motion Scale Factors	17
3.2.1	Parameters Used in Optimal Control Experiments	21
3.2.2	Initial Design: Optimal Fixed Damper Values	22
5.1	Comparison of Optimal Cost Function Values	27
5.2	Comparison of Peak Interstory Drifts	28
5.3	Comparison of Peak Accelerations	28
5.4	Comparison of Average Accelerations	29
5.5	Comparison of Total Energy Dissipation in Dampers	29
5.6	Comparison of Peak Shear Force	30
5.7	Comparison of Peak Damping Force	30
5.8	Peak Interstory Drifts	33
5.9	Peak Accelerations	34
5.10	Average Accelerations	34
5.11	Comparison of Total Energy Dissipations in Dampers	35
5.12	Comparison of Peak Shear Forces	36
5.13	Comparison of Peak Damping Forces	36
5.14	Comparison of Peak Interstory Drifts	37
5.15	Comparison of Peak Accelerations	37
5.16	Comparison of Average Accelerations	38

List of Figures

Figure	Description	Page
2.2.1	Floor Accelerations	46
2.2.2	Clamp Status vs. Time	46
2.3.1	Floor Accelerations ($\alpha = 0.0$)	46
2.3.2	Floor Accelerations ($\alpha = 0.5$)	46
2.3.3	Floor Accelerations ($\alpha = 0.9$)	47
3.1.1	Ground Position (EC)	47
3.1.2	Ground Velocity (EC)	47
3.1.3	Ground Acceleration (EC)	48
3.1.4	Ground Position (KC)	48
3.1.5	Ground Velocity (KC)	48
3.1.6	Ground Acceleration (KC)	48
3.1.7	Ground Position (PS)	49
3.1.8	Ground Velocity (PS)	49
3.1.9	Ground Acceleration (PS)	49
3.1.10	Ground Position (SF)	49
3.1.11	Ground Velocity (SF)	50
3.1.12	Ground Acceleration (SF)	50
3.1.13	Ground Position (WW)	50
3.1.14	Ground Velocity (WW)	50
3.1.15	Ground Acceleration (WW)	51
3.2.1	Interstory Drifts, Optimal Control (EC)	51
3.2.2	Floor Accelerations, Optimal Control (EC)	51
3.2.3	Damping Coefficients, Optimal Control (EC)	52
3.2.4	Energy Dissipation in Dampers, Optimal Control (EC)	52
3.2.5	Shear Force, Optimal Control (EC)	52
3.2.6	Damping Force, Optimal Control (EC)	52
3.3.1	Interstory Drifts, Minimax Design (EC)	53
3.3.2	Floor Accelerations, Minimax Design (EC)	53
3.3.3	Energy Dissipation in Dampers, Minimax Design (EC)	53
3.3.4	Shear Force, Minimax Design (EC)	53
3.3.5	Damping Force, Minimax Design (EC)	54
4.1	Interstory Drifts, S-D Moving Horizon (EC)	54
4.2	Floor Accelerations, S-D Moving Horizon (EC)	54
4.3	Damping Coefficients, S-D Moving Horizon (EC)	55
4.4	Energy Dissipation in Dampers, S-D Moving Horizon (EC)	55

4.5	Shear Force, S-D Moving Horizon (EC)	55
4.6	Damping Force, S-D Moving Horizon (EC)	55
4.7	Interstory Drifts, Moving Horizon (EC)	56
4.8	Floor Accelerations, Moving Horizon (EC)	56
4.9	Damping Coefficients, Moving Horizon (EC)	56
4.10	Energy Dissipation in Dampers, Moving Horizon (EC)	56
4.11	Shear Force, Moving Horizon (EC)	57
4.12	Damping Force, Moving Horizon (EC)	57
5.1	Interstory Drifts, Optimal Fixed (EC)	57
5.2	Floor Accelerations, Optimal Fixed (EC)	57
5.3	Energy Dissipation in Dampers, Optimal Fixed (EC)	58
5.4	Shear Force, Optimal Fixed (EC)	58
5.5	Damping Force, Optimal Fixed (EC)	58
5.6	Interstory Drifts, Optimal Control (EC)	59
5.7	Floor Accelerations, Optimal Control (EC)	59
5.8	Damping Coefficients, Optimal Control (EC)	59
5.9	Interstory Drifts, Minimax Design (EC)	59
5.10	Floor Accelerations, Minimax Design (EC)	60
5.11	Interstory Drifts, Moving Horizon (EC)	60
5.12	Floor Accelerations, Moving Horizon (EC)	60
5.13	Damping Coefficients, Moving Horizon (EC)	60

1. Introduction

The problem of controlling seismically excited vibrations in a terrestrial structure has features that make it significantly different from the problem of controlling vibrations in a structure caused by wind loading, or traffic, or from of controlling vibrations in a flexible space structure caused by docking maneuvers or space debris impacts. Seismic disturbances are of short duration, they are potentially of destructive intensity, and their occurrences are separated by long periods of quiescence. In addition, since seismic loading is applied only to the base of a structure, many of the methods of generating control forces for the elimination of wind loading and other types of excitation are not very effective in dealing with seismic disturbances.

The use of passive/active control to reduce the damage caused by earthquakes to buildings and other structures has become an area of considerable theoretical interest. There are several recent collections of papers on structural control [Lei.1, Lei.2, Cho.1, Wen.1] and many articles containing descriptions of control techniques applicable to the seismic damage control problem. For a representative sample of papers dealing with the control of structures subject to wind, traffic, and earthquake disturbances, see, e.g., [Abd.1, Cha.1, Kel.1, Mar.1, Kob.1,2, Mas.1, Roo.1, Yan.2 Yao.1], as well as the overview paper by T. T. Soong et al [Soo.2]. The recent text by T. T. Soong [Soo.1] demonstrates that the field of structural control is reaching a certain level of maturity. An interesting aspect of the research on the control of terrestrial structures is the range of actuation options that are being considered, such as active base isolation systems (see, e.g., [Kel.1]), the use of active tendons (see, e.g. [Roo.1]), active mass damping systems (see e.g., [Cha.1, Kob.2]), semi-active impact damping systems (see, e.g. [Deh.1]) and active variable structure control [Kob.1].

The control laws used in structural control often make use of state feedback in the form of instantaneous optimal control laws, based on the minimization of linear quadratic cost functions (see, e.g. [Yan.3, Soo.1, Che.1, Sat.1]), independent modal control, (see, e.g. [Mei.1, Yan.4, Mar.1]), pole assignment (see, e.g. [Abd.2]), sliding regimes (see, e.g. [Wan.1]), bang-bang control (see, e.g. [Kaw.1]), Lyapunov function based methods (see, e.g. [Lee.1, Kel.1]), and pulse control (see, e.g. [Deh.1, Pru.1, Mas.1]).

For reasons of reliability, the energy for operating the control system of a seismic resistant structure, ought to be stored locally. The actuator choices have a considerable impact both on the energy consumption and on the potential effectiveness of the resulting control system. For many active control schemes, such as active base isolation and active tendons, because of the enormous weight of a multistoried structure, the energy requirements can be very large indeed, and hence the development of safe energy storage methods for these types of actuators remains an open problem. The actuators proposed in [Deh.1, Kob.1] are distinguished by the fact that they use very little energy, which is highly desirable, but they raise the question as to how effectively one can control a structure without applying considerable external forces.

1. Introduction

Since in a variable structure one cannot apply external control forces, the function of a variable structure control system is to produce an impedance mismatch between the ground motion and the structure, so as to minimize the amount of ground motion energy that gets pumped into the structure. The success of such a control law, therefore, is bound to depend considerably on the spectral properties of the ground motion. The purpose of this study is to establish the capabilities of control laws for variable damping structures as well as for the simple variable stiffness structure proposed in [Kob.1].

In section 2.1, we present a model of the planar variable damping structure that we wish to study. Since the differential equations describing this model are stiff, simulations using this model are rather time consuming. We therefore proceed to develop a simplified model that may be useful for use in various preliminary studies, involving the use of sampled-data control laws. In Section 2.2, we examine the behavior of the most drastic simplification of our model, in which the mass of the auxiliary structure is neglected, and the variable dampers are assumed to function as on-off clamps only. In the process we examine the behavior of the original variable stiffness configuration proposed in [Kob.1], in which an auxiliary structure is connected to a main structure by means of controllable clamps, i.e, the stiffness variation is of the on-off variety. We show by analysis that, when operated in sampled-data relay mode, when the sampling period goes to zero, such a structure can be made to approximate a structure with stiffness values that lie anywhere in the convex hull of those of the main structure and the all-clamped structure. However, our experimental studies show that a variable structure, that is operated in sampled-data relay mode, exhibits very sharp, short duration acceleration peaks. Since these may cause buckling, the use of such a control method in practice may be problematic. We therefore abandoned this model, and, in Section 2.3, we construct a somewhat more sophisticated simplified model, in which the mass of the auxiliary structure is still neglected, so as to avoid creating stiff differential equations, but the on-off clamp action of the variable dampers is replaced by a smoothed out action. This model turned out to be adequate for use in preliminary studies, but not good enough to replace the original model entirely.

In Section 3, we establish performance bounds for a controlled variable damping structure. We begin in Section 3.1 by choosing an energy-based performance criterion that is close in spirit to the quadratic criteria used in many feedback laws. In Section 3.2, we then establish upper bounds on achievable performance for five well known earthquakes by determining the response of a variable damping structure with optimal damping modulation (using an algorithm from [Bak.1]), that is computed under the unrealistic assumption that the ground motion is known in advance. Then, in Section 3.3, we use an optimization algorithm (see [Pol.1,2]) to compute fixed damping coefficients that are minimax optimal, for our energy criterion, with respect to four of the earthquakes considered. The fifth, the El Centro 1940, earthquake was left out to be used as a control case, to determine whether a structure that has been minimax tuned for a given set of earthquakes performs well on other earthquakes. The performance of this minimax designed fixed structure determines a lower acceptable performance bound.

1. Introduction

Since the performance gap between the unrealistic optimally controlled structure and the minimax designed structure was found to be small, we decided to explore only the behavior of moving horizon control laws (see, e.g. [Pol.3]), since they have the best chance of giving behavior that falls in the gap between our upper and lower performance bounds. In Section 4, we present our moving horizon control laws: the first is of the sampled-data type, while the second one is a continuous control law.

In Section 5 we evaluate our numerical results. First, we found that the correlation between our energy criterion and such basic requirements as keeping interstory drifts within prescribed bounds and floor accelerations small, was adequate, though by no means exact. Second, we found that the minimax designed structure performed very well, even on the El Centro 1940 earthquake that was not used in its computations. Finally, we found that the use of a continuous moving horizon control law, with an accurate, 0.2 sec. prediction of the ground motion is capable of yielding performance that is better than our minimax design.

Our concluding thoughts are presented in Section 6. In particular, we arrive at two conclusions. The first is that sophisticated minimax design (see, e.g., [Pol.1,2]), taking a fairly small number of ground motions into account, is likely to yield structures that withstand seismic disturbances much better than structures designed by standard techniques. The second conclusion is that controlled variable structures are likely to be perform best at sites, such as landfills and dry lake beds, where resonances can be expected, but the resonance frequency cannot be estimated in advance.

2. System Models for Numerical Experimentation

As we will see, the natural model for a variable structure is numerically stiff, and hence numerical experiments using this model are rather time consuming. We will therefore develop a simplified model which results in much reduced simulation times and which is adequate for the tedious preliminary numerical experiments that we need to perform in order to establish effective weights in our cost function. As we will see, the simplest model that one can propose has nice theoretical properties, but does not sufficiently accurately model the acceleration response. Hence, a somewhat more complex, but still numerically well conditioned, simplified model had to be adopted.

2.1. Variable Structure System Model

We will consider the control of a planar variable three story structure consisting of a main structure and an auxiliary structure that are linked through variable damping elements, as shown in Fig. 2.1.1. We will assume that the mass of the main structure is concentrated in its floors, and that the mass of the auxiliary structure is concentrated at the points of connection of the auxiliary structure to the variable dampers. Hence our mathematical model corresponds to the situation in Fig. 2.1.2.

2.1. Variable Structure System Model

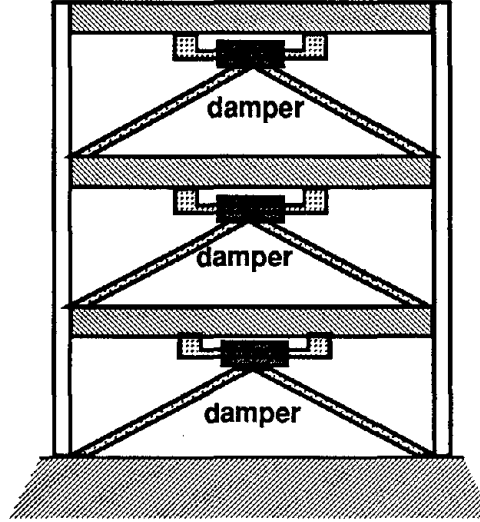


Fig. 2.1.1. Configuration of Variable Damping-Stiffness Structure

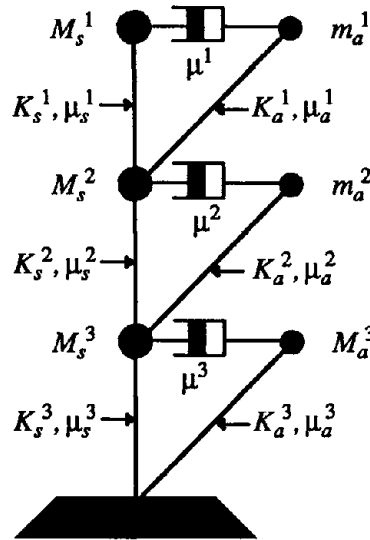


Fig. 2.1.2. Idealization of Variable Damping-Stiffness Structure

We will model the variable structure, as a planar structure with horizontal displacements only, in terms of absolute coordinates, as follows:

$$M\ddot{x}(t) + C\dot{x}(t) + Kx(t) + \sum_{i=1}^3 \mu^i(t) U_i \dot{x}(t) = C J_e \dot{x}_g(t) + K J_e x_g(t), \quad (2.1.1a)$$

where the vector $x \in \mathbb{R}^6$ is given by

$$x(t) = (x_s^1(t), x_s^2(t), x_s^3(t), x_a^1(t), x_a^2(t), x_a^3(t)), \quad (2.1.1b)$$

where the $x_s^i(t)$, $i = 1, 2, 3$, are the absolute displacement of the floors of the main

2.1. Variable Structure System Model

structure, the $x_a^i(t)$, $i = 1, 2, 3$, are the absolute displacement of the masses of the auxiliary structure, M is the mass matrix, C is the fixed damping matrix, K is the stiffness matrix, $\mu^i(t)$, $i = 1, 2, 3$, are the variable damper coefficients, U_i , $i = 1, 2, 3$, are location matrices for the variable dampers, J_e is a 6×1 vector with each element equal to 1, and $x_g(t)$ and $\dot{x}_g(t)$ are ground motion and ground velocity obtained from an earthquake record. We assume that at rest the positions of the floors and of the auxiliary masses are zero, in absolute coordinates.

The parameter values for our model are given in Table 2.1.1, where $i = 1, 2, 3$.

Next, defining the state vector $z \in \mathbb{R}^{12}$ by $z(t) = (\dot{x}(t), x(t))$, and $e(t) \in \mathbb{R}^2$ by $e(t) = (\dot{x}_g(t), x_g(t))$, equation (2.1.1) can be rewritten in the canonical state space form

$$\dot{z}(t) = Az(t) + \sum_{i=1}^3 u^i(t)B_i z(t) + De(t). \quad (2.1.2)$$

This system of differential equations turns out to be rather stiff, particularly when the variable damping coefficients are high, because the mass of the auxiliary structure is much smaller than the mass of the main structure. Hence numerical simulation times tend to be rather high. Therefore, in the next two subsections, we will attempt to develop a simplified, numerically well conditioned model that can be used in early stages of control system design.

M_s^1	$2.0 \times 10^5 \text{ kg}$
M_s^2	$1.2 \times 10^5 \text{ kg}$
M_s^3	$1.2 \times 10^5 \text{ kg}$
K_s^1	$1.96 \times 10^7 \text{ N/m}$
K_s^2	$1.96 \times 10^7 \text{ N/m}$
K_s^3	$2.45 \times 10^7 \text{ N/m}$
μ_s^i	$0.004K_s^i \text{ N s/m}$
M_a^i	$1.0 \times 10^4 \text{ Kg}$
K_a^i	$9.8 \times 10^7 \text{ N/m}$
μ_a^i	$0.004K_a^i \text{ N s/m}$

Table 2.1.1. Parameter Values for Variable Structure.

2.2. Simplified Variable Structure System Model I

Since one of the control laws that we propose to explore is a moving horizon sampled-data control law, we begin by exploring a simplification of the model (2.1.1), in which the mass of the auxiliary structure is neglected, and the variable dampers are modeled as on-off clamps. We will present a theoretical analysis that displays the capabilities of the resulting variable structure with a sampled-data clamp switching law, as well as a set of numerical experiments, designed to evaluate the validity of this simplified model of the dynamics and control action.

Consider the simple structure in Fig. 2.1.1, and suppose that the variable dampers act as on-off clamps. Since each clamp can be either open or closed, at each point of time, the behavior of the structure is determined by one of the eight possible combinations of the clamp states. To keep track of this situation, we introduce the clamping vector $c(t) \in \mathbb{R}^3$, $t \geq 0$, with the components $c^i(t)$, $i = 1, 2, 3$, assuming only the values of 0 or 1, i.e., $c(t) \in \mathbf{C}$, where

$$\mathbf{C} \triangleq \left\{ \begin{bmatrix} 0 \\ 0 \\ 0 \end{bmatrix} \begin{bmatrix} 0 \\ 1 \\ 0 \end{bmatrix} \begin{bmatrix} 0 \\ 0 \\ 1 \end{bmatrix} \begin{bmatrix} 0 \\ 1 \\ 1 \end{bmatrix} \begin{bmatrix} 1 \\ 0 \\ 0 \end{bmatrix} \begin{bmatrix} 1 \\ 1 \\ 0 \end{bmatrix} \begin{bmatrix} 1 \\ 0 \\ 1 \end{bmatrix} \begin{bmatrix} 1 \\ 1 \\ 1 \end{bmatrix} \right\}. \quad (2.2.1)$$

When $c^i(t) = 1$, the i -th clamp is closed, otherwise it is open. We will assume that $c(t)$ can only change at the sampling times kT , $k = 0, 1, 2, 3, \dots$, where T is the sampling period.

Hence, using coordinates relative to the inertial frame (i.e., absolute coordinates), for $t \geq 0$, to indicate the dependence of the motion of the system on the clamping vector $c(t)$, we will denote the resulting position of the i -th mass of the main structure by $x_s^i(t, c)$, $i = 1, 2, 3$, and the position of the i -th clamp by $x_a^i(t, c)$, $i = 1, 2, 3$. Finally, let $x_s^4(t, c) \triangleq x_g(t)$, the absolute position of the ground. We assume that the absolute ground motion is caused by a seismic disturbance, and that it is at least twice continuously differentiable.

Next, for $i = 1, 2, 3$, let

$$\Delta x_s^i(t, c) \triangleq x_s^i(t, c) - x_s^{i+1}(t, c), \quad (2.2.2a)$$

$$\Delta \dot{x}_s^i(t, c) \triangleq \dot{x}_s^i(t, c) - \dot{x}_s^{i+1}(t, c), \quad (2.2.2b)$$

$$\Delta x_a^i(t, c) \triangleq x_a^i(t, c) - x_s^{i+1}(t, c), \quad (2.2.2c)$$

$$c^0(t) = \Delta x_a^0(t, c) = \Delta x_s^0(t, c) = \Delta \dot{x}_s^0(t, c) \equiv 0, \quad (2.2.2d)$$

$$K_s^0 = \mu_s^0 = K_a^0 = \mu_a^0 = 0, \quad (2.2.2e)$$

where the last two relations are introduced so as to make it possible for us to write down

2.2. Simplified Variable Structure System Model I

the equations of motion of the controlled structure in compact form, as follows.

main structure. For $i = 1, 2, 3$,

$$\begin{aligned} M_s^i \ddot{x}_s^i(t, c) + (\mu_s^i + c^i(t)\mu_a^i) \Delta \dot{x}_s^i(t, c) + K_s^i \Delta x_s^i(t, c) + c^i(t) K_a^i \Delta x_a^i(t, c) \\ = (\mu_s^{i-1} + c^{i-1}(t)\mu_a^{i-1}) \Delta \dot{x}_s^{i-1}(t, c) \\ + K_s^{i-1} \Delta x_s^{i-1}(t, c) + c^{i-1}(t) K_a^{i-1} \Delta x_a^{i-1}(t, c), \end{aligned} \quad (2.2.3a)$$

auxillary structure. For $i = 1, 2, 3$,

$$\dot{x}_a^i(t, c) = c^i(t) \dot{x}_s^i(t, c) + (1 - c^i(t)) [\dot{x}_s^{i+1}(t, c) - \frac{K_a^i}{\mu_a^i} \Delta x_a^i(t, c)]. \quad (2.2.3b)$$

We assume that

$$x_s^i(0) = \dot{x}_s^i(0) = 0, \quad i = 1, 2, 3, 4, \quad (2.2.3c)$$

$$x_a^i(0) = \dot{x}_a^i(0) = 0, \quad i = 1, 2, 3, \quad (2.2.3d)$$

and that the ground motion $(x_g(t), \dot{x}_g(t))$ is given.

If we define the state vector $z \in \mathbb{R}^9$ by

$$z(t) \triangleq (x_s^1(t), x_s^2(t), x_s^3(t), \dot{x}_s^1(t), \dot{x}_s^2(t), \dot{x}_s^3(t), x_a^1(t), x_a^2(t), x_a^3(t)), \quad (2.2.3e)$$

and define the ground excitation function $e(t) \triangleq (x_g(t), \dot{x}_g(t))$, then we conclude from (2.2.2a), (2.2.2b) that $z(t)$ satisfies a differential equation of the form

$$\dot{z}(t) = A(c(t))z(t) + B(c(t))e(t), \quad (2.2.4a)$$

where the matrices $A(c(t))$ and $B(c(t))$ have the form

$$A(c(t)) = A_0 + \sum_{i=1}^3 c^i(t) A_i, \quad (2.2.4b)$$

$$B(c(t)) = B_0 + c^3(t) B_3, \quad (2.2.4c)$$

where the matrices A_i , $i = 0, 1, 2, 3$, and B_0 , B_3 are constant. Note that although the clamp status $c(t)$ is not necessarily continuous, by the fundamental theorem of differential equations, the state trajectory $z(t)$ is continuous.

To establish the potential capability of a variable damping-stiffness structure, we will show that the use of a relay clamp switching law enables us to endow the structure with any dynamics in a certain set. For this purpose, we assume that we need to analyze the behavior of the structure over the time interval $[0, T_f]$, and that our relay clamp switching law is based on a sampling time $T \triangleq T_f/NM$, where N and M are positive integers such that $[0, T_f]$ can be divided into N intervals $I_k = [kMT, (k+1)MT)$, for $k = 0, 1, \dots, N-1$. The clamping function $c(t)$ then has the property that each of the

2.2. Simplified Variable Structure System Model I

components $c^i(t)$ is constant over each sample period $[kT, (k+1)T)$ where $k \in \{0, 1, \dots, NM-1\}$. We then define the modulation function $m: \mathbb{R} \rightarrow [0, 1]^3$, by

$$m^i(t) = p_k^i/M, t \in I_k, i = 1, 2, 3, k = 0, 1, \dots, N-1, \quad (2.2.5)$$

where $0 \leq p_k^i \leq M$ is the number of subintervals in I_k for which the clamp connected to floor i is closed, (ie., $c^i(t) = 1$).

Now consider the ‘‘averaged’’ dynamics:

$$\dot{z}_{av}(t) = A_{av}(t)z_{av}(t) + B_{av}(t)e(t), \quad (2.2.6a)$$

where

$$A_{av}(t) = A_0 + \sum_{i=1}^3 m^i(t)A_i, \quad (2.2.6b)$$

$$B_{av}(t) = B_0 + m^3(t)B_3. \quad (2.2.6c)$$

Let $\delta A_i(t) \triangleq [c^i(t) - m^i(t)]A_i$, $i = 1, 2, 3$, and $\delta B_3(t) \triangleq [c^3(t) - m^3(t)]B_3$. Then, assuming that $z(0) = z_{av}(0) = 0$, we find that for $t \in [0, T_f]$,

$$\begin{aligned} z(t) - z_{av}(t) &= \int_0^t [A(c(s))z(s) - A_{av}(s)z_{av}(s) + (B(c(s)) - B_{av}(s))e(s)] ds \\ &= \int_0^t A_{av}(s)[z(s) - z_{av}(s)] ds \\ &\quad + \int_0^t [A(c(s)) - A_{av}(s)]z(s) ds \\ &\quad + \int_0^t [B(c(s)) - B_{av}(s)]e(s) ds. \end{aligned} \quad (2.2.7a)$$

Now,

$$A(c(s)) - A_{av}(s) = \sum_{i=1}^3 \delta A_i(s), \quad (2.2.7b)$$

and

$$B(c(s)) - B_{av}(s) = \delta B_3(s). \quad (2.2.7c)$$

Note that for any interval I_k , $k = 0, 1, \dots, N-1$, and $i = 1, 2, 3$,

$$\int_{kMT}^{(k+1)MT} [c^i(s) - m^i(s)]A_i z(kMT) ds = [p_k^i T - MT(p_k^i/M)]A_i z(kMT) = 0. \quad (2.2.7d)$$

Now, let L_z be the Lipschitz constant for $z(\cdot)$ on $[0, T_f]$, and $K_a < \infty$ be a constant such that $\|A_i\| \leq K_a$ for $i = 1, 2, 3$. Then for $k = 0, 1, \dots, N-1$, and $i = 1, 2, 3$,

$$\begin{aligned} \left\| \int_{kMT}^{(k+1)MT} \delta A_i(s) z(s) ds \right\| &\leq \int_{kMT}^{(k+1)MT} \|\delta A_i(s)\| \|z(s) - z(kMT)\| ds \\ &\quad + \left\| \int_{kMT}^{(k+1)MT} \delta A_i(s) z(kMT) ds \right\| \\ &\leq \int_{kMT}^{(k+1)MT} K_a L_z \|s - kMT\| ds \leq K_a L_z M^2 T^2. \end{aligned} \quad (2.2.7e)$$

For any $t \in [0, T_f]$, there exists $r \in \mathbb{N}$, $0 \leq r \leq N-1$ such that $rMT \leq t \leq (r+1)MT$ and

2.2. Simplified Variable Structure System Model I

hence,

$$\begin{aligned}
\| \int_0^t [A(c(s)) - A_{av}(s)]z(s) ds \| &\leq \sum_{k=0}^{r-1} \sum_{i=1}^3 \int_{kMT}^{(k+1)MT} \delta A_i(s)z(s) ds \| + \sum_{i=1}^3 \int_{rMT}^t \delta A_i(s)z(s) ds \| \\
&\leq 3rK_a L_z M^2 T^2 + 3(t - rMT)K_a K_z \\
&\leq 3NK_a L_z M^2 T^2 + 3MTK_a K_z \\
&= 3MTK_a [L_z T_f + K_z], \tag{2.2.7f}
\end{aligned}$$

where $K_z < \infty$ is such that $\|z(t)\| \leq K_z$ for all $t \in [0, T_f]$. Similarly, with L_e the Lipschitz constant for $e(\cdot)$ on $[0, T_f]$, $K_b < \infty$ such that $\|B_3\| \leq K_b$, and $K_e < \infty$ such that $\|e(t)\| \leq K_e$ for all $t \in [0, T_f]$, we get that

$$\| \int_0^t [B(c(s)) - B_{av}(s)]e(s) ds \| \leq MTK_b [L_e T_f + K_e]. \tag{2.2.7g}$$

Next, since $\|A_{av}(t)\|$ is bounded for all t , we can assume that there exists a constant $K_{av} < \infty$ such that $\|A_{av}(s)\| \leq K_{av}$ for all $s \in [0, T_f]$, and setting $K = 3K_a [L_z T_f + K_z] + K_b [L_e T_f + K_e]$, we conclude from (2.2.7a), (2.2.7f), and (2.2.7g) that

$$\|z(t) - z_{av}(t)\| \leq K_{av} \int_0^t \|z(s) - z_{av}(s)\| ds + KMT, \tag{2.2.7h}$$

It now follows from the Bellman-Gronwall Lemma that

$$\|z(t) - z_{av}(t)\| \leq KMT e^{K_{av} T_f} = K \frac{T_f}{N} e^{K_{av} T_f}, \tag{2.2.7i}$$

where we have used the fact that $MNT = T_f$.

Thus we see that as the number of samples N , in $[0, T_f]$, goes to infinity, the behavior of the relay clamp switched structure becomes the same as that of the averaged dynamics. Note that the error between the true and averaged dynamics does not necessarily go to zero as the sample size, T , goes to zero. In the case where N remains bounded, we have only shown a fixed upper bound on the error. However, when both N and M go to infinity, in the limit, the error goes to zero and the modulation function $m(t)$ can attain any value in a dense subset of $[0, 1]^3$. In the special case where $m(t) = m^*$ is constant, the relay clamp switched structure behaves as a linear system with dynamics defined by m^* .

numerical evaluation of the model. We carried out a numerical experiment using the model in this section so as to determine its validity. We used a sampling time $T = 0.2$ seconds, a final time $T_f = 5$ seconds, the earthquake ground motion supplied by the El Centro 1940 record, and a command signal constructed using a simple moving

2.2. Simplified Variable Structure System Model I

horizon control law. Plots of the resulting accelerations of the floors of the main structure, and the clamping vector $c(t)$, are shown in Fig. 2.2.1 and Fig. 2.2.2. Note that all plots included in this report follow the convention that the solid line refers to floor 1 (top) of the structure, or to the first component of the vector being plotted; the dashed line refers to floor 2 (middle) of the structure, or to the second component of the vector being plotted; and the dotted line refers to floor 3 (ground) of the structure, or to the third component of the vector being plotted. Referring to Fig. 2.2.1 and Fig. 2.2.2, we see large, short duration acceleration peaks that occur at the clamp opening and closing times. The reason for the acceleration peaks is that the opening and closing of a clamp causes impulsive forces to act on the main and auxiliary structures. Since large acceleration peaks may cause buckling failure in the structure, we will adopt a law for switching the dampers that is gradual, for use in sampled-data relay control. This results in a modified structural model that we will present in the next subsection.

2.3 Simplified Variable Structure System Model II

The numerical results presented in the last section indicate that even for preliminary studies, a more sophisticated model than the one presented in Section 2.2, for the structural system, is required. We will therefore replace the clamps by variable dampers whose damping coefficients can be varied from 0.0 N sec/m to $\mu_{\max} = 1.96 \times 10^8 \text{ N sec/m}$. As in Section 2.2, we will assume that the command signal $c(t) \in \mathbb{R}^3$ takes values in the set \mathbf{C} , defined in (2.2.1), and that it can only change at the sampling times kT , $k = 0, 1, 2, 3, \dots$, where T is the sampling period. Since the damping coefficients depend on the command signal, we will denote them by $\mu_c^i(t)$, $i = 1, 2, 3$, and we will assume that they respond to the command signal, $c(t)$, as follows:

$$\mu_c^i(t) = \begin{cases} \mu_{\max}((t - kT)/T_c)^r & \text{for } t \in [kT, kT + T_c] \\ \mu_{\max} & \text{for } t \in (kT + T_c, (k+1)T), \end{cases} \quad (2.3.1a)$$

if $c^i(kT - \epsilon) = 0$ and $c^i(kT) = 1$ (with $\epsilon \in (0, T)$);

$$\mu_c^i(t) = \begin{cases} \mu_{\max}(1 - (t - kT)/T_c)^r & \text{for } t \in [kT, kT + T_c] \\ 0 & \text{for } t \in (kT + T_c, (k+1)T), \end{cases} \quad (2.3.1b)$$

if $c^i(kT - \epsilon) = 1$ and $c^i(kT) = 0$;

$$\mu_c^i(t) = 0, \text{ for } t \in [kT, (k+1)T), \quad (2.3.1c)$$

if $c^i(kT - \epsilon) = 0$ and $c^i(kT) = 0$; and, finally,

$$\mu_c^i(t) = \mu_{\max}, \text{ for } t \in [kT, (k+1)T), \quad (2.3.1d)$$

if $c^i(kT - \epsilon) = 1$ and $c^i(kT) = 1$. The exponent $r \in \mathbb{N}$ will be chosen on the basis on

2.3 Simplified Variable Structure System Model II

numerical experimentation.

The introduction of a variable damper modifies the equations of motion (2.2.3a,b) as follows.

main structure. For $i = 1, 2, 3$,

$$\begin{aligned} & M_s^i \ddot{x}_s^i(t, c) + K_s^i \Delta x_s^i(t, c) + \mu_s^i \Delta \dot{x}_s^i(t, c) + \mu_c^i(t) (\dot{x}_s^i(t, c) - \dot{x}_a^i(t, c)) \\ &= K_s^{i-1} \Delta x_s^{i-1}(t, c) + \mu_s^{i-1} \Delta \dot{x}_s^{i-1}(t, c) + K_a^{i-1} \Delta x_a^{i-1}(t, c) + \mu_a^{i-1} \Delta \dot{x}_a^{i-1}(t, c), \end{aligned} \quad (2.3.2a)$$

auxiliary structure. For $i = 1, 2, 3$,

$$\mu_c^i(t) (\dot{x}_s^i(t, c) - \dot{x}_a^i(t, c)) = \mu_a^i \Delta \dot{x}_a^i(t, c) + K_a^i(t, c), \quad (2.3.2b)$$

Let $\mu_c(t) = (\mu_c^1(t), \mu_c^2(t), \mu_c^3(t))$ be the vector of damping coefficients corresponding to the three clamps. As before, by defining the state vector $z \in \mathbb{R}^9$ by

$$z(t) \triangleq (x_s^1(t), x_s^2(t), x_s^3(t), \dot{x}_s^1(t), \dot{x}_s^2(t), \dot{x}_s^3(t), x_a^1(t), x_a^2(t), x_a^3(t)), \quad (2.3.2c)$$

and the ground motion function $e(t) \triangleq (x_g(t), \dot{x}_g(t))$, then from (2.3.2a,b), we can show that $z(t)$ satisfies a differential equation of the form

$$\dot{z}(t) = \bar{A}(\mu_c(t))z(t) + \bar{B}(\mu_c(t))e(t), \quad (2.3.3a)$$

where the matrices $\bar{A}(\mu_c(t))$ and $\bar{B}(\mu_c(t))$ have the form

$$\bar{A}(\mu_c(t)) = A_0 + \sum_{i=1}^3 \bar{A}_i(\mu_c^i(t)), \quad (2.3.3b)$$

$$\bar{B}(\mu_c(t)) = B_0 + \bar{B}_3(\mu_c^3(t)), \quad (2.3.3c)$$

where the matrices $\bar{A}_i(\cdot)$, $i = 1, 2, 3$, and $\bar{B}_3(\cdot)$ are nonlinear, continuously differentiable functions of the damping coefficients $\mu_c^i(t)$, and A_0 and B_0 are defined as in Section 2.2.

The matrices $\bar{A}_i(\mu_c^i(t))$, $i=1,2,3$, have the property that $\bar{A}_i(0) = 0$ and $\bar{A}_i(\mu_c^i(t)) \rightarrow A_i$ as $\mu_c^i(t) \rightarrow \infty$. Also, $\bar{B}_3(0) = 0$ and $\bar{B}_3(\mu_c^3(t)) \rightarrow B_3$ as $\mu_c^3(t) \rightarrow \infty$. Hence, in the limit, as the damping coefficients corresponding to the clamps go to 0 or ∞ , the model given in (2.3.3a) becomes identical to that of (2.2.4a) with the corresponding clamp status set to 0 or 1 respectively.

Since the damping vector $\mu_c(c)$ is continuous, the matrices $\bar{A}(\mu_c(\cdot))$ and $\bar{B}(\mu_c(\cdot))$ are continuous functions of time, and by the fundamental theorem of differential equations, we see that both the state trajectories $z(t)$ and their derivatives $\dot{z}(t)$ are continuous for all $t \in [0, T_f]$.

Two issues still remain before the new model is completely specified. These are choosing an appropriate clamp transition time, T_c , and an exponent r for the damper response law in (2.3.1a,b). We carried out numerical experiments using the model in this section so as to establish reasonable values for these parameters. Once again, we used a

2.3 Simplified Variable Structure System Model II

sampling time $T = 0.2$ seconds, a final time $T_f = 5$ seconds, the earthquake ground motion supplied by the El Centro 1940 record, and a command signal constructed using a simple moving horizon control law.

exponent for damper response law r . We set $T_c = 0.9T$, which gives a sufficiently long clamp transition time to investigate the effects of different values of r in (2.3.1a,b). We found that $r = 4$ gave the most gradual transition, with smaller values of r resulting in most of the smoothing action occurring in the first fifth of the transition time, while larger values resulted in the smoothing action occurring in the last fifth of the transition time.

transition time T_c . To determine if the value $T_c = 0.9T$ should be replaced by another value, we carried out simulations using $T_c = \alpha T$, where $\alpha \in [0, 1)$, for several values of α . It was observed that as α becomes larger, the acceleration peaks in the response of the controlled structure become smaller. For example, see Figures 2.3.1 - 2.3.3, where Figure 2.3.1 shows the resulting accelerations using $\alpha = 0.0$, Figure 2.3.2 shows the accelerations for $\alpha = 0.5$, and Figure 2.3.3 shows the accelerations for $\alpha = 0.9$.

We define the peak acceleration magnitude vector \ddot{x}_{peak} by

$$\ddot{x}_{peak} \triangleq \left(\max_{t \in [0, T_f]} |\ddot{x}_s^1(t)|, \max_{t \in [0, T_f]} |\ddot{x}_s^2(t)|, \max_{t \in [0, T_f]} |\ddot{x}_s^3(t)| \right), \quad (2.3.4a)$$

the average acceleration vector \ddot{x}_{avg} by

$$\ddot{x}_{avg} \triangleq (1/T_f) \left(\int_0^{T_f} |\ddot{x}_s^1(t, c)| dt, \int_0^{T_f} |\ddot{x}_s^2(t, c)| dt, \int_0^{T_f} |\ddot{x}_s^3(t, c)| dt \right), \quad (2.3.4b)$$

and the maximum interstory drift vector x_d by

$$x_d \triangleq \left(\max_{t \in [0, T_f]} |\Delta x_s^1(t, c)|, \max_{t \in [0, T_f]} |\Delta x_s^2(t, c)|, \max_{t \in [0, T_f]} |\Delta x_s^3(t, c)| \right). \quad (2.3.4c)$$

Referring to Table 2.3.1, we see that both the peak and average accelerations become smaller as α increases.

α	\ddot{x}_{peak}^1	\ddot{x}_{peak}^2	\ddot{x}_{peak}^3	\ddot{x}_{avg}^1	\ddot{x}_{avg}^2	\ddot{x}_{avg}^3
0.0	575	1025	1200	103.9	164.6	232.7
0.5	550	800	550	113.0	149.7	128.4
0.9	440	460	410	102.0	109.5	132.6

Table 2.3.1. Effect of α on Peak and Average Accelerations.

Hence, our results seem to indicate that better performance in terms of reducing the accelerations of the floors of the structure can be obtained through the use of longer transition times. This result is quite important since it indicates that it may not be necessary to develop faster switching dampers in order to improve the response of the controlled structure. In the remaining simulations, we used the value $\alpha = 0.9$.

2.3 Simplified Variable Structure System Model II

In order to determine whether the simplified model considered in this section can always be used in numerical experiments in place of the original system model, simulations were performed using both models and identical command signals and ground motion records. The command signals were generated using a simple moving horizon sampled-data control law with sampling period $T = 0.2$ seconds, and the earthquake ground motions are given by the El Centro (1940) (EC), Kern County (1952) (KC), Puget Sound (1965) (PS), San Fernando (1971) (SF), and Western Washington (1949) (WW) records. A comparison of the peak interstory drifts is given in Table 2.3.2; a comparison of the peak accelerations is given in Table 2.3.3; and a comparison of average accelerations is given in Table 2.3.4.

Quake	simplified model			original model		
	x_d^1	x_d^2	x_d^3	x_d^1	x_d^2	x_d^3
EC	1.15	1.90	1.80	1.13	1.99	1.89
KC	1.70	2.90	3.00	1.79	2.92	3.22
PS	1.40	1.65	1.20	1.42	1.81	1.42
SF	1.00	1.65	1.00	0.97	1.73	1.37
WW	1.40	2.00	1.40	1.38	2.13	1.41

Table 2.3.2. Comparison of Peak Interstory Drifts (*cm*).

Quake	simplified model			original model		
	\ddot{x}_{peak}^1	\ddot{x}_{peak}^2	\ddot{x}_{peak}^3	\ddot{x}_{peak}^1	\ddot{x}_{peak}^2	\ddot{x}_{peak}^3
EC	625	475	525	566	358	350
KC	525	450	475	481	396	271
PS	390	360	375	384	361	362
SF	380	510	400	397	380	372
WW	275	220	380	289	243	284

Table 2.3.3. Comparison of Peak Accelerations (*cm/sec²*).

2.3 Simplified Variable Structure System Model II

Quake	simplified model			original model		
	\ddot{x}_{avg}^1	\ddot{x}_{avg}^2	\ddot{x}_{avg}^3	\ddot{x}_{avg}^1	\ddot{x}_{avg}^2	\ddot{x}_{avg}^3
EC	83.7	79.6	88.0	82.4	70.0	82.0
KC	79.0	74.1	55.3	67.1	57.8	44.5
PS	67.7	73.3	76.4	72.6	63.7	79.8
SF	70.7	62.3	64.0	65.4	53.3	54.9
WW	36.6	37.8	47.5	34.8	36.4	45.3

Table 2.3.4. Comparison of Average Accelerations (cm/sec^2)

In general, the simulations using the simplified model exhibit higher accelerations and lower interstory drifts than the simulations using the original model. These differences are too significant to ignore, and hence the simplified model can be used in preliminary experiments, but for final results, the original model must be used.

3. Estimation of Performance Bounds

Since the control system for an actively controlled variable structure cannot impart energy to the structure, it is not clear, a priori, what is its potential for earthquake damage mitigation. Hence, before attempting to develop control laws, we will establish upper and lower bounds on its performance. The upper bounds will be established using optimal control laws under the assumption that the earthquake ground motion is known in advance. A lower bound on acceptable performance will be obtained by carrying out a minimax optimal design that assigns fixed values to the variable dampers, on the basis of the histories of a fixed number of earthquakes. The first step in obtaining performance bounds is the development of a performance criterion that captures the essential performance requirements of interstory drift and acceleration limitation, and that is natural for use in moving horizon, as well as instantaneous optimal, feedback control laws.

3.1. Development of a Performance Criterion

We will assume that minimal performance requirements for a structure subjected to earthquakes, scaled to have the same peak velocity as the El Centro (1940 S00E) earthquake, are as specified in Table 3.1.1, which states maximum allowable deformations and shear forces that the structure can withstand before it breaks. In Table 3.1.1, D_{max} denotes the maximum allowable interstory drift, in cm, SF_{max} denotes the maximum allowable shear force, in N, and CF_{max} denotes the maximum allowable force on the damper, in N.

3.1. Development of a Performance Criterion

	Story 1	Story 2	Story 3
D_{\max}	$x_d^1 \leq 2.02$	$x_d^2 \leq 2.46$	$x_d^3 \leq 1.89$
SF_{\max}	8.33×10^5	7.448×10^5	5.782×10^5
CF_{\max}	1.372×10^6	1.372×10^6	1.372×10^6

Table 3.1.1. Design Performance Specifications

In addition, the accelerations of the floor masses must be kept as small as feasible, so as to help protect the contents of the structure during an earthquake.

The above requirements are best captured by a minimax type criterion. However, there are no commonly used feedback laws based on a minimax criterion, and, in addition, it would be rather cumbersome to implement a moving horizon control law based on a minimax criterion. Hence we will use a weighted energy criterion that reflects these requirements indirectly, but which relates naturally to common feedback laws. The weights will be tuned to make the energy criterion represent the performance requirements as well as possible.

Given a ground motion vector $e(t)$, the fact that the state of the variable structure is z_o at a time $T_o \geq 0$, and a damper coefficient modulation function $\mu(t)$, we will denote the resulting response of the structure, determined either by (2.1.1a,b) or by (2.3.2a,b), by $z(t; z_o, T_o, \mu, e)$. With each story of the structure, at time $t \geq T_o$, we will associate four energy functions, all of which depend on the variable damper modulation functions and the ground motion. Let $E_{s,K}^i(t; z_o, T_o, \mu, e)$ be the kinetic energy in i -th story of the main structure, $E_{s,P}^i(t; z_o, T_o, \mu, e)$, the potential energy in i -th story of the main structure, $E_{a,P}^i(t; z_o, T_o, \mu, e)$, the potential energy in the i -th story of the auxiliary structure, and $E_{a,K}^i(t; z_o, T_o, \mu, e)$, the kinetic energy in the i -th story of the auxiliary structure. Then, irrespective of whether model (2.1.1a,b) or model (2.3.2a,b) is used, we see that these are given by

$$E_{s,K}^i(t; z_o, T_o, \mu, e) \triangleq \frac{1}{2} M_s^i \dot{x}_s^i(t)^2, \quad i = 1, 2, 3, \quad (3.1.3a)$$

$$E_{s,P}^i(t; z_o, T_o, \mu, e) \triangleq \frac{1}{2} K_s^i (x_s^i - x_s^{i+1})^2, \quad i = 1, 2, 3, \quad (3.1.3b)$$

$$E_{a,K}^i(t; z_o, T_o, \mu, e) \triangleq \frac{1}{2} M_a^i \dot{x}_a^i(t)^2, \quad i = 1, 2, 3, \quad (3.1.3c)$$

$$E_{a,P}^i(t; z_o, T_o, \mu, e) \triangleq \frac{1}{2} K_a^i (x_a^i - x_s^{i+1})^2, \quad i = 1, 2, 3. \quad (3.1.3d)$$

We will use as our performance criterion a weighted energy function of the form

$$E(t; z_o, T_o, \mu, e) \triangleq \sum_{i=1}^3 w_{i,K} E_{s,K}^i(t; z_o, T_o, \mu, e) + \sum_{i=1}^3 w_{i,P} E_{s,P}^i(t; z_o, T_o, \mu, e), \quad (3.1.3e)$$

where the weights $w_{i,K}, w_{i,P} > 0, i = 1, 2, 3$.

3.1. Development of a Performance Criterion

The parameters $w = (w_{1,P}, w_{2,P}, w_{3,P}, w_{1,K}, w_{2,K}, w_{3,K})$ enable us to fine-tune the response of the controlled structure. Thus, increasing the potential energy parameters $w_{i,P}$ tends to decrease corresponding interstory drifts, while increasing the kinetic energy parameters $w_{i,K}$ tends to reduce the velocity of the i -th story mass.

Using the cruder model (2.3.2a,b), we performed a set of numerical experiments to determine the weights for the energy function in (3.1.3e) that result in good performance of the controlled structure. This involved performing simulations, using Moving Horizon Control Law 4.1, of the response of the controlled structure to the the 1940 El Centro (comp S00E) earthquake record for various weights. For these experiments, the initial time was $T_o = 0$, the initial state $z_o = 0$, the sampling time $T = 0.2$ seconds, and the final time $T_f = 5$ seconds.

Numerical experiments were performed for several values of weighting factors. A comparison of the resulting peak interstory drift values for each of the weighting factors is given in Table 3.1.2.

weighting factor w	interstory drifts (cm)		
	x_d^1	x_d^2	x_d^3
(1, 1, 1, 1, 1, 1)	1.85	1.40	4.20
(3, 3, 3, 1, 1, 1)	1.20	2.20	2.10
(3, 3.5, 3.5, 1, 1)	1.30	1.80	1.95
(3, 2.5, 4, 1, 1)	1.15	1.90	1.80

Table 3.1.2. Peak Interstory Drifts vs. Weighting Factor.

From these results, we see that changing the weights on the potential energy terms directly affects the resulting interstory drifts on the corresponding floors. The use of $w = (3, 2.5, 4, 1, 1)$ enabled the response of the structure to meet the interstory drift constraints given in Table 3.1.1, but the use of larger weights on the potential energy terms than those shown in the above results did not enable us to achieve better results. This seems to indicate that the amount of disturbance rejection possible with a variable structure system is limited.

The effectiveness of the weights $w = (3, 2.5, 4, 1, 1)$, was verified by performing numerical experiments on four additional earthquake records. In addition to the El Centro record, we used the Kern County (Taft) 1952 (comp S69E) record, the Puget Sound 1965 (comp S86W) record, the San Fernando (Pacoima) 1971 (comp S74W) record, and the Western Washington 1949 (comp N86E) record. Since these records represent earthquakes of varying intensities, the ground motion records needed to be scaled. It is common practice to scale the records so that the peak velocities are equal for all of the records. For our numerical experiments throughout this report, we used the El Centro

3.1. Development of a Performance Criterion

record as a standard and scaled the other earthquakes so that their peak velocities were equal to that of the El Centro record. Since these experiments were being run for only 5 seconds, only the first 5 seconds of each record were considered when determining the scaling factors. This resulted in the scaling factors shown in Table 3.1.3.

Earthquake	Scaling Factor
KC	1.825
PS	7.760
SF	0.563
WW	2.220

Table 3.1.3. Ground Motion Scale Factors.

The scaled ground acceleration, velocity, and position for each of the earthquakes are shown in Figures 3.1.1 - 3.1.15. The resulting experiments indicate that the use of $w = (3, 2.5, 4, 1, 1)$ provides reasonable performance, with the interstory drift constraints being met for all but the structure subjected to the Kern County earthquake.

3.2. Upper Performance Bounds: Optimal Controls

From now on we will use only the system model (2.1.1a,b). The five optimal control problems that we will solve differ only by the ground motion and ground velocity, obtained from an earthquake record, appearing in the system model (2.1.1a,b).

the optimal control problem. Since we will also need to use the optimal control algorithm in a moving horizon control law, we begin by stating a more general optimal control problem than is needed for this section alone. Let $0 < T_o < T_f < \infty$ be the initial and final times. Let $z(t; z_o, T_o, \mu, e)$ denote the response of the structure model (2.1.1a,b), with initial state z_o at time T_o to a ground motion $e(t)$, when controlled by the damper modulation function $\mu(t)$, let

$$\mathbf{M} = \{ \mu \in L_\infty^3[T_o, T_f] \mid 0 \leq \mu^i(t) \leq \mu_{\max}, \quad i = 1, 2, 3, \quad t \in [0, T_f] \}, \quad (3.2.1a)$$

and let $\Phi: \mathbf{M} \rightarrow \mathbb{R}$ be defined by

$$\Phi(\mu) \triangleq \int_{T_o}^{T_f} E(t; z_o, T_o, \mu, e) dt, \quad (3.2.1b)$$

where $E(t; z_o, T_o, \mu, e)$ is defined as in (3.1.3e). To compute an optimal damper modulation function (control) $\hat{\mu}(t)$, we propose to solve the following optimal control problem:

$$\mathbf{P} \quad \min_{\mu \in \mathbf{M}} \Phi(\mu). \quad (3.2.1c)$$

3.2. Upper Performance Bounds: Optimal Controls

In order to obtain a numerical solution to **P**, this problem must be replaced by a consistent finite dimensional approximation [Pol.4]. To obtain such an approximation, we replace the time interval $[T_o, T_f]$, by a grid of N equally spaced time points $t_k = k\Delta$, $k = 0, 1, \dots, N$, where $\Delta = [T_f - T_o]/N$, and assume that the the controls are constant between the grid points. Assuming without loss of generality that $T_o = 0$, results in controls having the finite parametric representation

$$\mu(t) = \sum_{k=1}^N u(k)\pi(t - (k-1)\Delta), \quad (3.2.2a)$$

where $u(k) \in \mathbb{R}^3$, for $k = 1, 2, \dots, N$, and

$$\pi(t) \triangleq \begin{cases} 1, & \text{for } 0 \leq t < \Delta, \\ 0, & \text{otherwise.} \end{cases} \quad (3.2.2b)$$

Hence the sequence $\{u(k)\}_{k=1}^N$ completely determines the control $\mu(t)$. The set of admissible discrete control sequences $u = \{u(k)\}_{k=1}^N$, that correspond to controls in the set **M**, is given by

$$\mathbf{U} \triangleq \{u = \{u(k)\}_{k=1}^N \mid u(k) \in \mathbf{V}, k = 1, 2, \dots, N\}, \quad (3.2.2c)$$

where

$$\mathbf{V} \triangleq \{v \in \mathbb{R}^3 \mid 0 \leq v^j \leq \mu_{\max}, j = 1, 2, 3\}. \quad (3.2.2d)$$

At the same time, the system equations (2.1.2) are replaced by the backwards Euler integration formula:

$$\bar{z}((k+1)\Delta) = \bar{z}(k\Delta) + \Delta(A + \sum_{i=1}^3 u^i((k+1)\Delta)B_i)\bar{z}((k+1)\Delta) + \Delta De((k+1)\Delta), \quad (3.2.3a)$$

where due to the linearity of the system with respect to the state variables, the implicit difference equations can be solved to yield the explicit difference equation

$$\bar{z}((k+1)\Delta) = (I - \Delta(A + \sum_{i=1}^3 u^i((k+1)\Delta)B_i))^{-1}(\bar{z}(k\Delta) + \Delta De((k+1)\Delta)). \quad (3.2.3b)$$

The backwards Euler integration method, which is the simplest implicit numerical integration method, is used here since for large values of $\mu(t)$, the state equations (2.1.2) become stiff.

Let $f : \mathbf{U} \rightarrow \mathbb{R}$ be defined by

$$f(u) \triangleq \Delta \sum_{k=1}^N E(k\Delta; z_o, T_o, u, e), \quad (3.2.4)$$

where E defined as in (3.1.3e), but with $\bar{z}(k\Delta)$ replacing $z(k\Delta)$ in equations (3.1.3a-d). The finite dimensional approximating optimization problem is then given by

$$\mathbf{P}_N \quad \min_{u \in \mathbf{U}} f(u). \quad (3.2.5)$$

The gradient of the cost function, $\nabla f(u)$ is an element of \mathbb{R}^{3N} . To retain an exact correspondence to the scalar product and norm in L_2 , we define the scalar product

3.2. Upper Performance Bounds: Optimal Controls

$\langle \cdot, \cdot \rangle_N : \mathbb{R}^{3N} \times \mathbb{R}^{3N} \rightarrow \mathbb{R}$ by

$$\langle x, y \rangle_N = \Delta \sum_{i=1}^N x_i^T y_i, \quad (3.2.6a)$$

where $x = \{x_i\}_{i=1}^N$, $y = \{y_i\}_{i=1}^N$, and $x_i, y_i \in \mathbb{R}^3$. The corresponding norm $\| \cdot \|_N : \mathbb{R}^{3N} \rightarrow \mathbb{R}$ is then given by

$$\|h\|_N^2 = \langle h, h \rangle_N. \quad (3.2.6b)$$

the optimal control algorithm. The finite dimensional optimization problem P_N can be solved numerically using a number of optimization algorithms. We will use the following generalization of the Armijo gradient method, which we have developed for optimization problems with simple, convex constraints, as in (3.2.5) (see [Bak.1, Pol.1, Pol.2]).

Constrained Armijo-Gradient Algorithm 3.2.1.

Parameters. $\alpha, \beta \in (0, 1), \gamma > 0, n_i =$ number of iterations.

Data. $T_o, T_f, z_o \in \mathbb{R}^{12}, e(\cdot), u_0 = \{u_0(k\Delta)\}_{k=1}^N \in \mathbf{U}$.

Step 0. Set $i = 0$.

Step 1. Compute the search direction:

$$h_i = \{ (h_i(\Delta), h_i(2\Delta), \dots, h_i(N\Delta)) \} \triangleq \arg \min_{h \in \mathbb{R}^{3N}} \{ \langle \nabla f(u_i), h \rangle_N + \frac{\gamma}{2} \|h\|_N^2 \mid u(k\Delta) + h(k\Delta) \in \mathbf{V}, j = 1, 2, 3, k = 1, 2, \dots, N \}. \quad (3.2.7a)$$

Step 2. Compute the step size:

$$\lambda_i = \max_{l \in \mathbb{N}} \{ \beta^l \mid f(u_i + \beta^l h(u_i)) - f(u_i) \leq \alpha \beta^l \langle \nabla f(u_i), h(u_i) \rangle_N, u(k\Delta) + \beta^l h(k\Delta) \in \mathbf{V}, j = 1, 2, 3, k = 1, 2, \dots, N \}. \quad (3.2.7b)$$

Step 3. Set $u_{i+1} = u_i + \lambda_i h_i$, replace i by $i+1$, and if $i \leq n_i$, go to Step 1. \square

The parameter γ is related to the second derivative of the cost function in the following way:

$$\inf_{u \in \mathbf{U}} \underline{\sigma}[f_{uu}(u)] \leq \gamma \leq \sup_{u \in \mathbf{U}} \overline{\sigma}[f_{uu}(u)], \quad (3.2.8a)$$

where $\underline{\sigma}[Q], \overline{\sigma}[Q]$ denote the smallest and largest singular values, respectively, of the matrix \overline{Q} . Since the second derivative matrix $f_{uu}(u)$ is quite tedious to compute, and since the value of γ only has to be in the range between the maximum and minimum singular values, an acceptable value may be computed simply setting

3.2. Upper Performance Bounds: Optimal Controls

$$\gamma = \frac{|f(u + \delta u) - f(u) - \langle \nabla f(u), \delta u \rangle_N|}{\frac{1}{2} \|\delta u\|_N^2}, \quad (3.2.8b)$$

for any $u \in U$ and $\delta u \in \mathbb{R}^{3N}$ such that $u + \delta u \in U$.

One final note on Algorithm 3.2.1 is that the stopping criterion may be changed to ensure that the algorithm continues until it approaches a local minimum rather than just for a specified number of iterations. For example, given some $\varepsilon > 0$, terminate the iteration when

$$-\langle \nabla f(u_i), h_i \rangle < \varepsilon. \quad (3.2.9)$$

In other words, when the directional derivative in the direction of the search direction becomes small (in magnitude), additional iterations will not produce any significant decreases in the value of the cost function, so the iteration should be terminated.

Initialization algorithm Optimal control problems require considerable computing time to solve, with the solution time depending strongly on the choice of the initial control. We therefore propose to solve the optimal control problems in two stages. The first consists of solving a simplified problem, in which the control is required to be constant for all times, for an initial control to be used in the second stage by Algorithm 3.2.1. Referring to (3.2.5), we see that the simplified problem must have the form

$$\min_{u \in U} \{ f(u) \mid u_1 = u_2 = \dots = u_N \}, \quad (3.2.10a)$$

or, equivalently,

$$\mathbf{P}_N^0 \quad \min_{v \in V} \bar{f}(v), \quad (3.2.10b)$$

where

$$\bar{f}(v) \triangleq f(u(v)), \quad (3.2.10c)$$

with $u(v) \triangleq \{ v \}_{k=1}^N$, i.e., $u_k(v) = v$ for all k .

Given the form of $\bar{f}(v)$, we see that we can compute its gradient by simply using the chain rule. The result is

$$\nabla \bar{f}(v) = u_v(v)^T \nabla f(u(v)), \quad (3.2.11)$$

where $u_v(v)^T = [I_3, I_3, \dots, I_3]$ is a $3 \times 3N$ matrix, with I_3 the 3×3 identity matrix. Hence, when applied to problem \mathbf{P}_N^0 , Algorithm 3.2.1 assumes the form

Constrained Armijo-Gradient Algorithm 3.2.1'

Parameters. $w_{1,P}, w_{2,P}, w_{3,P}, w_{1,K}, w_{2,K}, w_{3,K} > 0$, $\alpha, \beta \in (0, 1)$, $\gamma > 0$, $n_i =$ number of iterations.

Data. $v_0 \in V$.

Step 0. Set $i = 0$.

3.2. Upper Performance Bounds: Optimal Controls

Step 1. Compute the search direction:

$$h_i \triangleq \arg \min_{h \in V - v_i} \{ \langle \nabla \bar{f}(v_i), h \rangle_N + \frac{\gamma}{2} \|h\|_N^2 \}. \quad (3.2.12a)$$

Step 2. Compute the step size:

$$\lambda_i = \max_{l \in \mathbf{N}} \{ \beta^l | \bar{f}(v_i + \beta^l h_i) - \bar{f}(v_i) \leq \alpha \beta^l \langle \nabla f(u_i), h(u_i) \rangle_N, v_i + \beta^l h_i \in \mathbf{V} \}. \quad (3.2.12b)$$

Step 3. Set $u_{i+1} = u_i + \lambda_i h_i$, replace i by $i+1$, and if $i \leq n_i$, go to Step 1. □

Problem P_N^0 takes less time to solve than problem P_N , because the dimension of the search direction calculation in Step 1 of Algorithm 3.2.1' is N times smaller than in Algorithm 3.2.1. In addition, our computational experience indicates that, in general, fewer iterations are necessary to solve problem P_N^0 than problem P_N .

computational experiments The parameters used in our optimal control experiments, both for Algorithm 3.2.1 and Algorithm 3.2.1' are given in Table 3.2.1.

w	Δ (sec)	T_f (sec)	α	β	γ
(3, 2.5, 4, 1, 1, 1)	0.004	5	0.5	0.75	1×10^{-10}

Table 3.2.1. Parameters Used in Optimal Control Experiments

• **initialization** Optimal *constant* controls (i.e., fixed values for the damping coefficients), for use as initial controls by Algorithm 3.2.1, were computed using Algorithm 3.2.1' for each of the five scaled earthquake ground motion records. The parameter γ was selected by means of an expression analogous to (3.2.8b). The fact that gamma is quite small indicates that the cost function $\bar{f}(v)$ is close to being linear. All of the computations with Algorithm 3.2.1' required no more than 10 iterations for the termination test $|\langle \nabla \bar{f}(v_i), h_i \rangle| \leq 0.01 \bar{f}(v_0)$ to be satisfied.

The resulting optimal fixed damping coefficient values are shown in Table 3.2.2. We see that the optimal fixed damping coefficient for the third floor is largest and that the optimal fixed damping coefficients for the first and second floors are quite close. This intuitively makes sense since the weight on the potential energy terms for the cost function is largest for the third floor, while weights the first and second floors are smaller, and almost equal.

3.2. Upper Performance Bounds: Optimal Controls

Earthquake	μ^1	μ^2	μ^3
El Centro	7.5×10^6	6.8×10^6	1.45×10^7
Kern County	7.9×10^6	7.6×10^6	1.80×10^7
Puget Sound	9.1×10^6	8.7×10^6	1.71×10^7
San Fernando	1.72×10^7	1.63×10^7	3.15×10^7
Western Washington	1.43×10^7	1.44×10^7	3.20×10^7

Table 3.2.2. Initial Design: Optimal Fixed Damper Values

• **optimal controls.** For Algorithm 3.2.1, we used as initial controls μ_0 , the constant controls computed above. In contrast with our initialization computations using Algorithm 3.2.1', the computation of optimal controls using Algorithm 3.2.1 required as many as 25 iterations to reach the termination test. Also, as expected, each iteration of Algorithm 3.2.1 took somewhat longer than each iteration of Algorithm 3.2.1'. Our results indicate that in general, when the earthquake ground motions are small, the optimally modulated damping coefficients remain close to the initial fixed values, but when the ground motion becomes more severe, the optimally modulated damping coefficients can deviate significantly from the initial fixed values. We see that for each earthquake, the optimally controlled structure easily meets the interstory drift specifications in Table 3.1.1. A summary of the results of each of the computations will be given in Section 5 along with a detailed discussion of these results. In the interest of keeping the size of this report reasonable, we have included a full set of plots for only the computations which use the El Centro ground motion record. The plots are given in Figures 3.2.1-3.2.6, where Fig. 3.2.1 shows the interstory drifts, Fig. 3.2.2 shows the floor accelerations, Fig. 3.2.3 shows the modulated damping coefficients, Fig. 3.2.4 shows the energy dissipation in the variable dampers, Fig. 3.2.5 shows the shear force on the frame of the structure, and Fig. 3.2.6 shows the force on the variable dampers.

3.3. Lower Performance Bounds: Minimax-Optimal Fixed Structure

To justify the additional cost, a controlled variable structure must perform better than any well designed, comparable fixed structure. We propose to obtain minimax-optimal fixed values for the damping coefficients with respect to the Kern County, Puget Sound, San Fernando, and Western Washington earthquakes. The El Centro earthquake will not be included in our minimax design, so that we can later compare the responses of the optimally controlled structure and minimax-optimal designed fixed structure on an earthquake that was not included in the design of the fixed structure.

formulation of the minimax-optimal design problem. Again the continuous system dynamics must be discretized by the integration formula, as described in Section 3.2. For $j = 1, 2, 3, 4$, let $\bar{f}^j(v)$ be defined as in (3.2.13c), with the superscript j

3.3. Lower Performance Bounds: Minimax-Optimal Fixed Structure

denoting the particular earthquake exciting the dynamic equations (3.2.6a), as follows: $j = 1$ corresponds to Kern County, $j = 2$ corresponds to Puget Sound, $j = 3$ corresponds to San Fernando, and $j = 4$ corresponds to Western Washington. Then we propose to obtain fixed values for the dampers by solving the problem

$$\mathbf{P}_N^{mm} \quad \min_{v \in \mathbf{V}} \max_{j \in \mathbf{m}} \{ \bar{f}^j(v) \}, \quad (3.3.1)$$

where $\mathbf{m} = \{ 1, 2, 3, 4 \}$. Let

$$\psi(v) \triangleq \max_{j \in \mathbf{m}} \bar{f}^j(v). \quad (3.3.2)$$

The problem \mathbf{P}_N^{mm} can be solved by means of the following constrained minimax algorithm, which is a direct extension of Algorithm 3.2.1' (see [Bak.1, Pol.1, Pol.2]).

Constrained Minimax Algorithm 3.3.1.

Parameters. $w = (w_{1,P}, w_{2,P}, w_{3,P}, w_{1,K}, w_{2,K}, w_{3,K})$, $\alpha, \beta \in (0, 1)$, $\gamma > 0$, $n_i =$ number of iterations.

Data. $v \in \mathbf{V}$.

Step 0. Set $i = 0$.

Step 1. Compute the search direction h_i and value of the optimality function Θ_i :

$$h_i \triangleq \arg \min_{h \in \mathbf{V} - v_i} \max_{j \in \mathbf{m}} \{ \bar{f}_f^j(v_i) - \psi(v_i) + \langle \nabla \bar{f}^j(v_i), h \rangle + \frac{\gamma}{2} \|h\|^2 \}, \quad (3.3.3a)$$

$$\Theta_i \triangleq \min_{h \in \mathbf{V} - v_i} \max_{j \in \mathbf{m}} \{ \bar{f}^j(v_i) - \psi(v_i) + \langle \nabla \bar{f}^j(v_i), h \rangle + \frac{\gamma}{2} \|h\|^2 \}. \quad (3.3.3b)$$

Step 2. Compute the step size:

$$\lambda_i = \max_{k \in \mathbf{N}} \{ \beta^k \mid \psi(v_i + \beta^k h_i) - \psi(v_i) \leq \alpha \beta^k \Theta(v_i), v_i + \beta^k h_i \in \mathbf{V} \}. \quad (3.3.3c)$$

Step 3. Set $v_{i+1} = v_i + \lambda_i h_i$, replace i by $i+1$, and if $i \leq n_i$, go to Step 1. \square

An alternative stopping criterion for this algorithm is to stop iterating when $|\Theta_i| \leq \epsilon$, where $\epsilon > 0$ is small. This indicates that the current vector of damping coefficients, v_i , is close to a local minimizer of the max function $\psi(\cdot)$.

minimax-optimal design of fixed-structure. We set $\alpha = 0.9$, $\beta = 0.75$, and, as in the previous experiments, $\gamma = 1 \times 10^{-10}$. The initial damping coefficient vector was chosen to be $v_0 = (5 \times 10^6, 5 \times 10^6, 5 \times 10^6)$, Ns/m . Algorithm 3.3.1 required only 7 iterations to compute a v_i such that the stopping criterion $|\Theta(v_i)| \leq 0.01\psi(v_0)$ was satisfied. The resulting damping coefficient values were

$$\hat{v} = (0.90 \times 10^7, 0.87 \times 10^7, 1.70 \times 10^7) Nsec/m,$$

which happen to be nearly identical to the fixed optimal values computed for the Puget Sound earthquake, in the initialization stage of the optimal control computations of

3.3. Lower Performance Bounds: Minimax-Optimal Fixed Structure

Section 3.2. The response of the minimax designed structure was computed for each of the five earthquakes and a detailed evaluation will be carried out in Section 5. A full set of plots are included for the response of the minimax designed structure to the El Centro quake. Figure 3.3.1 shows the interstory drifts, Fig. 3.3.2 shows the floor accelerations, Fig. 3.3.3 shows the energy dissipation in the optimally chosen dampers, Fig. 3.3.4 shows the frame shear forces, and Fig. 3.3.5 shows the force on the dampers.

4. Moving Horizon Feedback Control Laws

We will now describe two moving horizon control laws that we evaluated with respect to our performance bounds. The first is a sampled-data relay type law that controls the dampers in on-off fashion, while the second is a continuous modulation type law. Both of these moving horizon control laws must be considered to be *conceptual*, since they requires knowledge of the ground motion one horizon ahead of the present time, which may not be available in a real time control system.

sampled-data moving horizon feedback control law Our sampled-data moving horizon control law is based on a sampling period T . At time $t = kT$, $k \in \mathbb{N}$ (i.e., at the beginning of the k -th sampling interval), the control law chooses an element $c_k \in \mathbf{C}$ that determines, via (2.3.1a-d) the action of the dampers over the k -th sampling interval, so as to minimize the cost function

$$E((k+1)T ; z(kT), kT, \mu_c, e). \quad (4.1)$$

For $i = 1, 2, \dots, 8$, let γ_i denote the elements of \mathbf{C} . Then our sampled-data moving horizon control law may be formally presented as follows:

Moving Horizon Control Law 4.1.

Parameters. $w = (w_{1,P}, w_{2,P}, w_{3,P}, w_{1,K}, w_{2,K}, w_{3,K})$.

Data. $c_0 \in \mathbf{C}$.

Step 0. Set $k = 0$.

Step 1. At $t = kT$, compute $E((k+1)T ; z(kT), kT, \mu_{\hat{c}_i}, e)$, $i = 1, 2, \dots, 8$, where

$$\hat{c}_i(t) = \gamma_i \text{ for } t \in [kT, (k+1)T) \text{ and } \hat{c}_i(t) = c(t) \text{ for } t \in [0, kT).$$

Step 2. Set $c_k = \arg \min_{\gamma_i \in \mathbf{C}} E((k+1)T ; z(kT), kT, \mu_{\hat{c}_i}, e)$, and for $t \in [kT, (k+1)T)$, set $c(t) = c_k$.

Step 3. Replace k by $k + 1$ and go to Step 1. □

With the sampling time set at $T = 0.2$ sec., the weight $w = (3, 2.5, 4, 1, 1)$, as selected in Section 3.1, the dynamics determined by (2.1.1a), and the damper modulation

4. Moving Horizon Feedback Control Laws

law by (2.3.1a-d), we simulated the response of the structure, controlled by Moving Horizon Control Law 4.1, with $c_0 = (0, 0, 0)$, subject to the ground motions specified by the first five seconds of our five earthquake records, scaled as specified Section 3.1. Our results indicate that the the response of the controlled structure to the Puget Sound, San Fernando, and Western Washington earthquakes meets the interstory drift constraints given in Table 3.1.1, the response to the El Centro earthquake slightly violates the constraints, and the response to the Kern County earthquake significantly violates the constraints. In Section 5, the performance of the control law for each of the five earthquakes is summarized and evaluated. For the structure subjected to the the El Centro earthquake, a full sets of plots is included in Figures 4.1 - 4.6, where Fig. 4.1 shows the interstory drifts, Fig. 4.2 shows the floor accelerations, Fig. 4.3 shows the variable damping coefficients generated by Control Law 4.1, Fig. 4.4 shows the energy dissipated by the variable dampers, Fig. 4.5 shows the frame shear forces, and Fig. 4.6 shows the forces on the variable dampers.

continuous time moving horizon feedback control law Our continuous time moving horizon control law is based on a horizon of T seconds. At time $t = kT$, $k \in \mathbb{N}$, the control law uses the Optimal Control Algorithm 3.2.1 to determine an optimal control $\hat{\mu}_k(t)$, which is then used over the time interval $[kT, (k+1)T)$.

Moving Horizon Control Law 4.2.

Parameters. $w = (w_{1,P}, w_{2,P}, w_{3,P}, w_{1,K}, w_{2,K}, w_{3,K})$.

Step 0. Set $k = 0$.

Step 1. At time $t = kT$, set up data for Algorithm 3.2.1: $z_0 = z(kT)$, $T_o = kT$, $T_f = (k+1)T$, and u_0 .

Step 2. Use Algorithm 3.2.1 to compute an optimal modulation function $\hat{\mu}_k(t)$, with $t \in [kT, (k+1)T)$.

Step 3. Apply the modulation function $\hat{\mu}_k(t)$, for $t \in [kT, (k+1)T)$.

Step 4. Replace k by $k + 1$ and go to Step 1. □

Note that the above Control Law does not require a specific rule for selecting u_0 in Step 1 above. For our experiments, we set $u_0(t) \equiv 0$ for $k = 0$, and $u_0(t) \equiv \hat{u}_{k-1}(kT)$, for $k > 0$.

For our numerical simulations, we once again used the weight $w = (3, 2.5, 4, 1, 1)$, the dynamics determined by (2.1.1a), and the ground motion given by each of our five scaled ground motion records. We set the horizon length T equal to 0.2 seconds. Our results indicate that the response of the controlled structure to each of the earthquakes easily satisfies the interstory drift constraints given in Table 3.1.1. A complete evaluation of the performance of Control Law 4.2 is given in Section 5. For the El Centro earthquake, we have included a full set of plots in Figures 4.7 - 4.12, where Fig. 4.7

4. Moving Horizon Feedback Control Laws

shows the interstory drifts, Fig. 4.8 shows the floor accelerations, Fig. 4.9 shows the variable damping coefficients generated by Control Law 4.2, Fig. 4.10 shows the energy dissipated by the variable dampers, Fig. 4.11 shows the frame shear forces, and Fig. 4.12 shows the forces on the variable dampers.

5. Evaluation of Numerical Results

We will now discuss the results of our numerical experiments. Because of the need to perform a very large number of numerical experiments, to reduce the total computation time, we performed experiments using only the first 5 seconds of each earthquake. In addition, to establish the validity of our conclusions based on these “short time” experiments, we performed one set of experiments using the ground motion supplied by the first 20 seconds of the El Centro earthquake. In this section, we will refer to the optimal designs of a fixed structure, obtained in Section 3.2, using Algorithm 3.2.1’, as initializations for the optimal control computations, as *optimal fixed designs*. To gain more insight into our evaluation of the controlled and minimax designed structures, we have computed the response of the optimal fixed designed structures subject to the respective earthquakes. The results are summarized and evaluated in this section. In addition, in Figures 5.1 - 5.5, we have included a set of plots of the response of the optimal fixed design for the El Centro earthquake. Specifically, Fig. 5.1 shows the interstory drifts, Fig. 5.2 shows the floor accelerations, Fig. 5.3 shows the total energy dissipation in the optimally chosen dampers, Fig. 5.4 shows the frame shear force, and Fig. 5.5 shows the force on the dampers.

In the tables below, EC denotes the El Centro 1940 (S00E) earthquake, KC denotes the Kern County (Taft) 1952 (comp S69E) earthquake, PS denotes the Puget Sound 1965 (comp S86W) earthquake, SF denotes the San Fernando (Pacoima) 1971 (comp S74W) earthquake, and WW denotes the Western Washington 1949 (comp N86E) earthquake.

optimal control versus minlmax design. We will compare the simulation results obtained using optimal control of the variable structure with those obtained using the fixed, minimax designed structure, so as to evaluate the available performance gap.

● **optimal cost gap.** We begin with the gap between the upper performance bounds resulting from using optimal control with perfect information about the earthquakes, and a lower acceptance bound based on our minimax design of fixed damping coefficient values.

First, we will examine the primary gap G_p , for each of our five earthquakes, in terms of the integral of our weighted energy function E , defined in (3.1.3e). We define the gap by the fractional relationship

5. Evaluation of Numerical Results

$$G_p \triangleq \frac{\bar{f}(\hat{v}_{MM}) - f(\hat{u})}{f(\hat{u})}, \quad (5.1)$$

where $f(\hat{u})$, defined in (3.2.4), is the cumulative weighted energy cost resulting from the use of an optimal control, for a particular earthquake, and $\bar{f}(\hat{v}_{MM})$, defined in (3.2.10c), is the cumulative weighted energy cost, for a particular earthquake, associated with the minimax designed structure.

Referring to Table 5.1, we see that the biggest gap, of 61%, occurs for the El Centro earthquake, for the remaining earthquakes, the gap varies from 27%, for the Kern County earthquake, to 41% for the San Fernando earthquake.

	Optimal Control	Minimax Design	Fixed Design	Moving Horizon	S-D Moving Horizon
Quake	$f(\hat{u})$	$\bar{f}(\hat{v}_{MM})$	$\bar{f}(\hat{v}_{FD})$	$f(\hat{u}_{MH})$	$f(\hat{u}_{SD})$
EC	2.77	4.46	4.41	3.26	4.93
KC	1.65	2.10	2.09	1.83	4.92
PS	1.93	2.51	2.51	2.65	3.56
SF	1.58	2.22	2.07	2.11	2.89
WW	1.21	1.57	1.49	1.27	2.08

Table 5.1. Comparison of Optimal Cost Function Values ($Nms \times 10^4$)

Next we will examine how the primary gaps translate themselves into gaps between the important response parameters, viz., peak and average accelerations of the floors, peak interstory drifts, total energy dissipation in the variable dampers, peak forces on the variable dampers, and peak shear forces on the main structure.

- peak interstory drifts.** We see from Table 5.2, that the peak interstory drifts reflect our choice of weights on the potential energy terms in the energy function, i.e., the drifts are highest on the second floor, where the weight on the potential energy was the smallest. For the El Centro earthquake, the peak interstory drift of the minimax design is 64% larger than that of the optimally controlled structure, and so we see that the use of optimal control produces a considerable reduction in maximum interstory drift over the minimax design for this particular earthquake. However, for the other earthquakes, the superiority of the optimal control law was not clear.

5. Evaluation of Numerical Results

	Optimal Control			Minimax Design			Optimal Design		
Quake	x_d^1	x_d^2	x_d^3	x_d^1	x_d^2	x_d^3	x_d^1	x_d^2	x_d^3
EC	0.80	1.45	1.10	1.30	1.90	1.75	1.20	1.90	1.60
KC	0.65	1.45	1.00	0.75	1.25	1.10	0.90	1.30	1.00
PS	0.75	1.18	0.70	0.65	0.95	1.00	0.60	1.00	1.00
SF	0.62	1.12	1.08	0.85	1.30	1.15	0.75	1.15	1.15
WW	0.75	1.30	0.80	0.65	1.05	0.90	0.60	0.85	0.80

Table 5.2. Comparison of Peak Interstory Drifts (*cm*)

• **peak accelerations.** Referring to Table 5.3, we see that for the El Centro earthquake, the minimax designed structure exhibits 30 - 70% larger accelerations than the one controlled by optimal control, with the biggest difference occurring on the top floor. However, for the remaining earthquakes, the superiority of the optimally controlled structure is again not clear.

	Optimal Control			Minimax Design			Optimal Design		
Quake	\ddot{x}_{peak}^1	\ddot{x}_{peak}^2	\ddot{x}_{peak}^3	\ddot{x}_{peak}^1	\ddot{x}_{peak}^2	\ddot{x}_{peak}^3	\ddot{x}_{peak}^1	\ddot{x}_{peak}^2	\ddot{x}_{peak}^3
EC	290	260	280	500	410	360	460	375	340
KC	320	275	290	350	280	280	340	275	280
PS	260	220	330	235	255	320	230	250	325
SF	310	300	360	315	280	210	350	310	225
WW	280	260	290	265	220	225	310	260	240

Table 5.3. Comparison of Peak Accelerations (*cm/sec²*)

• **average accelerations.** Referring to Table 5.4, we see that the optimally controlled structure sustained 10-20% higher average accelerations on the ground floor than the minimax design, but the minimax design sustained up to 65% higher average accelerations on the top two floors than the optimally controlled structure, with the largest difference occurring for the El Centro earthquake.

5. Evaluation of Numerical Results

Quake	Optimal Control			Minimax Design			Optimal Design		
	\ddot{x}_{avg}^1	\ddot{x}_{avg}^2	\ddot{x}_{avg}^3	\ddot{x}_{avg}^1	\ddot{x}_{avg}^2	\ddot{x}_{avg}^3	\ddot{x}_{avg}^1	\ddot{x}_{avg}^2	\ddot{x}_{avg}^3
EC	59.6	57.5	79.8	98.5	80.2	72.8	91.6	75.4	72.1
KC	38.0	36.5	50.3	50.4	43.4	44.1	45.1	42.6	44.2
PS	43.8	50.5	77.9	64.0	58.6	70.6	64.0	58.6	70.7
SF	46.1	47.2	59.8	54.4	47.6	49.9	62.7	52.2	50.5
WW	35.8	35.3	45.3	35.8	34.2	41.3	41.8	39.3	43.7

Table 5.4. Comparison of Average Accelerations (cm/sec^2)

• **variable damper energy dissipation.** In Table 5.5, we denote the total energy dissipated in the variable damper connected to the i th floor of the structure, up to time $T_f = 5$ seconds, by E_T^i . Referring to Table 5.5, we see that a significant advantage of using optimal control, over a minimax design, is that it results in considerably lower energy dissipation in the dampers. We see that the dampers of the minimax design must dissipate up to 2.5 times more energy than the dampers of the optimally controlled structure.

Quake	Optimal Control			Minimax Design			Optimal Design		
	E_T^1	E_T^2	E_T^3	E_T^1	E_T^2	E_T^3	E_T^1	E_T^2	E_T^3
EC	1.20	3.75	3.10	2.60	6.20	4.60	2.60	6.44	4.53
KC	0.70	2.10	1.20	1.00	2.40	1.80	1.06	2.51	1.62
PS	0.61	1.50	1.40	0.90	2.1	1.70	0.93	2.10	1.66
SF	0.41	1.52	0.81	1.00	2.35	1.80	0.73	1.72	1.24
WW	0.33	0.87	0.50	0.46	1.12	0.92	0.42	0.96	0.67

Table 5.5. Comparison of Total Energy Dissipation in Dampers ($Nm \times 10^4$)

• **main structure shear force.** In Table 5.6, we denote the peak shear force at the i -th floor of the main structure by F_s^i . We see from Table 5.6 that for the El Centro and San Fernando earthquakes, the minimax structure exhibits 4% - 65% higher structural shear forces than the optimally controlled structure, but for the other earthquakes, the advantage of the use of optimal control over a minimax design is not as clear.

5. Evaluation of Numerical Results

	Optimal Control			Minimax Design			Optimal Design		
Quake	F_S^1	F_S^2	F_S^3	F_S^1	F_S^2	F_S^3	F_S^1	F_S^2	F_S^3
EC	1.7	2.8	2.6	2.6	3.8	4.3	2.5	3.7	4.0
KC	1.4	2.4	2.9	1.7	2.5	2.6	1.8	2.6	2.4
PS	1.5	2.3	1.7	1.2	1.9	2.5	1.2	1.9	2.5
SF	1.2	2.2	2.7	1.7	2.6	2.8	1.5	2.3	2.9
WW	1.4	2.5	2.0	1.3	2.0	2.2	1.2	1.7	2.0

Table 5.6. Comparison of Peak Shear Force ($N \times 10^5$)

• **peak damper force.** The peak force on the damper connecting the i -th level of the main and auxiliary structures is denoted in Table 5.7 as F_μ^i . Referring to Table 5.7, we see that for the El Centro earthquake, the peak force on the variable dampers is 25%-50% larger for the minimax design than for the optimally controlled structure, but for the remaining earthquakes, the controlled structure exhibits up to 30% higher forces on the dampers than the minimax design.

	Optimal Control			Minimax Design			Optimal Design		
Quake	F_μ^1	F_μ^2	F_μ^3	F_μ^1	F_μ^2	F_μ^3	F_μ^1	F_μ^2	F_μ^3
EC	5.3	8.5	9.6	7.5	11.5	14.0	6.9	10.4	12.8
KC	5.2	9.0	10.0	5.7	8.3	10.0	5.4	8.0	9.8
PS	4.6	6.7	7.4	3.6	5.2	6.8	3.6	5.2	6.8
SF	5.1	9.1	10.0	4.9	7.7	9.6	5.7	8.8	10.5
WW	5.2	7.9	7.7	4.3	6.3	7.5	5.1	7.5	8.8

Table 5.7. Comparison of Peak Damping Force ($N \times 10^5$)

• **conclusions.** As expected, on all earthquakes, the optimally controlled structure results in smaller cost function values than the minimax design, with the gap being largest for the El Centro earthquake. Our results also show that, with the exception of the El Centro earthquake, the primary performance gap G_p does not clearly translate into a corresponding gap in structural response performance. Overall, the performance gap between the realistic, minimax designed structure and the conceptual, optimally controlled structure is fairly small, and thus it may be quite difficult to obtain a feedback control law that does significantly better than the minimax design.

5. Evaluation of Numerical Results

evaluation of minimax design. Our minimax design was based on a very small number of earthquakes. We will now examine how well the minimax design performs relative to the unattainable design of a fixed structure specifically reconfigured for each of the earthquakes used in the minimax design, as well as relative to a fixed optimal design for the El Centro earthquake, which was not used in the minimax design.

- **optimal cost gap.** First, we will consider the gap in the optimal cost function values between the minimax design and the optimal fixed design. Referring to Table 5.1, we see that the optimal cost function values for the minimax design are no more than 7% larger than those for the optimal fixed design. The minimax cost function value and damping coefficient values are nearly identical with those obtained for fixed optimal design for the Puget Sound earthquake. Note that for the El Centro earthquake, although the minimax design used no knowledge of the El Centro ground motions, the optimal cost function value for the minimax design structure is within 2% of that of the optimal fixed design, which used full ground motion knowledge.

- **peak Interstory drifts.** Referring to Table 5.2, we see that for the San Fernando and Western Washington earthquakes, the minimax design exhibits up to 25% larger peak interstory drifts than the optimal fixed designs. For the El Centro earthquake, the minimax design exhibits no more than 10% larger interstory drifts. For the Kern County and Puget Sound Earthquakes, neither of the designs has a clear advantage.

- **peak accelerations.** Referring to Table 5.3, we see that for the El Centro earthquake, the minimax design sustained no more than 10% larger peak accelerations than the optimal fixed design. For the Kern County and Puget Sound quakes, the peak accelerations in the two designs are nearly equal, while for the San Fernando and Western Washington quakes, the optimal fixed designs sustain up to 20% more peak accelerations.

- **average accelerations.** Referring to Table 5.4, we see that for the El Centro and Kern County earthquakes, the minimax design sustained no more than 8% more average accelerations than the optimal fixed designs; for the Puget Sound earthquake, the average accelerations are nearly identical for the two designs; and for the San Fernando and Western Washington earthquakes, the optimal fixed designs exhibit up to 15% more average accelerations than the minimax design.

- **variable damper energy dissipation.** Referring to Table 5.5, we see that for the El Centro, Kern County, and Puget Sound earthquakes, neither the minimax nor fixed optimal designs have a clear advantage, while for the San Fernando and Western Washington earthquakes, the minimax design requires up to 45% more energy to be dissipated in the dampers than for the optimal fixed designs.

- **main structure shear force.** Referring to Table 5.6, we see that for the El Centro and Western Washington earthquakes, the minimax design sustained up to 18% more shear force than the optimal fixed designs, while for the remaining earthquakes, neither of the designs exhibits a clear advantage.

5. Evaluation of Numerical Results

- **peak damper force.** Finally, referring to Table 5.7, we see that for the El Centro and Kern County earthquakes, the minimax design requires no more than 11% larger damper forces than the optimal fixed designs. For the Puget Sound earthquake, the peak damper forces are equal for both designs; and for the San Fernando and Western Washington earthquakes, the optimal fixed designs require up to 20% larger forces to be applied by the variable dampers than for the minimax design.
- **conclusions.** The above results show that the minimax design is surprisingly nonconservative, and that a minimax design carried out using a small number of earthquakes results in excellent performance on earthquakes not used in the design.

evaluation of the feedback control laws. Next, we turn to an evaluation of the performance of our moving horizon feedback laws presented in Section 4, so as to determine how well they perform relative to one another and to the performance bounds provided by the minimax designed structure and the optimally controlled structure.

- **cost gap.** For each of our simulations of the controlled structure, we computed cost function values using the same cost function $f(u)$ (3.2.7) that was used in the optimal control experiments, but with u equal to the control constructed by the moving horizon control laws. Referring to Table 5.1, we see that the the cost function values for the sampled-data moving horizon law simulations range from 1.3 to 2.7 times as large as the corresponding cost function values for the continuous moving horizon law simulations.

With the exception of the Puget Sound earthquake, the cost function values for the moving horizon controlled structure are roughly half way between those of the optimally controlled structure and those of the minimax designed structure. For the Puget Sound earthquake, the cost function value for the moving horizon controlled structure is 6% larger than that of the minimax design.

- **peak interstory drifts.** Referring to Table 5.8, we see that with the exception of x_d^2 , the peak drift between floors 2 and 3, corresponding to the El Centro earthquake, the peak interstory drifts of the structure with the sampled-data moving horizon control law are up to 2.6 times larger than those of the structure with the continuous moving horizon control law.

Comparing the interstory drifts of the structure with the continuous moving horizon control law, in Table 5.8, with the interstory drifts of the minimax design, shown in Table 5.2, we see that for the El Centro and San Fernando earthquakes, the minimax design exhibits up to 67% larger interstory drifts than the structure with the continuous moving horizon control law. For the remaining earthquakes, the structure with the continuous moving horizon control law exhibits no more than 51% larger interstory drifts than the minimax design. The use of optimal control almost invariably results in up to 40% smaller interstory drifts than the use of the continuous moving horizon control law.

5. Evaluation of Numerical Results

Quake	S-D Moving Horizon			Moving Horizon		
	x_d^1	x_d^2	x_d^3	x_d^1	x_d^2	x_d^3
EC	1.34	1.46	2.00	0.78	1.59	1.31
KC	1.74	2.86	3.17	0.89	1.50	1.18
PS	1.56	1.89	1.49	0.77	1.47	1.20
SF	0.76	1.65	1.72	0.71	1.27	0.97
WW	1.93	2.27	1.19	0.75	1.58	0.87

Table 5.8. Peak Interstory Drifts (*cm*)

● **peak accelerations.** Referring to Table 5.9, we see that except for the ground floors of the structures in the Kern County and Western Washington simulations, the peak accelerations sustained by the structure controlled by the moving horizon sampled-data control law are up to 75% larger than the corresponding accelerations sustained by the structure controlled by the continuous moving horizon control law.

Referring to Tables 5.2 and 5.9, we see that for the El Centro earthquake, the minimax designed structure sustained 10%-42% larger peak accelerations than the continuous moving horizon controlled structure. For the Kern County and Puget Sound earthquakes, neither the minimax designed structure nor the continuous moving horizon controlled structure exhibits a clear advantage. For the San Fernando and Western Washington earthquakes, the continuous moving horizon controlled structure sustained up to 88% higher peak accelerations than the minimax designed structure.

With the exception of the Western Washington earthquake, the continuous moving horizon control law resulted in no more than 20% higher peak accelerations on all floors, than the optimal control law. But for the Western Washington earthquake the peak acceleration, resulting from the use of the continuous moving horizon control law, on the ground floor was higher than with the optimal control law, while the accelerations on the upper two floors were lower than with the optimal control law.

● **average accelerations.** Referring to Table 5.10, we see that the sampled-data moving horizon controlled structure sustained up to 70% larger average accelerations than the continuous moving horizon controlled structure, for all earthquakes considered, except Western Washington, where neither control law shows a clear advantage.

Comparing the structure with the continuous moving horizon control law and the minimax designed structure, see Table 5.4, we see that for all earthquakes other than the San Fernando earthquake, the continuous moving horizon controlled structure sustained lower average accelerations than the minimax designed structure on the top two floors, but higher average accelerations on the ground floor. The minimax design sustained up

5. Evaluation of Numerical Results

Quake	S-D Moving Horizon			Moving Horizon		
	\ddot{x}_{peak}^1	\ddot{x}_{peak}^2	\ddot{x}_{peak}^3	\ddot{x}_{peak}^1	\ddot{x}_{peak}^2	\ddot{x}_{peak}^3
EC	579	385	392	351	279	329
KC	460	395	272	390	317	321
PS	452	363	364	258	221	329
SF	417	342	453	369	341	359
WW	283	230	229	276	226	423

Table 5.9. Peak Accelerations (cm/sec^2)

to 40% larger accelerations on the top two floors, while the controlled structure sustained no more than 20% larger accelerations on the ground floor.

Except for Western Washington, the continuous moving horizon controlled structure sustained up to 26% larger accelerations on the top two floors, than the optimally controlled structure, while the optimally controlled structure sustained up to 12% higher accelerations on the ground floor. For the Western Washington earthquake, the two control laws produced almost equal average accelerations.

Quake	S-D Moving Horizon			Moving Horizon		
	\ddot{x}_{avg}^1	\ddot{x}_{avg}^2	\ddot{x}_{avg}^3	\ddot{x}_{avg}^1	\ddot{x}_{avg}^2	\ddot{x}_{avg}^3
EC	102.9	91.3	94.3	70.4	64.5	74.8
KC	70.2	55.3	46.0	41.3	36.5	45.0
PS	61.6	65.8	80.2	55.3	53.2	72.2
SF	59.3	54.1	80.8	57.3	50.4	59.4
WW	38.1	33.9	40.5	32.7	34.5	44.7

Table 5.10. Average Accelerations (cm/sec^2)

● **variable damper energy dissipation.** Referring to Table 5.11, we see that the continuous moving horizon controlled structure dissipates up to 3.5 times more energy in each of the variable dampers than the sampled-data moving horizon controlled structure, except in the Western Washington earthquake simulations, where neither control law has a clear advantage.

Referring to Table 5.5, we see that the minimax designed structure dissipates up to 2 times more energy in each of the variable dampers than the continuous moving horizon controlled structure, except for the second floor of the San Fernando simulations, where the continuous moving horizon controlled structure dissipates about 20% more energy

5. Evaluation of Numerical Results

than the minimax design.

The energy dissipation in each of the variable dampers of the moving horizon controlled structure is up to 85% larger than in the optimally controlled structure.

Quake	S-D Moving Horizon			Moving Horizon		
	E_T^1	E_T^2	E_T^3	E_T^1	E_T^2	E_T^3
EC	0.83	1.59	2.25	1.32	4.06	4.23
KC	0.65	1.46	1.62	0.69	2.10	1.68
PS	0.25	0.72	1.15	0.63	2.00	1.34
SF	0.27	0.81	0.84	0.74	2.80	1.39
WW	0.50	0.89	0.76	0.32	1.04	0.57

Table 5.11. Comparison of Total Energy Dissipation in Dampers ($Nm \times 10^4$)

- main structure shear force.** Referring to Table 5.12, we see that except for the second floor in the El Centro simulations, the use of the sample-data moving horizon control law results in up to 2.7 times higher shear forces than the use of the continuous moving horizon control law.

Comparing the peak shear forces in the structure with the continuous moving horizon control law with those in the minimax designed structure, shown in Table 5.6, we see that for the El Centro and San Fernando earthquakes, the minimax designed structure exhibits up to 73% larger shear forces. For the Kern County earthquake, neither structure has a clear advantage; and for the Puget Sound and Western Washington earthquakes, the continuous moving horizon controlled structure exhibits no more than 55% larger shear forces than the minimax design.

The structure with the continuous moving horizon control law exhibited up 75% larger peak shear forces than the optimally controlled structure (see Table 5.6).

- peak damper force.** Finally, referring to Table 5.13, we see that for all but the San Fernando earthquake, the sampled-data moving horizon controlled structure exhibits up to 66% larger forces on the variable dampers than the continuous moving horizon controlled structure. For the San Fernando earthquake, neither control law clearly exhibits an advantage.

Comparing the continuous moving horizon controlled structure with the minimax designed structure, see Table 5.7, we find that for the El Centro earthquake, the dampers in the minimax design apply up to 50% larger forces than the dampers of the continuous moving horizon controlled structure. For the remaining earthquakes, the dampers of the

5. Evaluation of Numerical Results

Quake	S-D Moving Horizon			Moving Horizon		
	F_S^1	F_S^2	F_S^3	F_S^1	F_S^2	F_S^3
EC	2.7	2.9	4.9	1.5	3.1	3.2
KC	3.4	5.6	7.8	1.8	2.9	2.9
PS	3.1	3.7	3.7	1.5	2.9	3.0
SF	1.5	3.2	4.2	1.4	2.5	2.4
WW	3.8	4.5	2.9	1.5	3.1	2.1

Table 5.12. Comparison of Peak Shear Force ($N \times 10^5$)

continuous moving horizon controlled structure apply no more than 50% larger forces than the dampers of the minimax designed structure.

The continuous moving horizon controlled structure exhibited no more than 42% higher peak forces on the variable dampers than the optimally controlled structure.

Quake	S-D Moving Horizon			Moving Horizon		
	F_μ^1	F_μ^2	F_μ^3	F_μ^1	F_μ^2	F_μ^3
EC	9.8	13.7	13.6	5.9	8.9	9.3
KC	9.5	14.9	18.5	7.4	11.5	12.7
PS	7.4	12.2	13.3	4.8	7.8	10.0
SF	7.3	9.7	12.0	6.6	10.7	12.1
WW	7.4	10.4	10.0	5.3	7.9	8.3

Table 5.13. Comparison of Peak Damping Force ($N \times 10^5$)

• **conclusions.** Because of the rather small gap between the the performance gap between the realistic, minimax designed structure and the conceptual, optimally controlled structure, finding a feedback law that is better than the minimax design is quite difficult. Moving horizon laws using estimates of ground motion one short horizon ahead seem to have the best chance of falling into the performance gap. However, even using unrealistic projections of the the ground motion, our simple, sampled-data moving horizon feedback law led to worse results than our minimax design. On the other hand, our continuous moving horizon feedback law, again using unrealistic projections of the the ground motion, resulted in better performance than the minimax design, particularly on the severe, El Centro earthquake.

5. Evaluation of Numerical Results

validation of “short time” experiments. To establish confidence in our experimental results that examined only the first 5 seconds of the response of a structure to a ground motion excitation, we performed one set of experiments using the the first 20 seconds of the El Centro earthquake. The experiments performed were an optimal control computation, a simulation of the response of the minimax designed structure, and a simulation of the response of the structure controlled using the continuous moving horizon control law (4.2). Other than using a final time T_f equal to 20 seconds, the parameters used for the optimal control experiment were the same as those used in Section 3.2, and the parameters for the moving horizon simulation were the same as those used in Section 4. The resulting interstory drifts, floor accelerations, variable damping coefficients are shown in Figures 5.6 - 5.13.

Referring to Table 5.2, Table 5.8, and Table 5.14, we see that the peak interstory drifts in the 20 second experiments are very close to those obtained in the 5 second experiments.

	x_d^1	x_d^2	x_d^3
Optimal Control	0.74	1.33	0.99
Minimax Design	1.31	1.91	1.77
Moving Horizon	0.83	1.61	1.17

Table 5.14. Comparison of Peak Interstory Drifts (*cm*)

Comparing the results in Table 5.15 with with the corresponding results in Table 5.3, we see that the peak accelerations for the 20 second and 5 second optimal control experiments are nearly equal, as are the peak accelerations for the 20 second and 5 second simulations using the minimax designed structure. Referring to Table 5.9 and Table 5.15, we see that the peak accelerations sustained by the continuous moving horizon controlled structure are somewhat larger for the 20 second simulation than for the 5 second simulation, but the difference is not large enough to change any of the conclusions obtained from the 5 second simulation results.

	\ddot{x}_{peak}^1	\ddot{x}_{peak}^2	\ddot{x}_{peak}^3
Optimal Control	283	253	273
Minimax Design	498	417	365
Moving Horizon	375	373	337

Table 5.15. Comparison of Peak Accelerations (*cm/sec*²)

Referring to Table 5.4, Table 5.10, and Table 5.16, we see that the average

5. Evaluation of Numerical Results

accelerations for the 20 second experiments are all smaller than for the 5 second experiments, but the conclusions obtained from the 5 second experiment about the relative size of the average accelerations also hold for the 20 second experiment results.

	\ddot{x}_{avg}^1	\ddot{x}_{avg}^2	\ddot{x}_{avg}^3
Optimal Control	40.4	37.5	47.2
Minimax Design	61.0	50.2	46.3
Moving Horizon	48.5	42.9	45.8

Table 5.16. Comparison of Average Accelerations (cm/sec^2)

We conclude from the above results, that the 5 second variable structure experiments give an adequate indication of the performance of the various designs over a 20 second horizon. Thus, it seems quite likely that the conclusions resulting from the 5 second experiments will be equally valid for longer time horizons.

6. Conclusion

Using the responses to seismic excitation of an optimally controlled variable structure and of a minimax optimally designed fixed structure, we have established an upper bound on the achievable performance and a lower bound on the acceptability of a control system for a variable damping structure. The gap between the upper and lower bounds is rather small, which indicates that to design a control system that results in a variable structure that is clearly superior to a minimax optimal designed fixed structure is a very difficult task indeed. Our experimental results indicate that a controlled variable structure is likely to perform better than a fixed structure in the case of moderate to severe earthquakes. Further reflection leads us to believe that controlled variable structures are likely to perform best at sites, such as landfills and dry lake beds, where resonances can be expected, but the resonance frequency cannot be estimated in advance. The reason for this is that a variable structure will adjust itself for an impedance mismatch (i.e., for anti-resonance), while a fixed structure is not capable of such adaptation.

In addition, we have found that even fairly simple minimax formulations of the design of a fixed structure, based on a small number of ground motions, produce very good results, in the sense that the resulting structure meets specifications on interstory drifts, shear forces, and floor accelerations not only for the earthquakes considered in the design process, but also for other earthquakes scaled to comparable intensity. Sophisticated minimax design techniques (see, e.g., [Pol.1,2]), using direct measures of performance requirements in the form of bounds on instantaneous interstory drifts, shear forces, accelerations, etc., are likely to produce even better results.

6. Conclusion

Finally, we have found that a continuous moving horizon control law, using a horizon of only 0.2 seconds, produces quite acceptable performance in a variable structure. However, the implementation of this control law will require the resolution of two issues. The first is that of speed of computation, and will require finding suitable hardware as well as developing particularly efficient software. The second issue is that of ground motion prediction over an interval of 0.2 seconds. It will be necessary to determine whether such a prediction can be made by using ground motion monitoring sensors located a small distance away from the site.

7. References

- [Abd.1] Abdel-Rohman, M. and Leipholz, H. H. E., "General Approach to Active Structural Control", *J. Eng. Mech. Div. ASCE*, Vol. 105, (1979), pp. 1007-1923.
- [Abd.2] Abdel-Rohman, M. and Liepholz, H. H. E., "Structural Control by Pole Assignment Method," *Journal of Engineering Mechanics*, Vol. 104 (1978), pp. 1157-1175.
- [Bak.1] Baker, T. E., and Polak, E., "On the optimal control of systems described by evolution equations," Memorandum No: UCB/ERL M89/113, Electronics Research Laboratory, University of California (Berkeley, CA, 1989).
- [Cha.1] Chang, J. C. H. and Soong, T. T., "Structural Control Using Active Tuned Mass Drivers", *J. Eng. Mech. Div. ASCE*, Vol. 106, 00 (1980), pp. 1091-1098.
- [Che.1] Cheng, F. Y., Choi, C.-K., Juang, D.-S., "Development of Optimum Design and Control of Seismic Structures," in: Chang, K.P., Liu, S.C., Li, J.C. eds., *Intelligent Structures* (Elsevier Applied Science, New York 1990).
- [Cho.1] Chong, K. P., Liu, S. C., and Li, J. C., editors, *Intelligent Structures*", (Elsevier Applied Science, New York, 1990).
- [Deh.1] Dehghanyar, T. J, Masri, S. F., Miller, R. K, and Caughey, T. K., "On-line parameter control of nonlinear flexible structures," in: Liepholz, H.H.E ed., *Structural Control* (Martinus Nijhoff Publishers, Dordrecht, The Netherlands, 1987).
- [Kel.1] Kelly, J. M., Leitmann, G., and Soldatos, A., "Robust Control of Base-Isolated Structures Under Earthquake Excitation," *Jour. Optim. Theory and Appl.*, Vol. 53, No. 2, (1987). pp. 1834-1938.
- [Mar.1] Martin, C. R. and Soong, T. T., "Modal Control of Multistory Structures," *J. Eng. Mech. Div., ASCE*, Vol. 102, No. EM4, (1976) pp. 613-632.
- [Kob.1] Kobori, T., et al, "Experimental Study of Seismic Response Control with Active Variable Stiffness System", *Jour. of Structural Engin*, Vol. 35B, (1989).
- [Kob.2] Kobori, T. et al, "Seismic-Response-Controlled Structure with Active Mass

7. References

- Driver System. Part 1: Design", *Earthquake Engineering and Structural Dynamics*", Vol. 20, (1991) pp. 133-149.
- [Lei.1] Leipholz, H. H. E. editor, *Structural Control*, (North-Holland, 1980).
- [Mas.1] Masri, S. F., Bekey, G. A. and Caughey, T. K. "Optimum Pulse Control of Flexible Structures", *J. Appl. Mech. ASME*, Vol. 48, (1982) pp. 619-626.
- [Mei.1] Meirovitch, L. and Oz, H., "Active Control of Structures by Modal Synthesis," in: Leipholz, H.H.E ed., *Structural Control* (North Holland, Amsterdam, 1980) pp. 505-521.
- [Pol.1] Polak, E., "Minimax algorithms for structural optimization," *Proc. IUTAM Symposium on Structural Optimization* (Melbourne, Australia, 1988).
- [Pol.2] Polak, E., "Nonsmooth optimization algorithms for the design of controlled flexible structures," Marsden, J. E., Krishnaprasad, P. S., and Simo, J. C., eds., *Contemporary Mathematics* vol. 97 (American Math Soc., Providence RI, 1989) pp. 337-371.
- [Pol.3] Polak, E., and Yang, T. H., "Moving horizon control of linear systems with input saturation, disturbances, and plant uncertainty, Part I: robustness", To appear in *Int. J. Control*.
- [Pol.4] Polak, E., "On the use of consistent approximations in the solution of semi-infinite optimization and optimal control problems", *University of California, Berkeley, Electronics Research Laboratory Memo No. UCB/ERL M92/36*, 13 April 1992
- [Pru.1] Prucz, Z., Soong, T. T., and Reinhorn, A. M., "An Analysis of Pulse Control for Simple Mechanical Systems," *Journal of Dynamic Systems Measurement Control* Vol. 107 (1985) pp. 123-131.
- [Roo.1] Roorda, J., "Tendon Control in Tall Structures", *J Struct. Div. ASCE*, Vol. 101, (1975) pp. 505-521.
- [Soo.1] Soong, T. T., *Active Structural Control: Theory and Practice*, (Wiley, New York, 1990).
- [Soo.2] Soong, T. T., Masri, S. F. and Housner, G. W., "An overview of Active Structural Control under Seismic Loads", *Earthquake Spectra*, Vol. 7, No.3, (1991) pp. 483-505.
- [Sat.1] Sata, T., Toki, K., "Active control of seismic response of structures," Chang, K. P., Liu, S. C., Li, J. C. eds., *Intelligent Structures* (Elsevier Applied Science, New York, 1990).
- [Wan.1] Wang, K. W. and Kim, Y. S., "Semi-Active Vibration Control of Structures via Variable Damping Elements," *Mechanical Systems and Signal Processing*, Vol. 5 No. 5 (1991) pp. 421-430.
- [Wen.1] Wen, Y. K., editor, *Intelligent Structures-2*, (Elsevier Applied Science, New York, 1992).

7. References

- [Yan.2] Yang, J. N., Lin, M. J. and Sae-Ung, S.. "Optimal Open-Loop Control of Tall Buildings Under Earthquake Excitation," Proceedings of the *Third International Conference on Structural Safety and Reliability*, (Norway, 1981).
- [Yan.3] Yang, J. N., Li, Z., Danielians, A., Liu, S. C., "Aseismic Hybrid Control of Nonlinear and Hysteretic Structures I," *Journal of Engineering Mechanics*, Vol.18 No. 7 (July, 1992).
- [Yan.4] Yang, H. T. Y., Liaw, D. G., Hsu, D. S., Fu, H. C., "A simple model for optimal control of high rise buildings," in: Chang, K.P., Liu, S.C., Li, J.C. eds., *Intelligent Structures* (Elsevier Applied Science, New York 1990).
- [Yan.5] Yang, J. N., Akbarpour, A., and Ghaemmaghami, P., "Optimal control algorithms for earthquake-excited building structures" Liepholz, H. H. E. ed., *Structural Control* Martinus Nijhoff Publishers, Dordrecht, The Netherlands 1987.
- [Yao.1] Yao, J. T. P., "Adaptive Systems for Seismic Structures," Proceedings *NSF-UCEER Earthquake Eng. Res. Conf.*, U.C. Berkeley, (1969) pp. 142-150.

Appendix: Discretized Gradient Computation

In this appendix, we will derive in detail the formula for the computation of the gradient of the cost function $f(u)$ (3.2.4) for the discretized optimal control problem described in section 3.2. We begin by considering the more general problem of the computation of the gradient of the cost function for an optimal control problem with dynamics of the form

$$\dot{x}(t) = \bar{h}(x(t), \mu(t)), \quad t \in [0, T_f], \quad x(0) = 0, \quad (\text{A.1})$$

where $\mu \in \mathbf{M}$ with \mathbf{M} defined in (3.2.1a), and $x \in \mathbb{R}^n$. The cost function is assumed to be of the form

$$F(\mu) = g(x^\mu(T_f)), \quad (\text{A.2})$$

where $g(\cdot)$ is continuously differentiable and $x^\mu(\cdot)$ is the solution of (A.1) subject to the control μ . We assume that the function $h(\cdot, \cdot)$ is continuously differentiable and that $h_x(\cdot, \cdot)$ and $h_\mu(\cdot, \cdot)$ are Lipschitz continuous. The problem to be considered is

$$\mathbf{P}_1 \quad \min_{\mu \in \mathbf{M}} F(\mu). \quad (\text{A.3})$$

In order to obtain a numerical solution to \mathbf{P}_1 , this problem must be replaced by a consistent finite dimensional approximation [Pol.4]. To obtain such an approximation, we discretize the time interval and replace the control by the finite parametric representation (3.2.2a,b) as shown in Section 3.2. Once again, the backwards Euler method is used to integrate the system equations:

$$\bar{x}((k+1)\Delta) = \bar{x}(k\Delta) + \Delta \bar{h}(\bar{x}((k+1)\Delta), u((k+1)\Delta)), \quad \bar{x}(0) = 0, \quad (\text{A.4})$$

where we assume that the equations may be solved exactly.

The discretized cost function then becomes

$$F(u) = g(\bar{x}^u(N\Delta)), \quad (\text{A.5})$$

where $\{\bar{x}^u(k\Delta)\}_{k=0}^N$ represents the solution of the difference equation (A.5) subject to the control sequence $u = \{u(k)\}_{k=1}^N$.

To compute the gradient of the cost function, $\nabla F(u)$ we first look at the differential of the solution to the difference equation (A.4) at time $N\Delta$, $D\bar{x}^u(N\Delta; \delta u) = \delta \bar{x}^{\delta u}(N\Delta)$, where for $k = 0, 1, \dots, N$, $\delta \bar{x}^{\delta u}(k\Delta)$ is the solution of the following difference equation:

$$\begin{aligned} \delta \bar{x}((k+1)\Delta) - \delta \bar{x}(k\Delta) &= \Delta \bar{h}_x(\bar{x}^u((k+1)\Delta), u(k+1)) \delta \bar{x}((k+1)\Delta) \\ &+ \Delta \bar{h}_u(\bar{x}^u((k+1)\Delta), u(k+1)) \delta u(k+1), \end{aligned} \quad (\text{A.6a})$$

subject to $\delta \bar{x}(0) = 0$. Rearranging terms, we get

$$\delta \bar{x}((k+1)\Delta) = A_{k+1} \delta \bar{x}(k\Delta) + A_{k+1} B_{k+1} \delta u(k+1), \quad (\text{A.6b})$$

where $A_{k+1} = (I - \Delta \bar{h}_x(\bar{x}^u((k+1)\Delta), u(k+1)))^{-1}$, and $B_{k+1} = \Delta \bar{h}_u(\bar{x}^u((k+1)\Delta), u(k+1))$.

Appendix: Discretized Gradient Computation

Let $\Phi^u(\cdot, \cdot)$ be the state transition matrix for (A.6b), i.e., for any $N \geq k \geq j \geq 0$, $\Phi^u(k\Delta, j\Delta)$ is the solution to the matrix difference equation

$$\Phi((k+1)\Delta, j\Delta) = A_{k+1}\Phi(k\Delta, j\Delta), \quad \Phi(j\Delta, j\Delta) = I. \quad (\text{A.6c})$$

From (A.6b,c), we obtain the following expression for $\delta\bar{x}^{\delta u}(N\Delta)$:

$$\delta\bar{x}^{\delta u}(N\Delta) = \sum_{k=0}^{N-1} \Phi(N\Delta, (k+1)\Delta)A_{k+1}B_{k+1}\delta u(k+1). \quad (\text{A.6d})$$

Next, applying the chain rule to the function $F(u) = g(\bar{x}^u(N\Delta))$, we get

$$DF(u; \delta u) = \langle \nabla_x g(\bar{x}^u(N\Delta)), D\bar{x}^u(N\Delta; \delta u) \rangle. \quad (\text{A.7a})$$

Using the fact that $D\bar{x}^u(N\Delta; \delta u) = \delta\bar{x}^{\delta u}(N\Delta)$, and noting from (A.6c), that $\Phi(N\Delta, (k+1)\Delta)A_{k+1} = \Phi(N\Delta, k\Delta)$, we see that

$$\begin{aligned} DF(u; \delta u) &= \sum_{k=0}^{N-1} \langle B_{k+1}^T \Phi(N\Delta, k\Delta)^T \nabla_x g(\bar{x}^u(N\Delta)), \delta u(k+1) \rangle \\ &= \sum_{k=0}^{N-1} \langle B_{k+1}^T \bar{p}^u(k\Delta), \delta u(k+1) \rangle, \end{aligned} \quad (\text{A.7b})$$

where for $k = 0, 1, \dots, N$,

$$\bar{p}^u(k\Delta) = \Phi(N\Delta, k\Delta)^T \nabla_x g(\bar{x}^u(N\Delta)). \quad (\text{A.7c})$$

The computation of the adjoint $\bar{p}^u(\cdot)$ by computing the state transition matrix $\Phi(\cdot, \cdot)$ and using equation (A.7c) is not particularly efficient, and in fact requires n times more operations than are required by the more efficient scheme described below. From (A.7c) we get

$$\bar{p}^u(k\Delta) - \bar{p}^u((k+1)\Delta) = [\Phi(N\Delta, k\Delta)^T - \Phi(N\Delta, (k+1)\Delta)^T] \nabla_x g(\bar{x}^u(N\Delta)). \quad (\text{A.7d})$$

Using the fact that $\Phi(N\Delta, (k+1)\Delta)A_{k+1} = \Phi(N\Delta, k\Delta)$, we get that

$$\Phi(N\Delta, k\Delta) - \Phi(N\Delta, (k+1)\Delta) = \Phi(N\Delta, k\Delta) \Delta \bar{h}_x(\bar{x}^u((k+1)\Delta), u(k+1)). \quad (\text{A.7e})$$

Combining (A.7d) and (A.7e) results in

$$\begin{aligned} \bar{p}^u(k\Delta) - \bar{p}^u((k+1)\Delta) &= \Delta \bar{h}_x(\bar{x}^u((k+1)\Delta), u(k+1))^T \Phi(N\Delta, k\Delta)^T \nabla_x g(\bar{x}^u(N\Delta)) \\ &= \Delta \bar{h}_x(\bar{x}^u((k+1)\Delta), u(k+1))^T \bar{p}^u(k\Delta), \end{aligned} \quad (\text{A.7f})$$

subject to $\bar{p}^u(N\Delta) = \nabla_x g(\bar{x}^u(N\Delta))$. Thus, we see that the adjoint is computed backwards in time, again using a backwards Euler formula.

The optimal control problem (3.2.1) considered in Section 3.2 has an integral, rather than endpoint cost function, so the above results cannot be directly applied to problem (3.2.1). However, as we will show, it is not difficult to transform an optimal control problem with an integral cost into a problem with an endpoint cost. Consider the system model (2.1.2). For notational convenience, we will denote the system equations by

Appendix: Discretized Gradient Computation

$$\dot{z}(t) = h(z(t), \mu(t)), \quad z(0) = 0, \quad (\text{A.8a})$$

and the cost function by

$$\Phi(\mu) = \int_0^{T_f} e^{z^\mu(t)} dt, \quad (\text{A.8b})$$

where $z^\mu(\cdot)$ is the solution of the differential equation (A.8a) subject to the control $\mu(\cdot)$. The discretized system equations are then given by

$$\bar{z}((k+1)\Delta) = \bar{z}(k\Delta) + \Delta h(\bar{z}((k+1)\Delta), u(k+1)), \quad \bar{z}(0) = 0, \quad (\text{A.9a})$$

and the discretized cost function is given by

$$f(u) = \Delta \sum_{k=1}^N e^{\bar{z}^u(k\Delta)}, \quad (\text{A.9b})$$

where $\{\bar{z}^u(k\Delta)\}_{k=0}^N$ is the solution of the difference equation (A.9a) subject to the control sequence $\{u(k)\}_1^N$.

To convert this to a problem of the form considered in (A.4, A.5), we define for $k = 0, 1, \dots, N$, the augmented state

$$\bar{x}(k\Delta) = (\bar{z}(k\Delta), \bar{f}(k)), \quad (\text{A.10a})$$

where $\bar{z}(k\Delta) \in \mathbb{R}^{12}$ is the system state defined by equation (A.9a), and $\bar{f}(k) \in \mathbb{R}$ is defined by

$$\bar{f}(k) = \Delta \sum_{j=1}^k e^{\bar{z}(j\Delta)}. \quad (\text{A.10b})$$

The augmented system equations are then

$$\begin{bmatrix} \bar{z}((k+1)\Delta) \\ \bar{f}(k+1) \end{bmatrix} = \begin{bmatrix} \bar{z}(k\Delta) \\ \bar{f}(k) \end{bmatrix} + \Delta \begin{bmatrix} h(\bar{z}((k+1)\Delta), u(k+1)) \\ e^{\bar{z}((k+1)\Delta)} \end{bmatrix}, \quad (\text{A.10c})$$

subject to $\bar{x}(0) = 0$, which is in the form (A.4). The cost function $f(u)$ is then given by

$$f(u) = \langle e^{13}, \bar{x}^u(N\Delta) \rangle, \quad (\text{A.10d})$$

where $e^{13} \in \mathbb{R}^{13}$ denotes the 13th column of a 13×13 identity matrix. Thus, we see that the original problem has been converted to the form (A.4, A.5).

To compute the gradient for the discretized optimal control problem (A.9), we will first apply the results derived for the problem (A.4, A.5) to the augmented system (A.10). From (A.7b), we see that

$$Df(u; \delta u) = \Delta \sum_{k=0}^{N-1} \langle \bar{h}_u(\bar{x}^u((k+1)\Delta), u(k+1))^T \bar{p}^u(k\Delta), \delta u(k+1) \rangle. \quad (\text{A.11a})$$

For $k = 0, 1, \dots, N$, let $\bar{p}^u(k\Delta)$ equal the first 12 components of $\bar{p}^u(k\Delta)$, and let $p_e^u(k\Delta)$ be the 13th component of $\bar{p}^u(k\Delta)$. Then, from (A.7f), we get

Appendix: Discretized Gradient Computation

$$\begin{aligned} \begin{bmatrix} \bar{p}^u(k\Delta) \\ p_e^u(k\Delta) \end{bmatrix} &= \begin{bmatrix} \bar{p}^u((k+1)\Delta) \\ p_e^u((k+1)\Delta) \end{bmatrix} \\ &+ \Delta \begin{bmatrix} h_z(\bar{z}^u((k+1)\Delta), u(k+1))^T & \nabla_z e(\bar{z}^u((k+1)\Delta))^T \\ 0 & 0 \end{bmatrix} \begin{bmatrix} \bar{p}^u(k\Delta) \\ p_e^u(k\Delta) \end{bmatrix} \end{aligned} \quad (\text{A.11b})$$

subject to $\bar{p}^u(N\Delta) = \nabla_x f(u) = e^{13}$. From the above equations, we can conclude that for $k = 0, 1, \dots, N$, $p_e^u(k\Delta) = p_e^u(N\Delta) = 1$. Thus, equation (A.11b) becomes

$$\bar{p}^u(k\Delta) = A_p((k+1)\Delta)\bar{p}^u((k+1)\Delta) + \Delta A_p((k+1)\Delta)\nabla_z e(\bar{z}^u((k+1)\Delta))^T, \quad (\text{A.11c})$$

subject to $\bar{p}^u(N\Delta) = 0$, where $A_p((k+1)\Delta) = (I - \Delta h_z(\bar{z}^u((k+1)\Delta), u(k+1)))^{-1}$.

The equation for $Df(u; \delta u)$, may be similarly simplified by substituting the expression for $\bar{h}_u(\bar{z}^u((k+1)\Delta), u(k+1))$ into equation (A.11a), which becomes

$$\begin{aligned} Df(u; \delta u) &= \Delta \sum_{k=0}^{N-1} \left\langle \begin{bmatrix} h_u(\bar{z}^u((k+1)\Delta), u(k+1))^T & 0 \end{bmatrix} \begin{bmatrix} \bar{p}^u(k\Delta) \\ p_e^u(k\Delta) \end{bmatrix}, \delta u(k+1) \right\rangle \\ &= \Delta \sum_{k=0}^{N-1} \langle h_u(\bar{z}^u((k+1)\Delta), u(k+1))^T \bar{p}^u(k\Delta), \delta u(k+1) \rangle. \end{aligned} \quad (\text{A.11d})$$

Referring to the finite dimensional scalar product formula (3.2.6b) and equation (A.11d), we see by inspection that for $k = 1, 2, \dots, N$,

$$\nabla f(u)(k) = h_u(\bar{z}^u(k\Delta), u(k))^T \bar{p}^u((k-1)\Delta). \quad (\text{A.12})$$

Fig. 2.2.1: Floor Accelerations

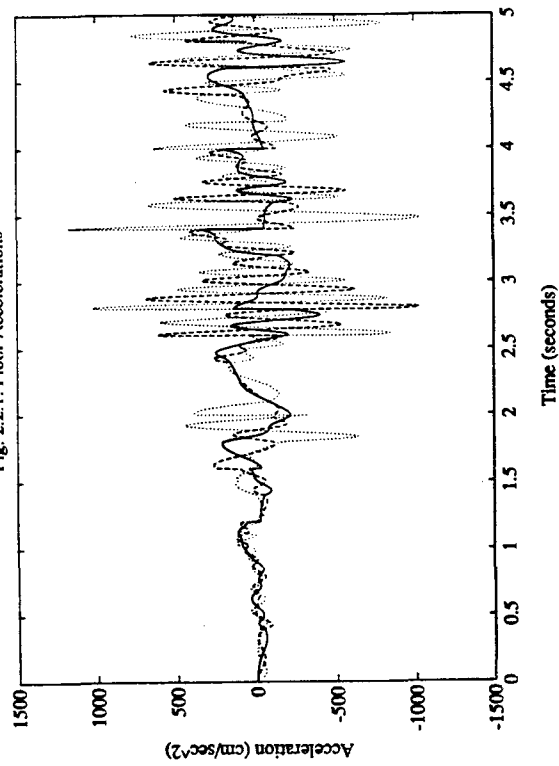


Fig. 2.3.1: Floor Accelerations (alpha = 0.0)

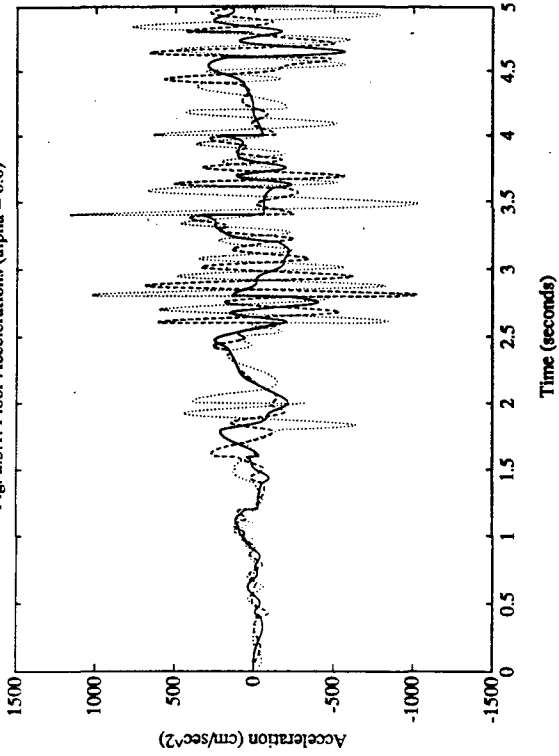


Fig. 2.2.2: Clamp Status vs. Time

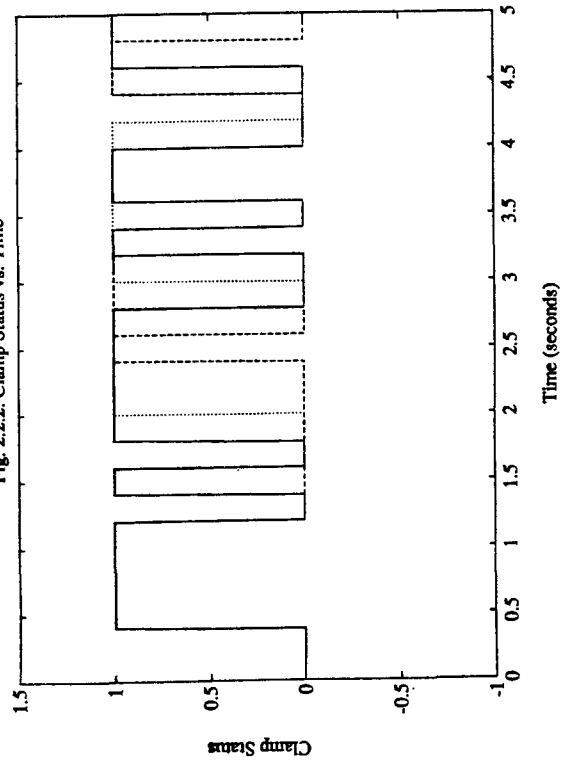
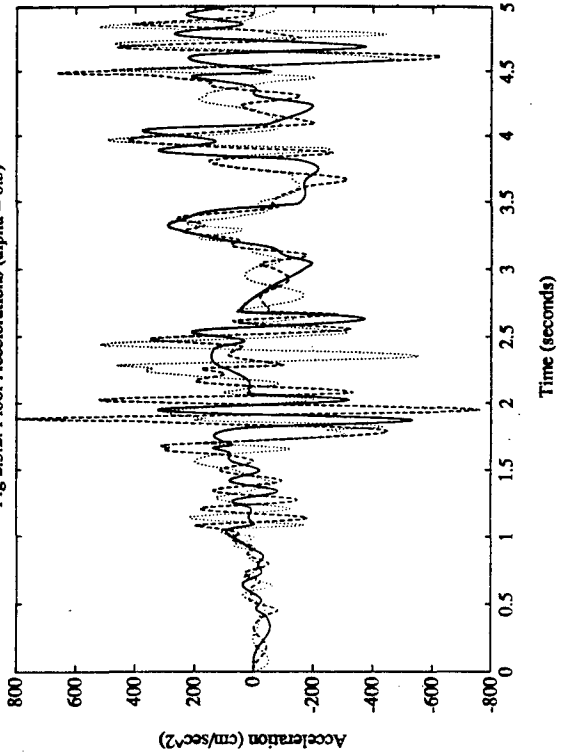


Fig. 2.3.2: Floor Accelerations (alpha = 0.5)



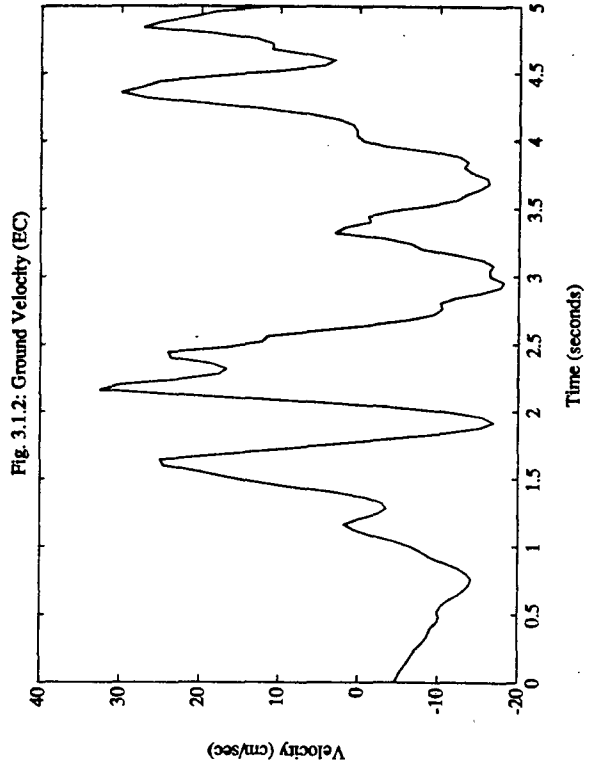
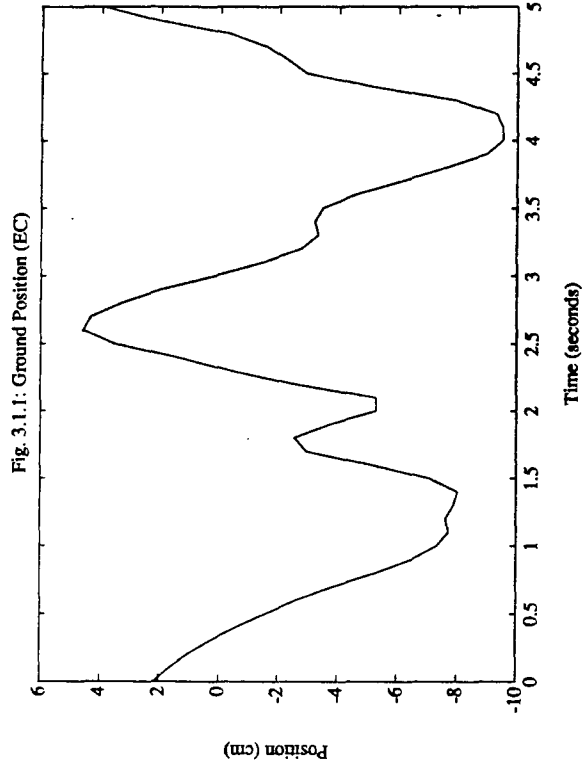
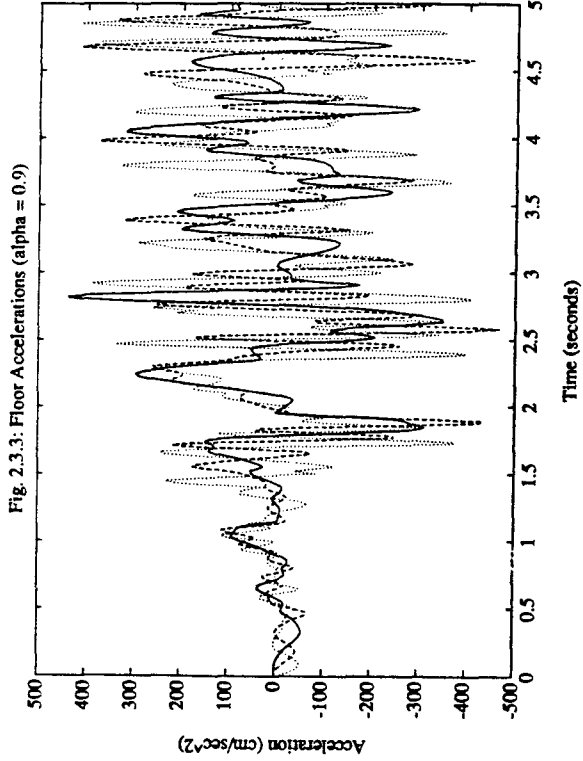


Fig. 3.1.3: Ground Acceleration (EC)

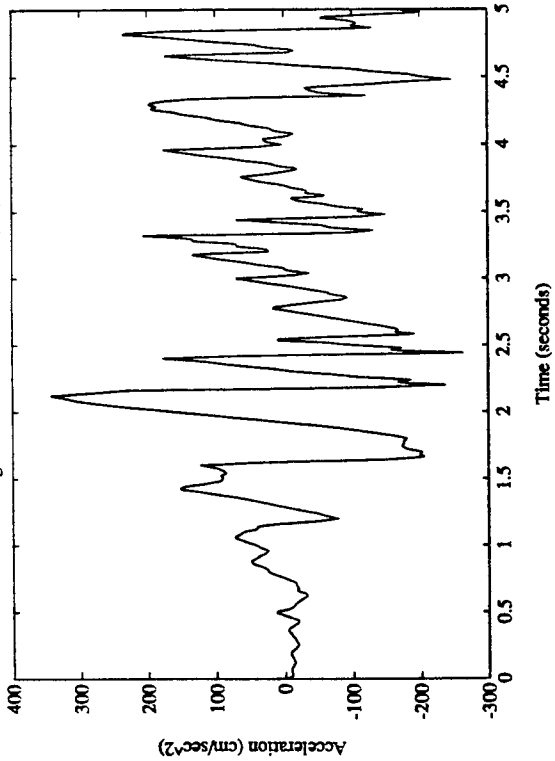


Fig. 3.1.5: Scaled Ground Velocity (KC)

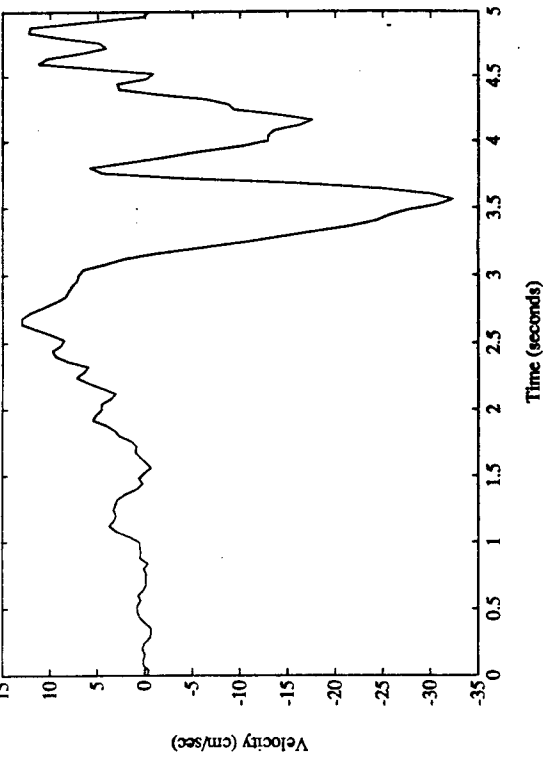


Fig. 3.1.4: Scaled Ground Position (KC)

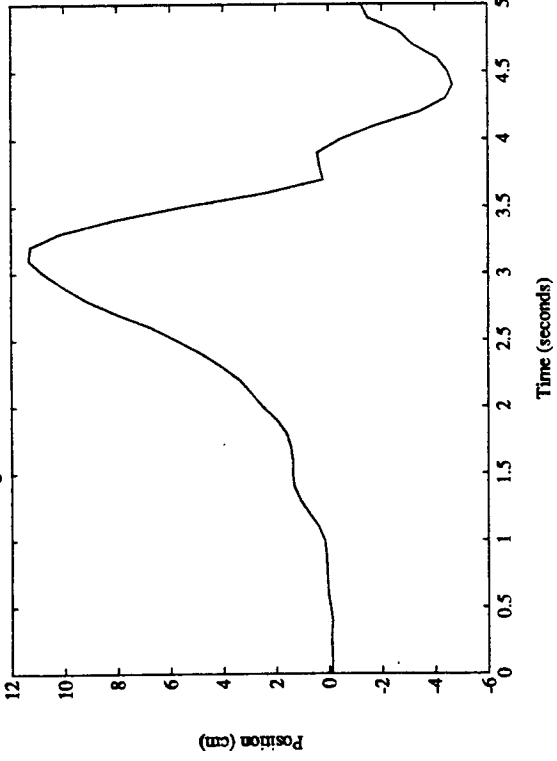
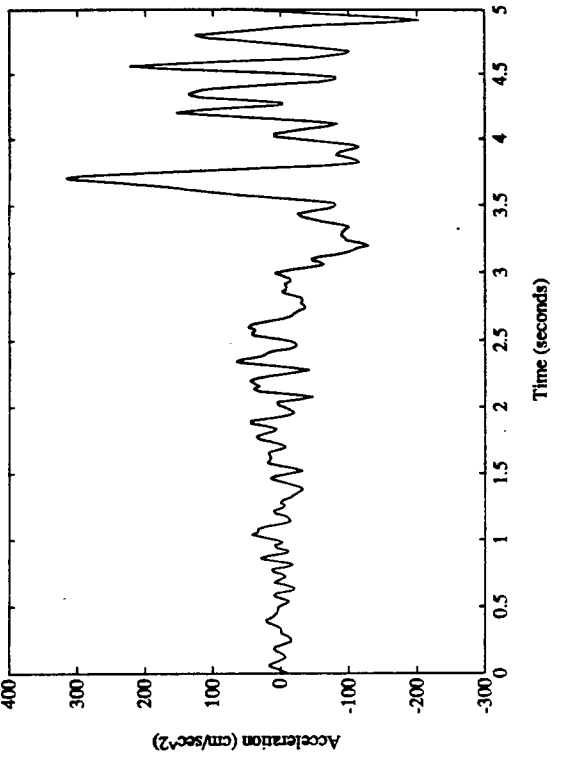
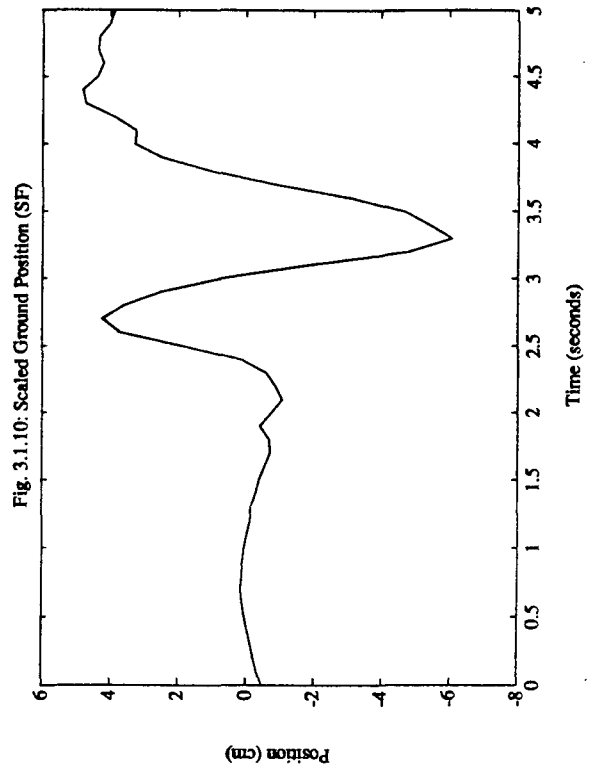
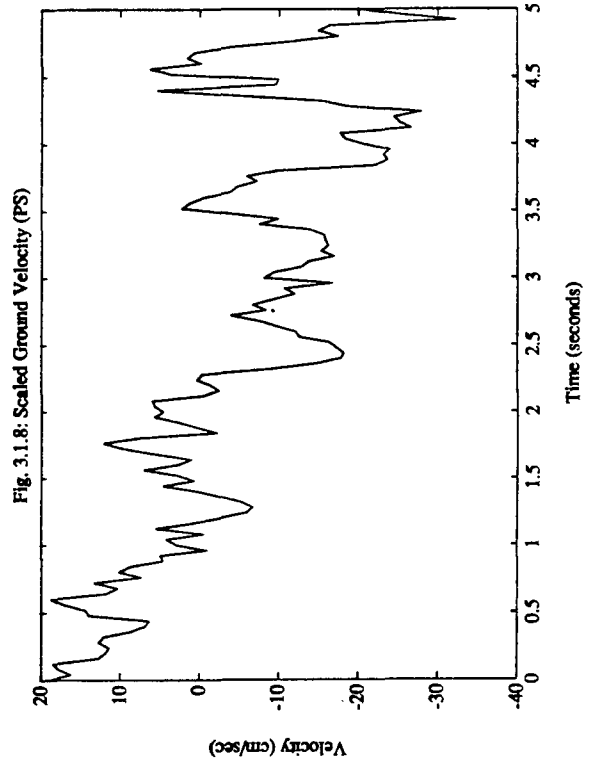
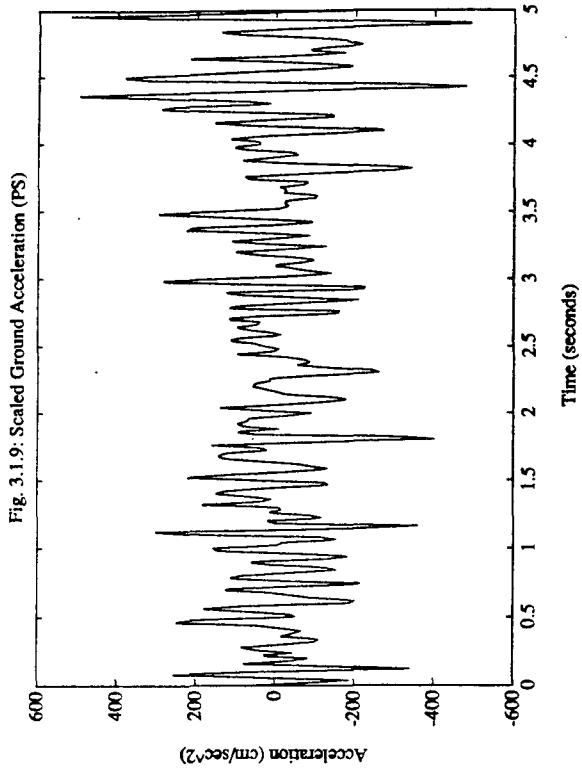
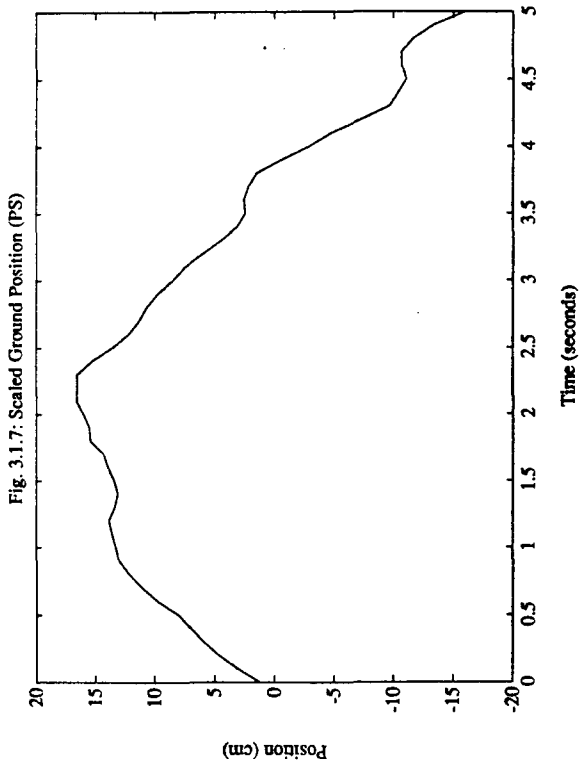
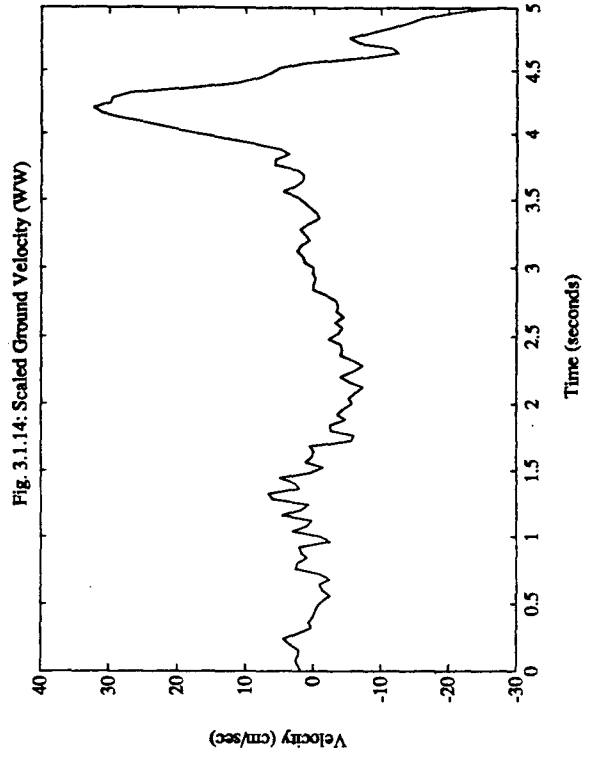
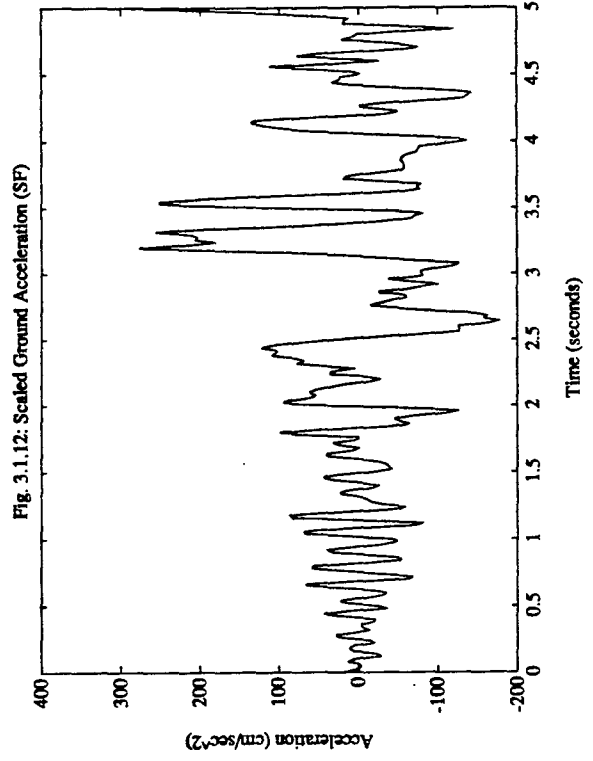
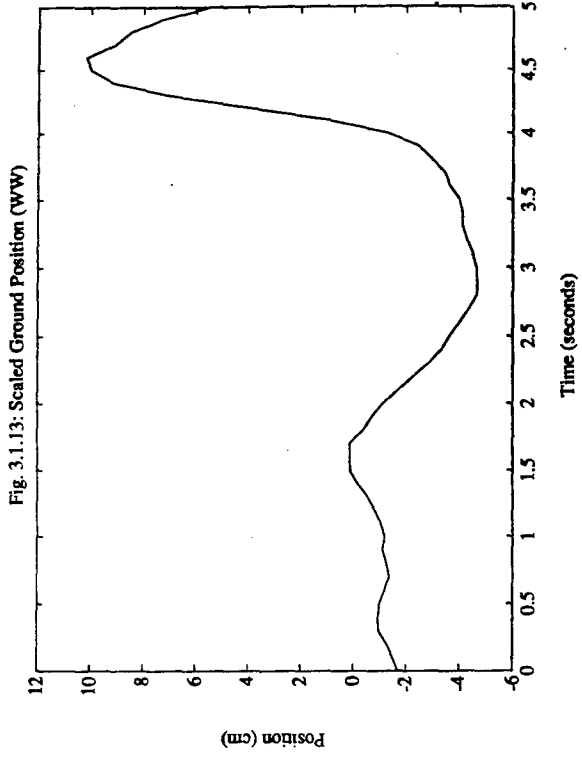
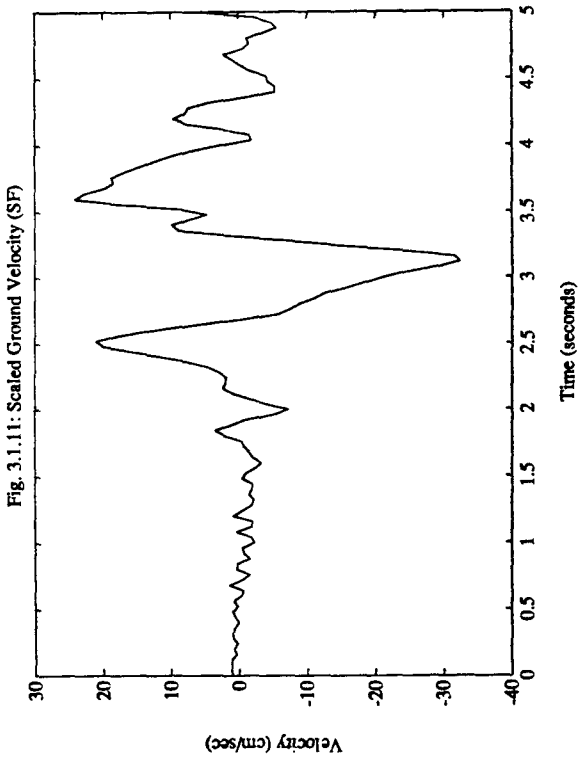
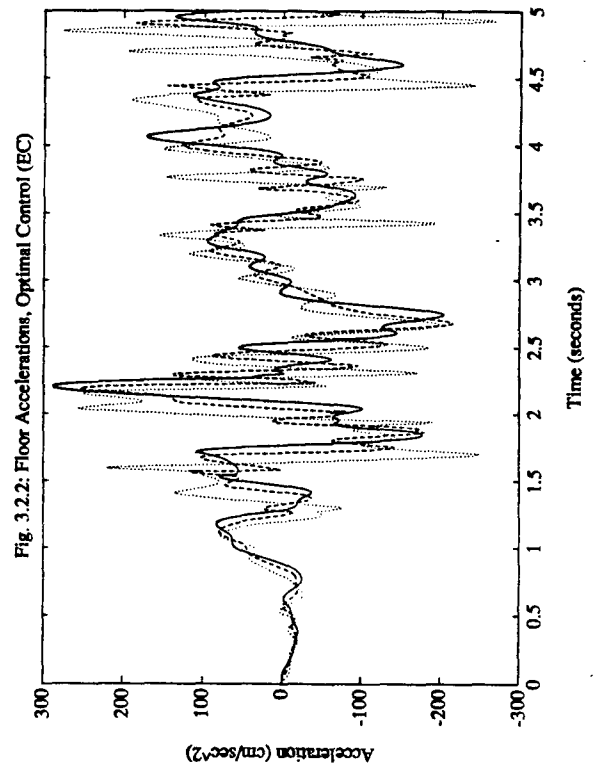
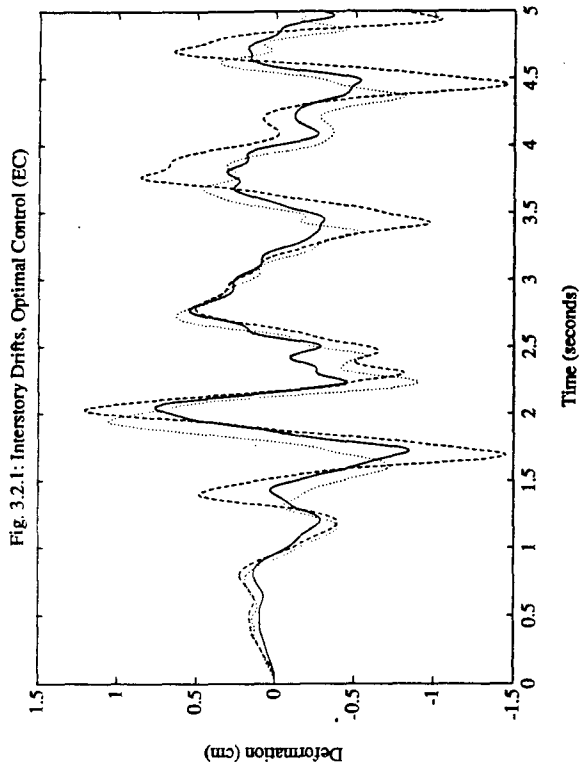
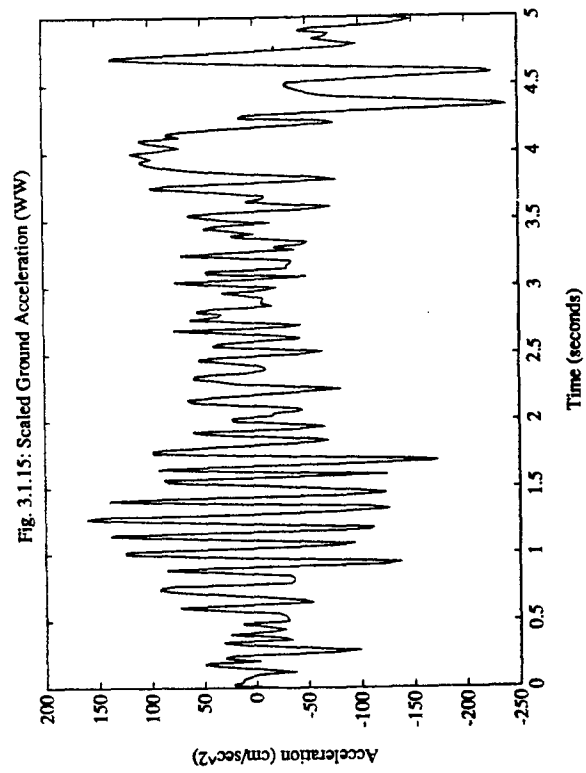


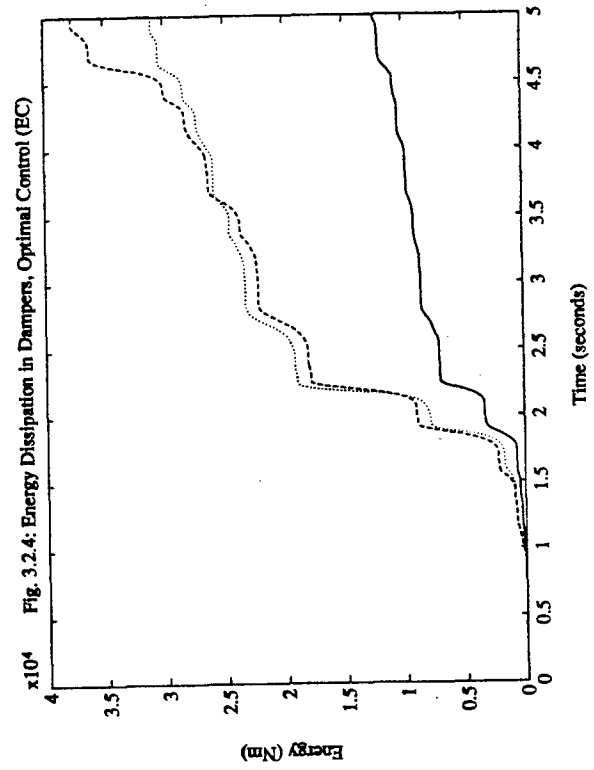
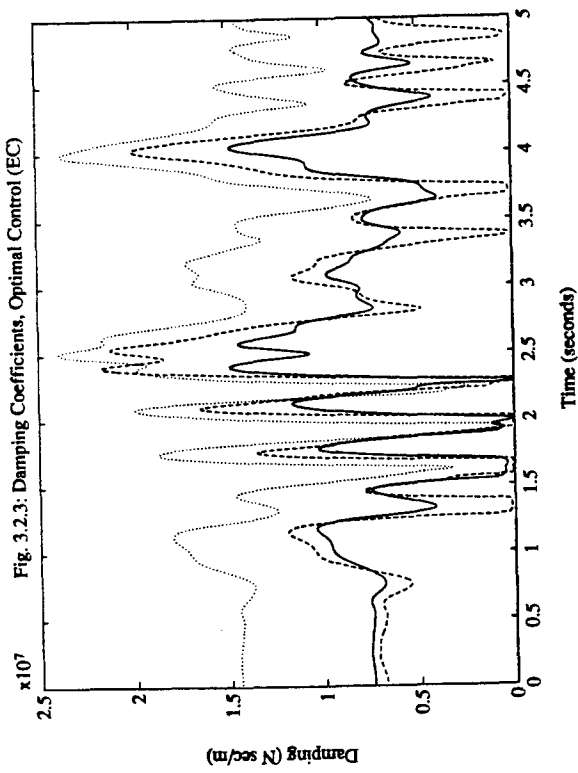
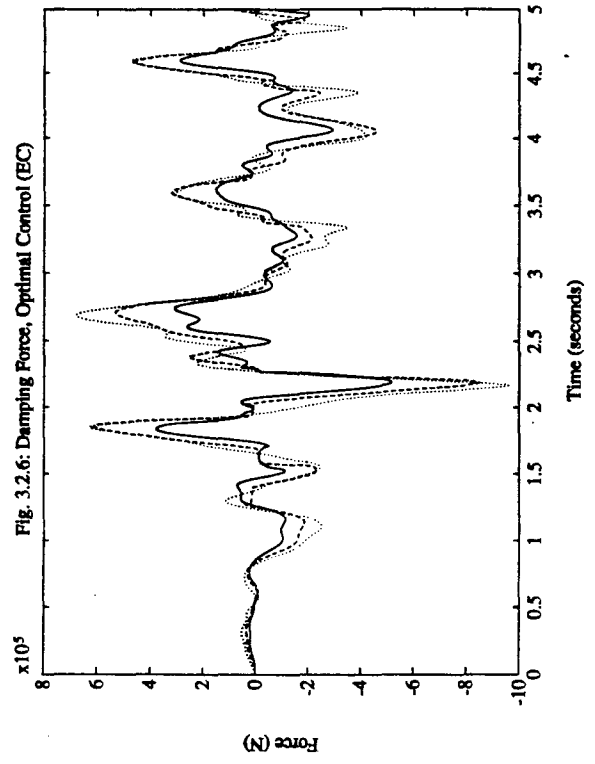
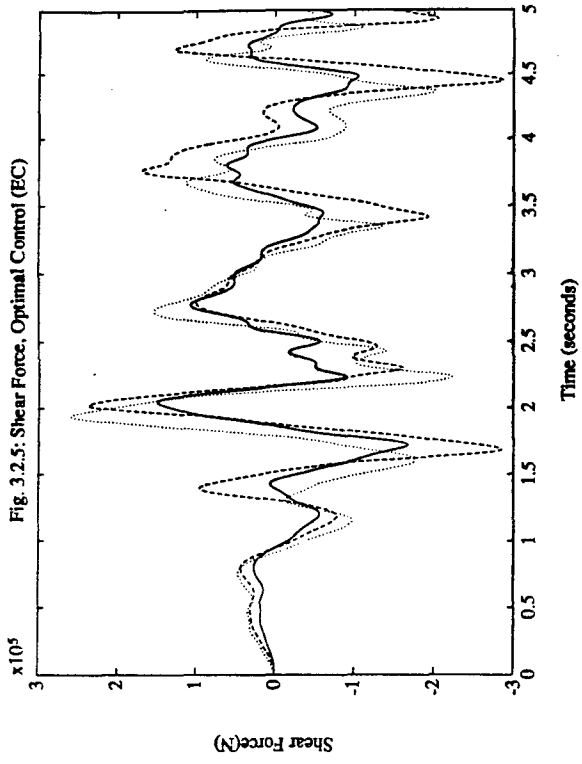
Fig. 3.1.6: Scaled Ground Acceleration (KC)

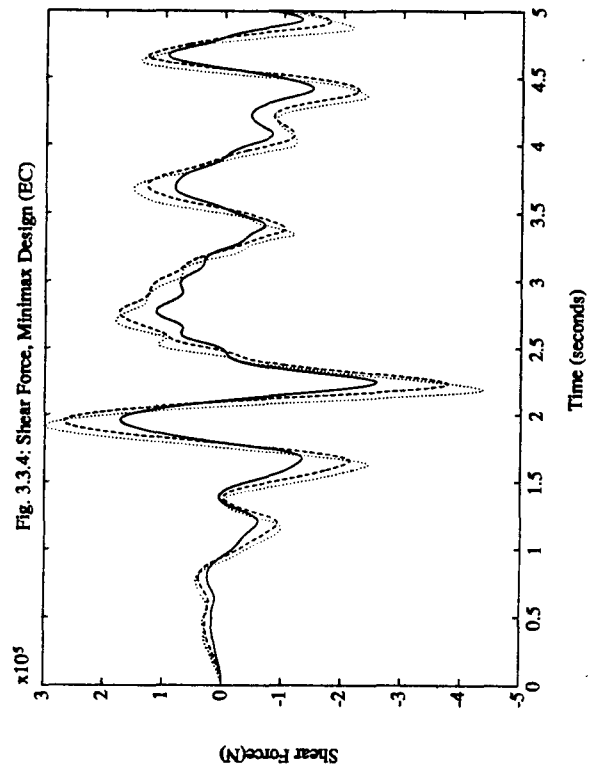
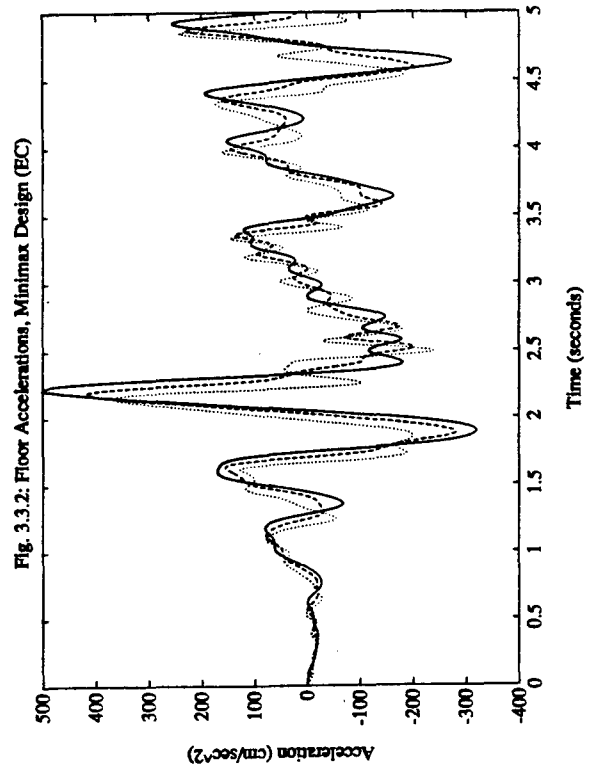
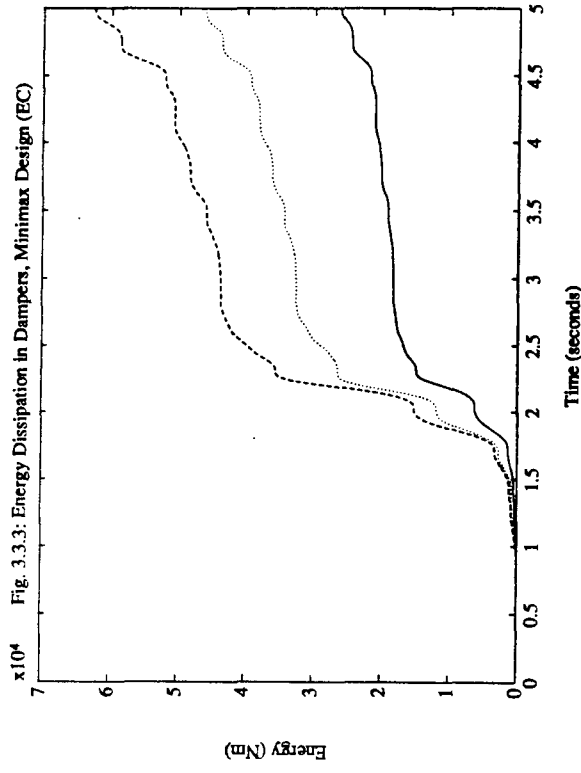
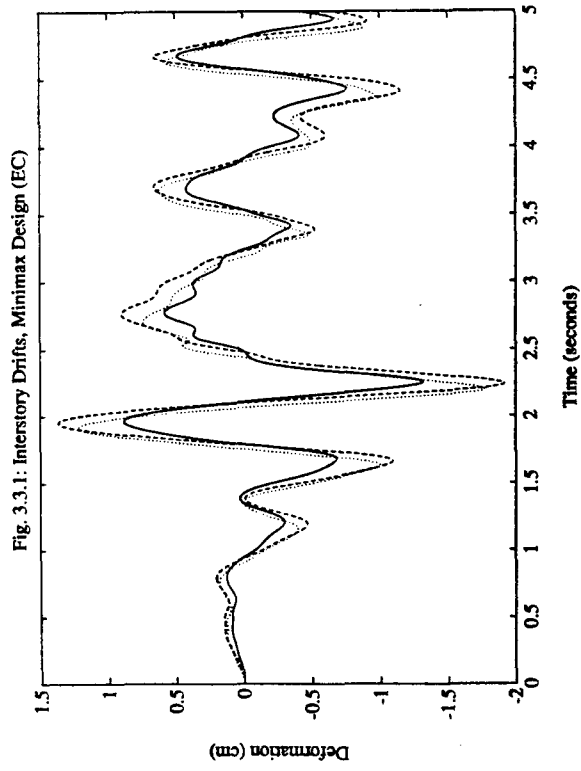


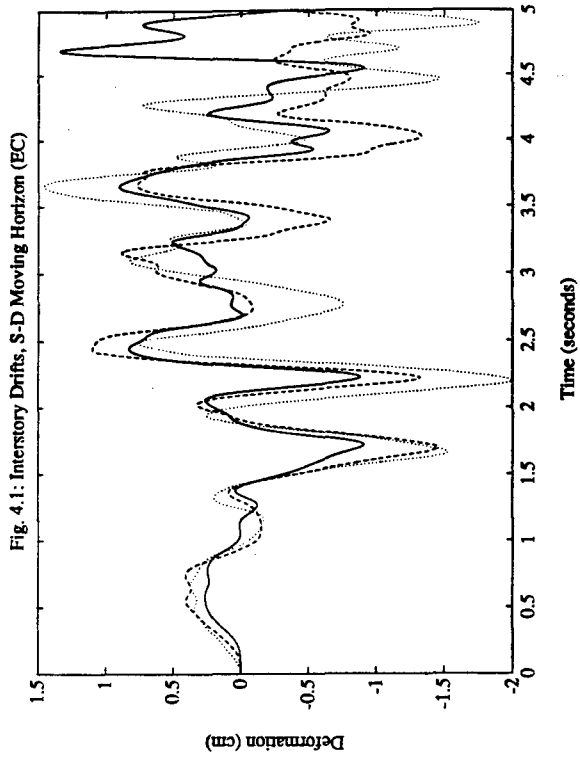
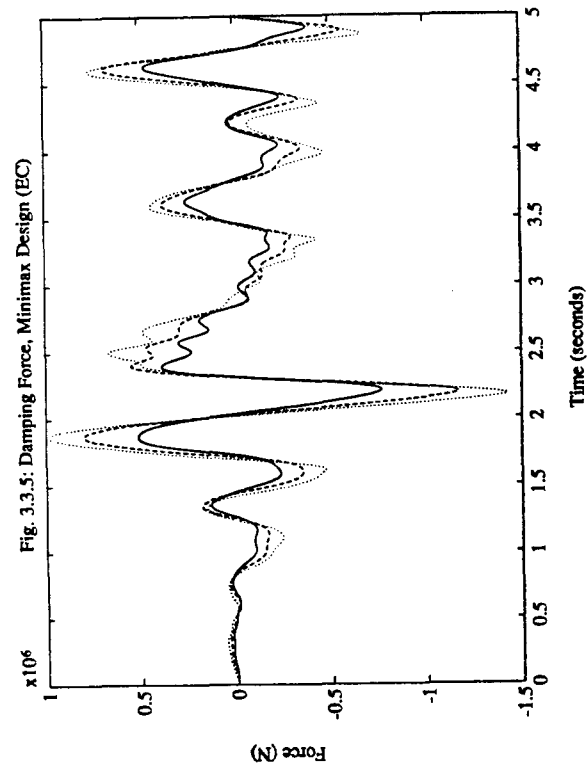


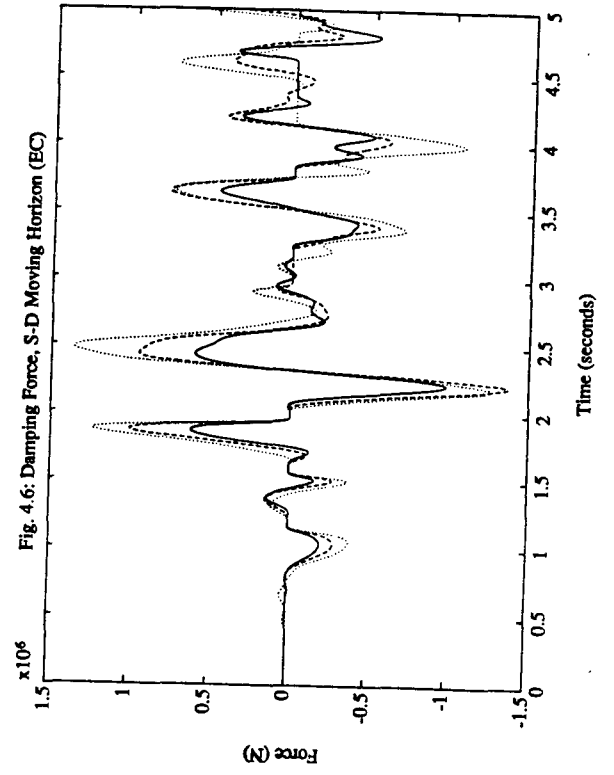
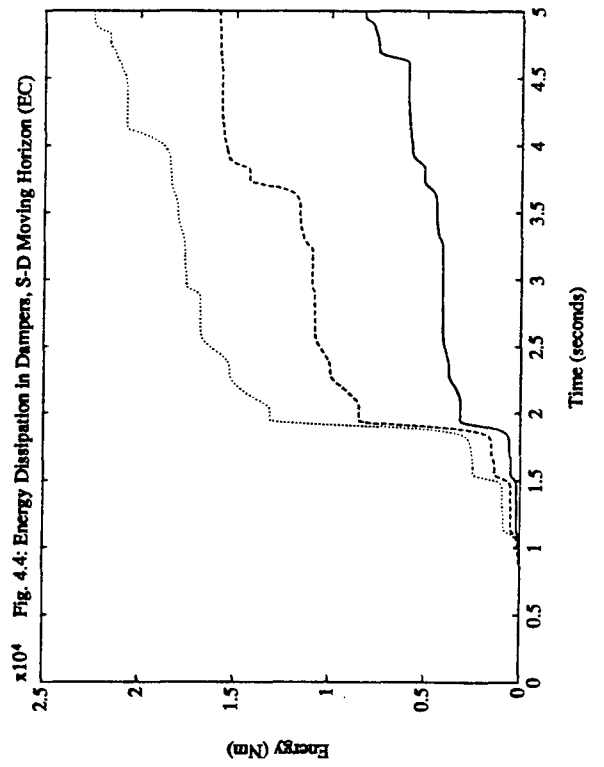
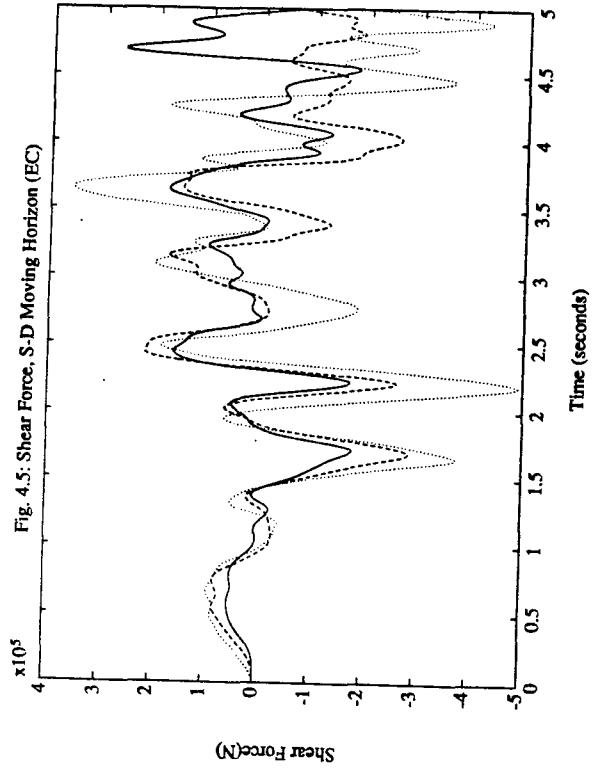
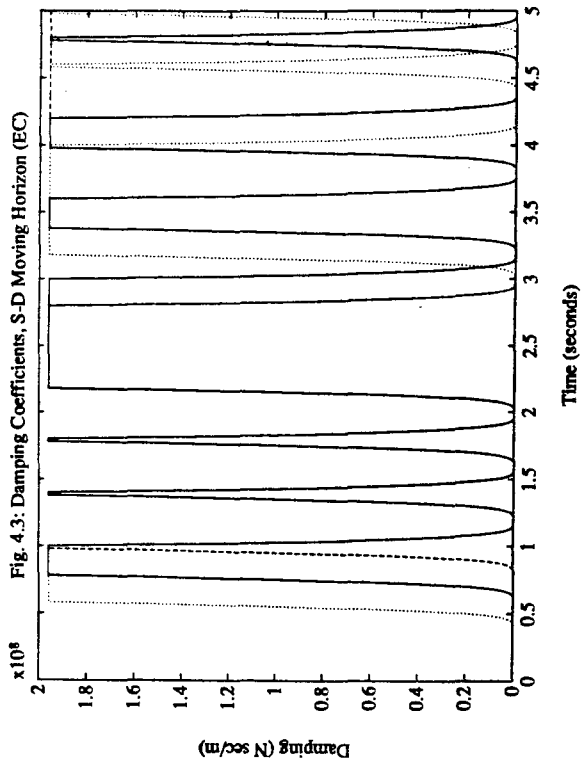


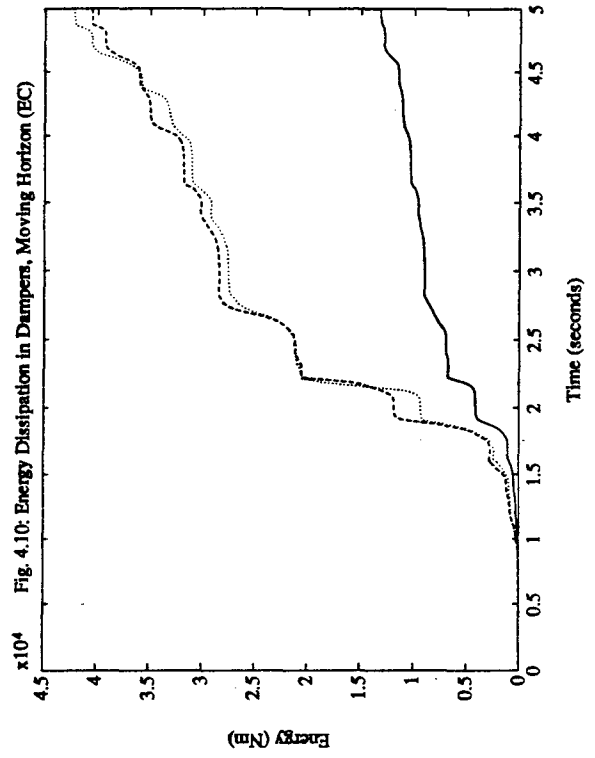
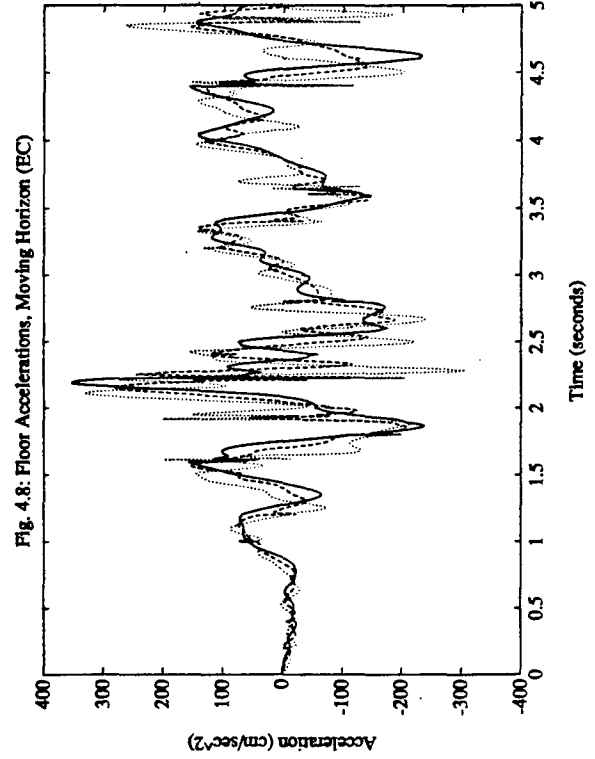
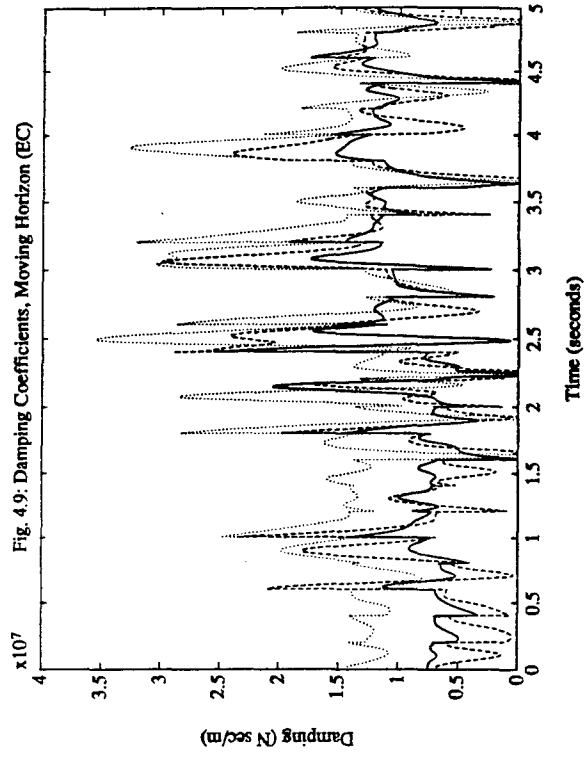
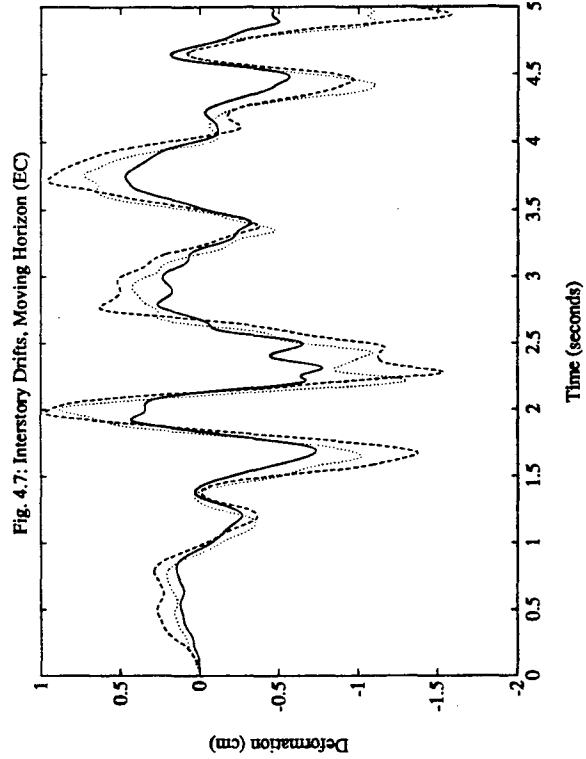












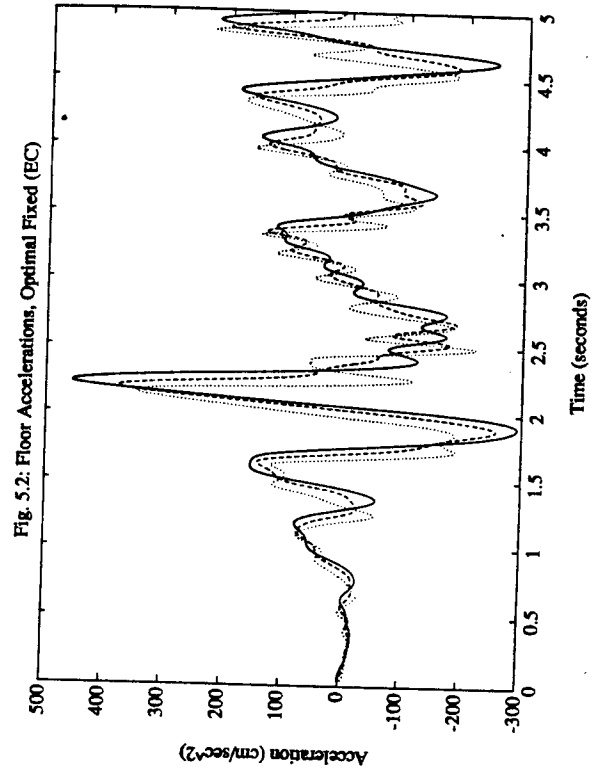
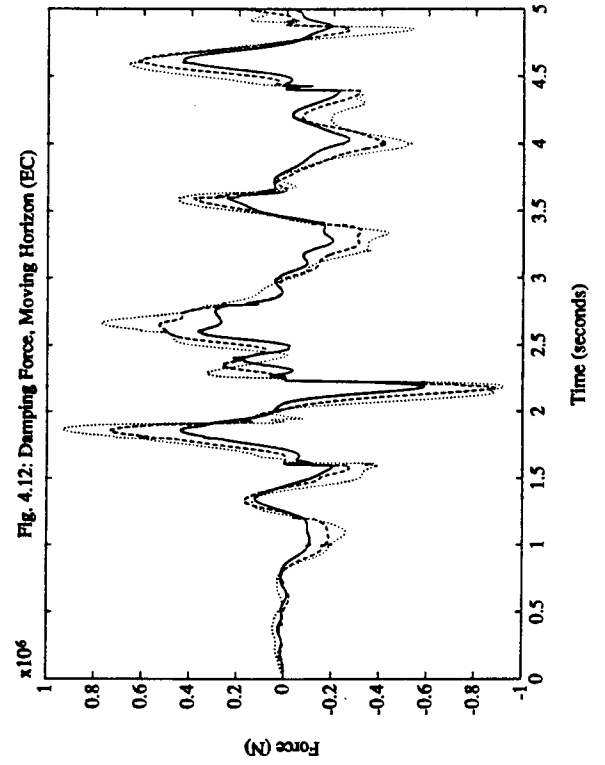
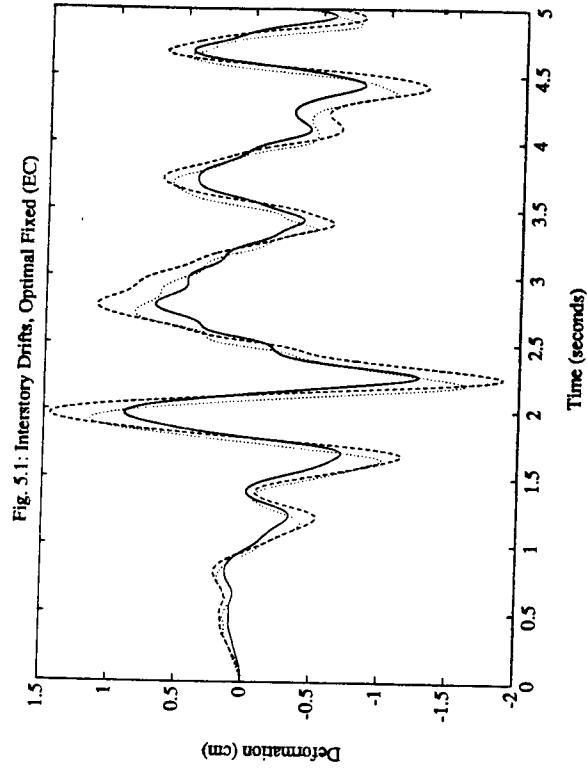
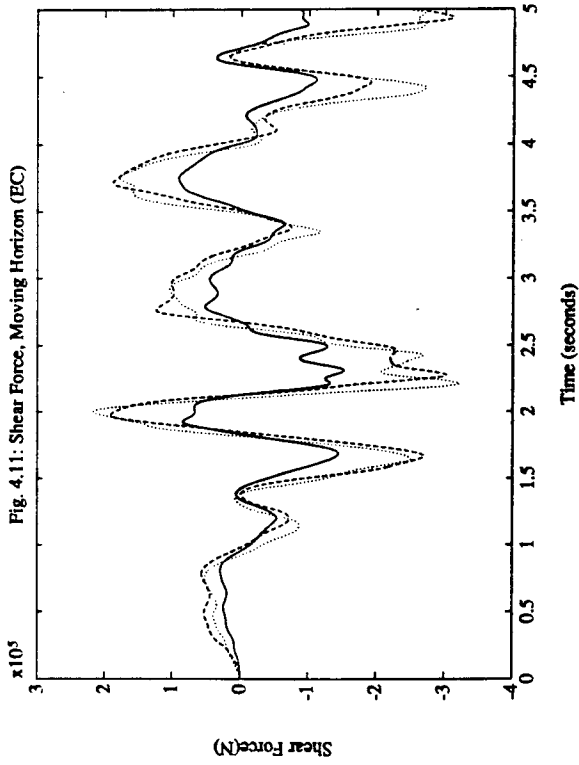


Fig. 5.3: Energy Dissipation in Dampers, Optimal Fixed (EC)

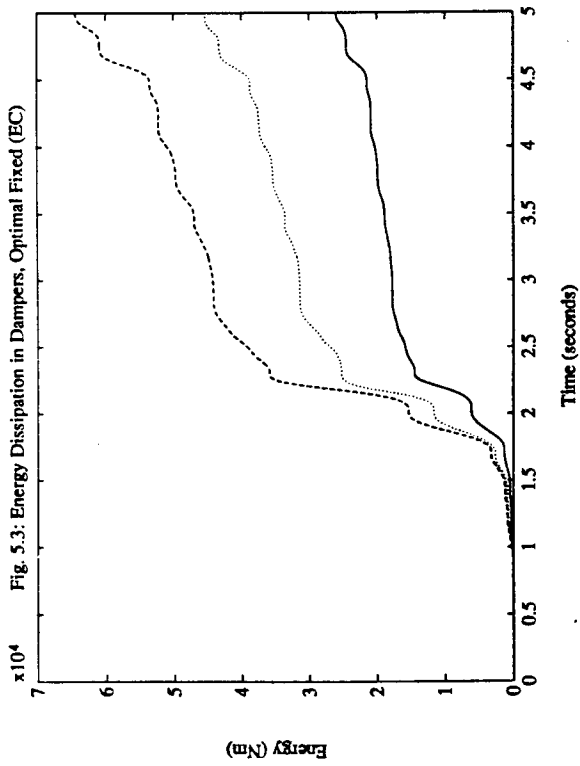


Fig. 5.5: Damping Force, Optimal Fixed (EC)

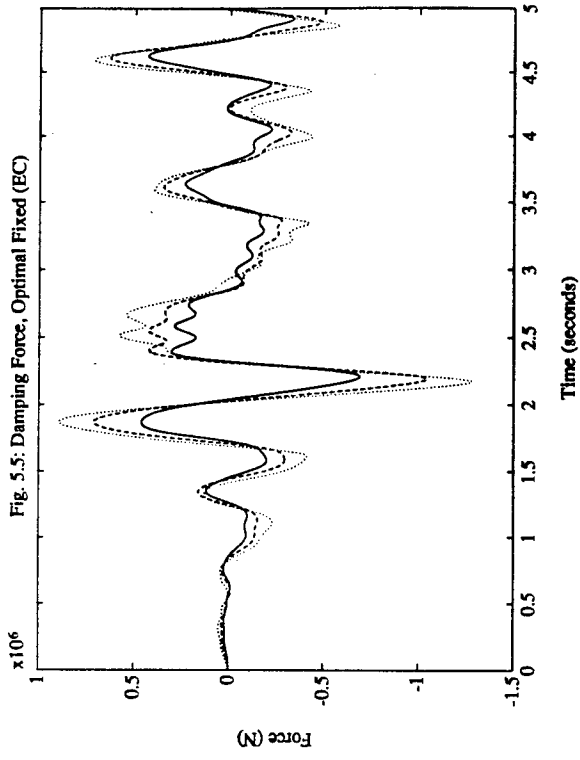
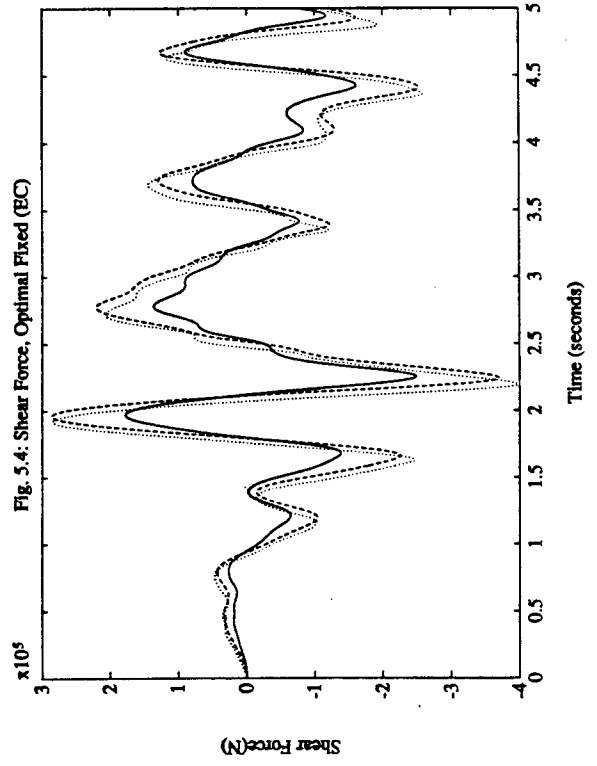
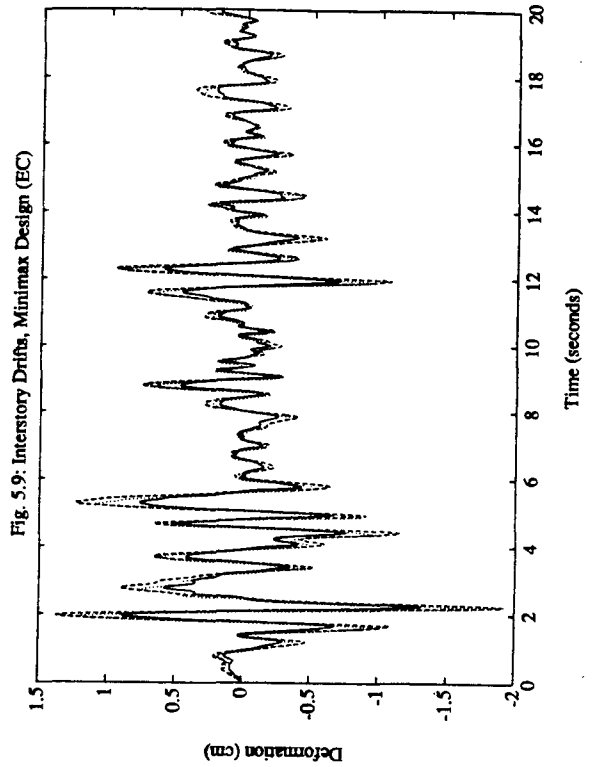
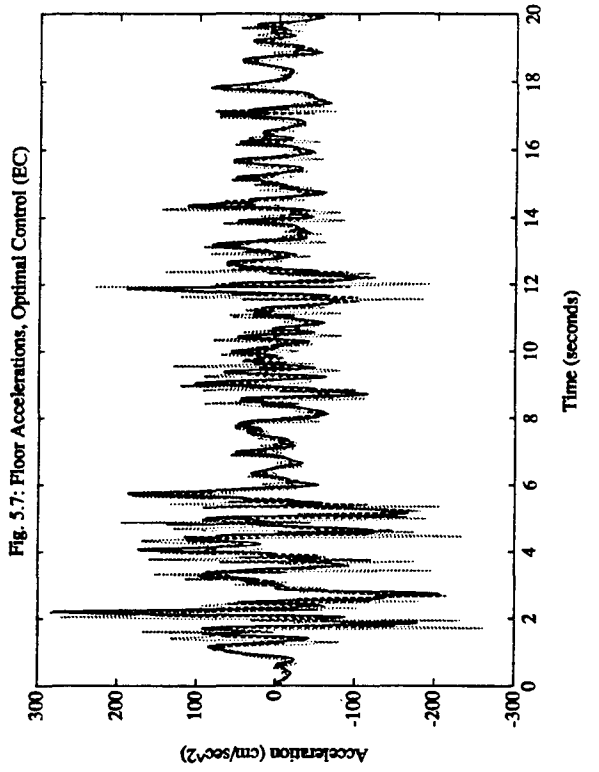
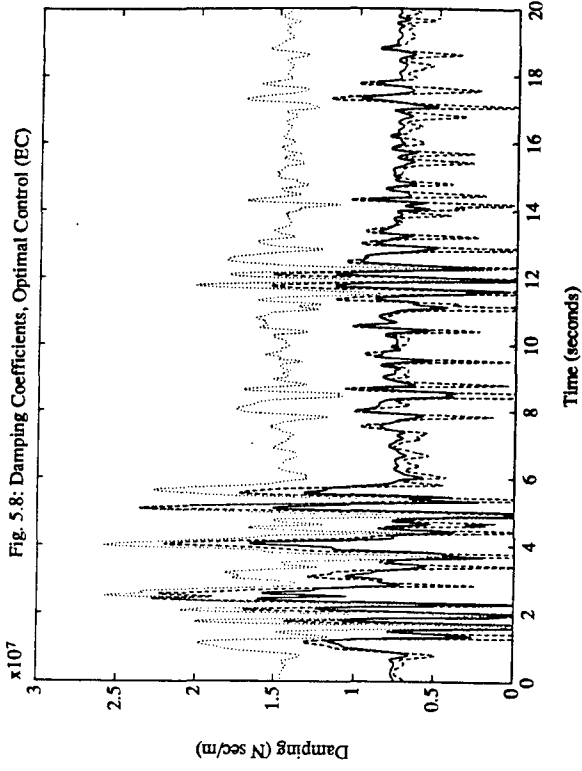
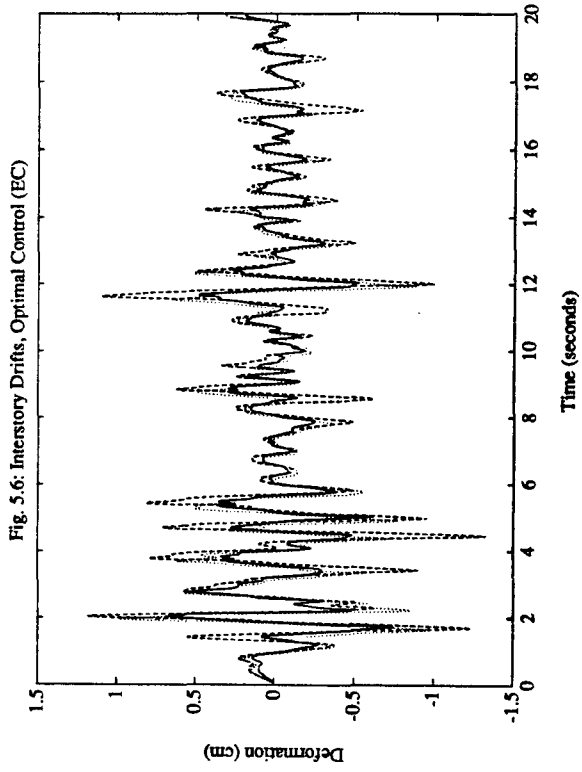
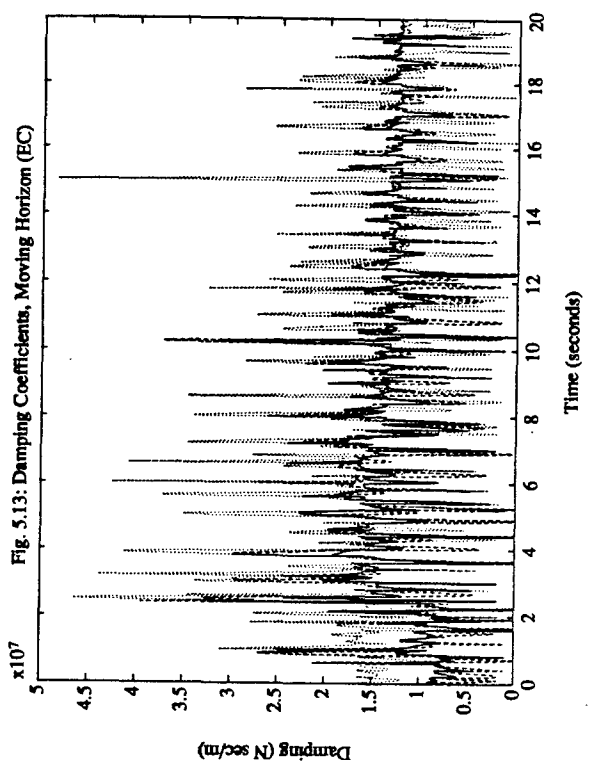
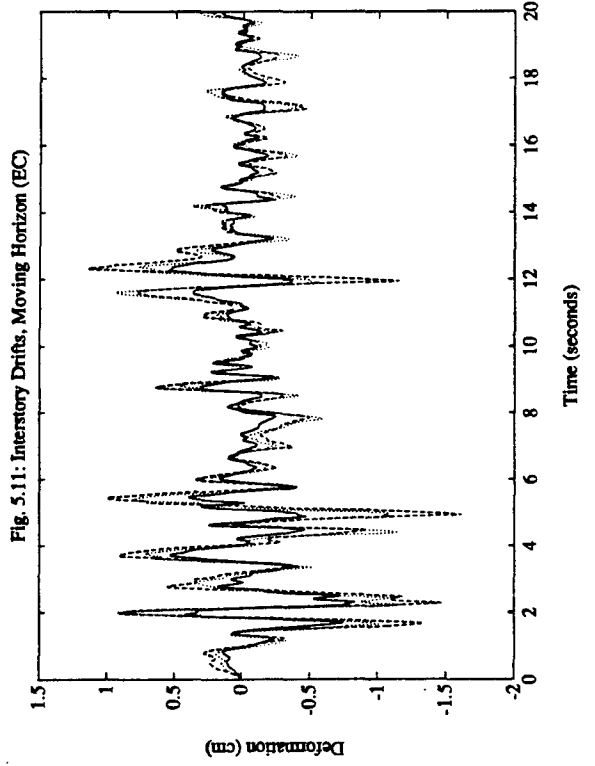
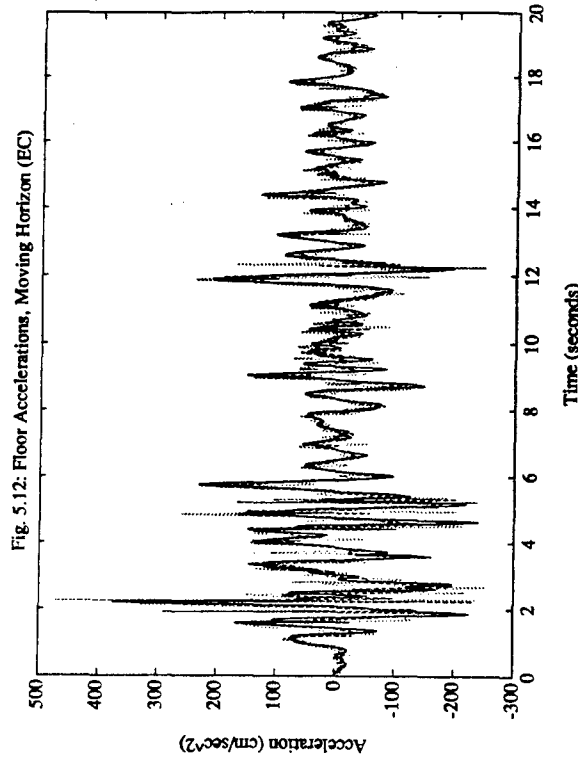
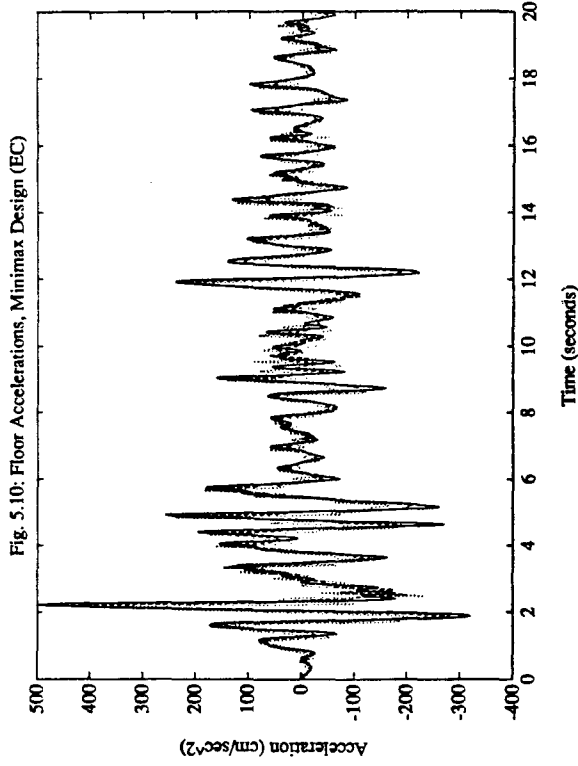


Fig. 5.4: Shear Force, Optimal Fixed (EC)







EARTHQUAKE ENGINEERING RESEARCH CENTER REPORT SERIES

EERC reports are available from the National Information Service for Earthquake Engineering (NISEE) and from the National Technical Information Service (NTIS). Numbers in parentheses are Accession Numbers assigned by the National Technical Information Service; these are followed by a price code. Contact NTIS, 5285 Port Royal Road, Springfield Virginia, 22161 for more information. Reports without Accession Numbers were not available from NTIS at the time of printing. For a current complete list of EERC reports (from EERC 67-1) and availability information, please contact University of California, EERC, NISEE, 1301 South 46th Street, Richmond, California 94804.

- UCB/EERC-82/01 "Dynamic Behavior of Ground for Seismic Analysis of Lifeline Systems," by Sato, T. and Der Kiureghian, A., January 1982, (PB82 218 926)A05.
- UCB/EERC-82/02 "Shaking Table Tests of a Tubular Steel Frame Model," by Ghanaat, Y. and Clough, R.W., January 1982, (PB82 220 161)A07.
- UCB/EERC-82/03 "Behavior of a Piping System under Seismic Excitation: Experimental Investigations of a Spatial Piping System supported by Mechanical Shock Arrestors," by Schneider, S., Lee, H.-M. and Godden, W. G., May 1982, (PB83 172 544)A09.
- UCB/EERC-82/04 "New Approaches for the Dynamic Analysis of Large Structural Systems," by Wilson, E.L., June 1982, (PB83 148 080)A05.
- UCB/EERC-82/05 "Model Study of Effects of Damage on the Vibration Properties of Steel Offshore Platforms," by Shahrivar, F. and Bouwkamp, J.G., June 1982, (PB83 148 742)A10.
- UCB/EERC-82/06 "States of the Art and Practice in the Optimum Seismic Design and Analytical Response Prediction of R/C Frame Wall Structures," by Aktan, A.E. and Bertero, V.V., July 1982, (PB83 147 736)A05.
- UCB/EERC-82/07 "Further Study of the Earthquake Response of a Broad Cylindrical Liquid-Storage Tank Model," by Manos, G.C. and Clough, R.W., July 1982, (PB83 147 744)A11.
- UCB/EERC-82/08 "An Evaluation of the Design and Analytical Seismic Response of a Seven Story Reinforced Concrete Frame," by Charney, F.A. and Bertero, V.V., July 1982, (PB83 157 628)A09.
- UCB/EERC-82/09 "Fluid-Structure Interactions: Added Mass Computations for Incompressible Fluid," by Kuo, J.S.-H., August 1982, (PB83 156 281)A07.
- UCB/EERC-82/10 "Joint-Opening Nonlinear Mechanism: Interface Smeared Crack Model," by Kuo, J.S.-H., August 1982, (PB83 149 195)A05.
- UCB/EERC-82/11 "Dynamic Response Analysis of Techi Dam," by Clough, R.W., Stephen, R.M. and Kuo, J.S.-H., August 1982, (PB83 147 496)A06.
- UCB/EERC-82/12 "Prediction of the Seismic Response of R/C Frame-Coupled Wall Structures," by Aktan, A.E., Bertero, V.V. and Piazza, M., August 1982, (PB83 149 203)A09.
- UCB/EERC-82/13 "Preliminary Report on the Smart 1 Strong Motion Array in Taiwan," by Bolt, B.A., Loh, C.H., Penzien, J. and Tsai, Y.B., August 1982, (PB83 159 400)A10.
- UCB/EERC-82/14 "Seismic Behavior of an Eccentrically X-Braced Steel Structure," by Yang, M.S., September 1982, (PB83 260 778)A12.
- UCB/EERC-82/15 "The Performance of Stairways in Earthquakes," by Roha, C., Axley, J.W. and Bertero, V.V., September 1982, (PB83 157 693)A07.
- UCB/EERC-82/16 "The Behavior of Submerged Multiple Bodies in Earthquakes," by Liao, W.-G., September 1982, (PB83 158 709)A07.
- UCB/EERC-82/17 "Effects of Concrete Types and Loading Conditions on Local Bond-Slip Relationships," by Cowell, A.D., Popov, E.P. and Bertero, V.V., September 1982, (PB83 153 577)A04.
- UCB/EERC-82/18 "Mechanical Behavior of Shear Wall Vertical Boundary Members: An Experimental Investigation," by Wagner, M.T. and Bertero, V.V., October 1982, (PB83 159 764)A05.
- UCB/EERC-82/19 "Experimental Studies of Multi-support Seismic Loading on Piping Systems," by Kelly, J.M. and Cowell, A.D., November 1982, (PB90 262 684)A07.
- UCB/EERC-82/20 "Generalized Plastic Hinge Concepts for 3D Beam-Column Elements," by Chen, P. F.-S. and Powell, G.H., November 1982, (PB83 247 981)A13.
- UCB/EERC-82/21 "ANSR-III: General Computer Program for Nonlinear Structural Analysis," by Oughourlian, C.V. and Powell, G.H., November 1982, (PB83 251 330)A12.
- UCB/EERC-82/22 "Solution Strategies for Statically Loaded Nonlinear Structures," by Simons, J.W. and Powell, G.H., November 1982, (PB83 197 970)A06.
- UCB/EERC-82/23 "Analytical Model of Deformed Bar Anchorages under Generalized Excitations," by Ciampi, V., Eligehausen, R., Bertero, V.V. and Popov, E.P., November 1982, (PB83 169 532)A06.
- UCB/EERC-82/24 "A Mathematical Model for the Response of Masonry Walls to Dynamic Excitations," by Sucuoglu, H., Mengi, Y. and McNiven, H.D., November 1982, (PB83 169 011)A07.
- UCB/EERC-82/25 "Earthquake Response Considerations of Broad Liquid Storage Tanks," by Cambra, F.J., November 1982, (PB83 251 215)A09.
- UCB/EERC-82/26 "Computational Models for Cyclic Plasticity, Rate Dependence and Creep," by Mosaddad, B. and Powell, G.H., November 1982, (PB83 245 829)A08.
- UCB/EERC-82/27 "Inelastic Analysis of Piping and Tubular Structures," by Mahasuverachai, M. and Powell, G.H., November 1982, (PB83 249 987)A07.
- UCB/EERC-83/01 "The Economic Feasibility of Seismic Rehabilitation of Buildings by Base Isolation," by Kelly, J.M., January 1983, (PB83 197 988)A05.
- UCB/EERC-83/02 "Seismic Moment Connections for Moment-Resisting Steel Frames," by Popov, E.P., January 1983, (PB83 195 412)A04.
- UCB/EERC-83/03 "Design of Links and Beam-to-Column Connections for Eccentrically Braced Steel Frames," by Popov, E.P. and Malley, J.O., January 1983, (PB83 194 811)A04.
- UCB/EERC-83/04 "Numerical Techniques for the Evaluation of Soil-Structure Interaction Effects in the Time Domain," by Bayo, E. and Wilson, E.L., February 1983, (PB83 245 605)A09.
- UCB/EERC-83/05 "A Transducer for Measuring the Internal Forces in the Columns of a Frame-Wall Reinforced Concrete Structure," by Sause, R. and Bertero, V.V., May 1983, (PB84 119 494)A06.

- UCB/EERC-83/06 "Dynamic Interactions Between Floating Ice and Offshore Structures," by Croteau, P., May 1983, (PB84 119 486)A16.
- UCB/EERC-83/07 "Dynamic Analysis of Multiply Tuned and Arbitrarily Supported Secondary Systems," by Igusa, T. and Der Kiureghian, A., July 1983, (PB84 118 272)A11.
- UCB/EERC-83/08 "A Laboratory Study of Submerged Multi-body Systems in Earthquakes," by Ansari, G.R., June 1983, (PB83 261 842)A17.
- UCB/EERC-83/09 "Effects of Transient Foundation Uplift on Earthquake Response of Structures," by Yim, C.-S. and Chopra, A.K., June 1983, (PB83 261 396)A07.
- UCB/EERC-83/10 "Optimal Design of Friction-Braced Frames under Seismic Loading," by Austin, M.A. and Pister, K.S., June 1983, (PB84 119 288)A06.
- UCB/EERC-83/11 "Shaking Table Study of Single-Story Masonry Houses: Dynamic Performance under Three Component Seismic Input and Recommendations," by Manos, G.C., Clough, R.W. and Mayes, R.L., July 1983, (UCB/EERC-83/11)A08.
- UCB/EERC-83/12 "Experimental Error Propagation in Pseudodynamic Testing," by Shing, P.B. and Mahin, S.A., June 1983, (PB84 119 270)A09.
- UCB/EERC-83/13 "Experimental and Analytical Predictions of the Mechanical Characteristics of a 1/5-scale Model of a 7-story R/C Frame-Wall Building Structure," by Aktan, A.E., Bertero, V.V., Chowdhury, A.A. and Nagashima, T., June 1983, (PB84 119 213)A07.
- UCB/EERC-83/14 "Shaking Table Tests of Large-Panel Precast Concrete Building System Assemblages," by Oliva, M.G. and Clough, R.W., June 1983, (PB86 110 210/AS)A11.
- UCB/EERC-83/15 "Seismic Behavior of Active Beam Links in Eccentrically Braced Frames," by Hjelmstad, K.D. and Popov, E.P., July 1983, (PB84 119 676)A09.
- UCB/EERC-83/16 "System Identification of Structures with Joint Rotation," by Dimsdale, J.S., July 1983, (PB84 192 210)A06.
- UCB/EERC-83/17 "Construction of Inelastic Response Spectra for Single-Degree-of-Freedom Systems," by Mahin, S. and Lin, J., June 1983, (PB84 208 834)A05.
- UCB/EERC-83/18 "Interactive Computer Analysis Methods for Predicting the Inelastic Cyclic Behaviour of Structural Sections," by Kaba, S. and Mahin, S., July 1983, (PB84 192 012)A06.
- UCB/EERC-83/19 "Effects of Bond Deterioration on Hysteretic Behavior of Reinforced Concrete Joints," by Filippou, F.C., Popov, E.P. and Bertero, V.V., August 1983, (PB84 192 020)A10.
- UCB/EERC-83/20 "Correlation of Analytical and Experimental Responses of Large-Panel Precast Building Systems," by Oliva, M.G., Clough, R.W., Velkov, M. and Gavrilovic, P., May 1988, (PB90 262 692)A06.
- UCB/EERC-83/21 "Mechanical Characteristics of Materials Used in a 1/5 Scale Model of a 7-Story Reinforced Concrete Test Structure," by Bertero, V.V., Aktan, A.E., Harris, H.G. and Chowdhury, A.A., October 1983, (PB84 193 697)A05.
- UCB/EERC-83/22 "Hybrid Modelling of Soil-Structure Interaction in Layered Media," by Tzong, T.-J. and Penzien, J., October 1983, (PB84 192 178)A08.
- UCB/EERC-83/23 "Local Bond Stress-Slip Relationships of Deformed Bars under Generalized Excitations," by Elgehausen, R., Popov, E.P. and Bertero, V.V., October 1983, (PB84 192 848)A09.
- UCB/EERC-83/24 "Design Considerations for Shear Links in Eccentrically Braced Frames," by Malley, J.O. and Popov, E.P., November 1983, (PB84 192 186)A07.
- UCB/EERC-84/01 "Pseudodynamic Test Method for Seismic Performance Evaluation: Theory and Implementation," by Shing, P.-S.B. and Mahin, S.A., January 1984, (PB84 190 644)A08.
- UCB/EERC-84/02 "Dynamic Response Behavior of Kiang Hong Dian Dam," by Clough, R.W., Chang, K.-T., Chen, H.-Q. and Stephen, R.M., April 1984, (PB84 209 402)A08.
- UCB/EERC-84/03 "Refined Modelling of Reinforced Concrete Columns for Seismic Analysis," by Kaba, S.A. and Mahin, S.A., April 1984, (PB84 234 384)A06.
- UCB/EERC-84/04 "A New Floor Response Spectrum Method for Seismic Analysis of Multiply Supported Secondary Systems," by Asfura, A. and Der Kiureghian, A., June 1984, (PB84 239 417)A06.
- UCB/EERC-84/05 "Earthquake Simulation Tests and Associated Studies of a 1/5th-scale Model of a 7-Story R/C Frame-Wall Test Structure," by Bertero, V.V., Aktan, A.E., Charney, F.A. and Sause, R., June 1984, (PB84 239 409)A09.
- UCB/EERC-84/06 "Unassigned," by Unassigned, 1984.
- UCB/EERC-84/07 "Behavior of Interior and Exterior Flat-Plate Connections Subjected to Inelastic Load Reversals," by Zee, H.L. and Moehle, J.P., August 1984, (PB86 117 629/AS)A07.
- UCB/EERC-84/08 "Experimental Study of the Seismic Behavior of a Two-Story Flat-Plate Structure," by Moehle, J.P. and Diebold, J.W., August 1984, (PB86 122 553/AS)A12.
- UCB/EERC-84/09 "Phenomenological Modeling of Steel Braces under Cyclic Loading," by Ikeda, K., Mahin, S.A. and Dermitzakis, S.N., May 1984, (PB86 132 198/AS)A08.
- UCB/EERC-84/10 "Earthquake Analysis and Response of Concrete Gravity Dams," by Fenves, G.L. and Chopra, A.K., August 1984, (PB85 193 902/AS)A11.
- UCB/EERC-84/11 "EAGD-84: A Computer Program for Earthquake Analysis of Concrete Gravity Dams," by Fenves, G.L. and Chopra, A.K., August 1984, (PB85 193 613/AS)A05.
- UCB/EERC-84/12 "A Refined Physical Theory Model for Predicting the Seismic Behavior of Braced Steel Frames," by Ikeda, K. and Mahin, S.A., July 1984, (PB85 191 450/AS)A09.
- UCB/EERC-84/13 "Earthquake Engineering Research at Berkeley - 1984," by EERC, August 1984, (PB85 197 341/AS)A10.
- UCB/EERC-84/14 "Moduli and Damping Factors for Dynamic Analyses of Cohesionless Soils," by Seed, H.B., Wong, R.T., Idriss, I.M. and Tokimatsu, K., September 1984, (PB85 191 468/AS)A04.
- UCB/EERC-84/15 "The Influence of SPT Procedures in Soil Liquefaction Resistance Evaluations," by Seed, H.B., Tokimatsu, K., Harder, L.F. and Chung, R.M., October 1984, (PB85 191 732/AS)A04.

- UCB/EERC-84/16 "Simplified Procedures for the Evaluation of Settlements in Sands Due to Earthquake Shaking," by Tokimatsu, K. and Seed, H.B., October 1984, (PB85 197 887/AS)A03.
- UCB/EERC-84/17 "Evaluation of Energy Absorption Characteristics of Highway Bridges Under Seismic Conditions - Volume I (PB90 262 627)A16 and Volume II (Appendices) (PB90 262 635)A13," by Imbsen, R.A. and Penzien, J., September 1986.
- UCB/EERC-84/18 "Structure-Foundation Interactions under Dynamic Loads," by Liu, W.D. and Penzien, J., November 1984, (PB87 124 889/AS)A11.
- UCB/EERC-84/19 "Seismic Modelling of Deep Foundations," by Chen, C.-H. and Penzien, J., November 1984, (PB87 124 798/AS)A07.
- UCB/EERC-84/20 "Dynamic Response Behavior of Quan Shui Dam," by Clough, R.W., Chang, K.-T., Chen, H.-Q., Stephen, R.M., Ghanaat, Y. and Qi, J.-H., November 1984, (PB86 115177/AS)A07.
- UCB/EERC-85/01 "Simplified Methods of Analysis for Earthquake Resistant Design of Buildings," by Cruz, E.F. and Chopra, A.K., February 1985, (PB86 112299/AS)A12.
- UCB/EERC-85/02 "Estimation of Seismic Wave Coherency and Rupture Velocity using the SMART 1 Strong-Motion Array Recordings," by Abrahamson, N.A., March 1985, (PB86 214 343)A07.
- UCB/EERC-85/03 "Dynamic Properties of a Thirty Story Condominium Tower Building," by Stephen, R.M., Wilson, E.L. and Stander, N., April 1985, (PB86 118965/AS)A06.
- UCB/EERC-85/04 "Development of Substructuring Techniques for On-Line Computer Controlled Seismic Performance Testing," by Dermitzakis, S. and Mahin, S., February 1985, (PB86 132941/AS)A08.
- UCB/EERC-85/05 "A Simple Model for Reinforcing Bar Anchorages under Cyclic Excitations," by Filippou, F.C., March 1985, (PB86 112 919/AS)A05.
- UCB/EERC-85/06 "Racking Behavior of Wood-framed Gypsum Panels under Dynamic Load," by Oliva, M.G., June 1985, (PB90 262 643)A04.
- UCB/EERC-85/07 "Earthquake Analysis and Response of Concrete Arch Dams," by Fok, K.-L. and Chopra, A.K., June 1985, (PB86 139672/AS)A10.
- UCB/EERC-85/08 "Effect of Inelastic Behavior on the Analysis and Design of Earthquake Resistant Structures," by Lin, J.P. and Mahin, S.A., June 1985, (PB86 135340/AS)A08.
- UCB/EERC-85/09 "Earthquake Simulator Testing of a Base-Isolated Bridge Deck," by Kelly, J.M., Buckle, I.G. and Tsai, H.-C., January 1986, (PB87 124 152/AS)A06.
- UCB/EERC-85/10 "Simplified Analysis for Earthquake Resistant Design of Concrete Gravity Dams," by Fenves, G.L. and Chopra, A.K., June 1986, (PB87 124 160/AS)A08.
- UCB/EERC-85/11 "Dynamic Interaction Effects in Arch Dams," by Clough, R.W., Chang, K.-T., Chen, H.-Q. and Ghanaat, Y., October 1985, (PB86 135027/AS)A05.
- UCB/EERC-85/12 "Dynamic Response of Long Valley Dam in the Mammoth Lake Earthquake Series of May 25-27, 1980," by Lai, S. and Seed, H.B., November 1985, (PB86 142304/AS)A05.
- UCB/EERC-85/13 "A Methodology for Computer-Aided Design of Earthquake-Resistant Steel Structures," by Austin, M.A., Pister, K.S. and Mahin, S.A., December 1985, (PB86 159480/AS)A10.
- UCB/EERC-85/14 "Response of Tension-Leg Platforms to Vertical Seismic Excitations," by Liou, G.-S., Penzien, J. and Yeung, R.W., December 1985, (PB87 124 871/AS)A08.
- UCB/EERC-85/15 "Cyclic Loading Tests of Masonry Single Piers: Volume 4 - Additional Tests with Height to Width Ratio of 1," by Sveinsson, B., McNiven, H.D. and Sucuoglu, H., December 1985, (PB87 165031/AS)A08.
- UCB/EERC-85/16 "An Experimental Program for Studying the Dynamic Response of a Steel Frame with a Variety of Infill Partitions," by Yanev, B. and McNiven, H.D., December 1985, (PB90 262 676)A05.
- UCB/EERC-86/01 "A Study of Seismically Resistant Eccentrically Braced Steel Frame Systems," by Kasai, K. and Popov, E.P., January 1986, (PB87 124 178/AS)A14.
- UCB/EERC-86/02 "Design Problems in Soil Liquefaction," by Seed, H.B., February 1986, (PB87 124 186/AS)A03.
- UCB/EERC-86/03 "Implications of Recent Earthquakes and Research on Earthquake-Resistant Design and Construction of Buildings," by Bertero, V.V., March 1986, (PB87 124 194/AS)A05.
- UCB/EERC-86/04 "The Use of Load Dependent Vectors for Dynamic and Earthquake Analyses," by Leger, P., Wilson, E.L. and Clough, R.W., March 1986, (PB87 124 202/AS)A12.
- UCB/EERC-86/05 "Two Beam-To-Column Web Connections," by Tsai, K.-C. and Popov, E.P., April 1986, (PB87 124 301/AS)A04.
- UCB/EERC-86/06 "Determination of Penetration Resistance for Coarse-Grained Soils using the Becker Hammer Drill," by Harder, L.F. and Seed, H.B., May 1986, (PB87 124 210/AS)A07.
- UCB/EERC-86/07 "A Mathematical Model for Predicting the Nonlinear Response of Unreinforced Masonry Walls to In-Plane Earthquake Excitations," by Mengi, Y. and McNiven, H.D., May 1986, (PB87 124 780/AS)A06.
- UCB/EERC-86/08 "The 19 September 1985 Mexico Earthquake: Building Behavior," by Bertero, V.V., July 1986.
- UCB/EERC-86/09 "EACD-3D: A Computer Program for Three-Dimensional Earthquake Analysis of Concrete Dams," by Fok, K.-L., Hall, J.F. and Chopra, A.K., July 1986, (PB87 124 228/AS)A08.
- UCB/EERC-86/10 "Earthquake Simulation Tests and Associated Studies of a 0.3-Scale Model of a Six-Story Concentrically Braced Steel Structure," by Uang, C.-M. and Bertero, V.V., December 1986, (PB87 163 564/AS)A17.
- UCB/EERC-86/11 "Mechanical Characteristics of Base Isolation Bearings for a Bridge Deck Model Test," by Kelly, J.M., Buckle, I.G. and Koh, C.-G., November 1987, (PB90 262 668)A04.
- UCB/EERC-86/12 "Effects of Axial Load on Elastomeric Isolation Bearings," by Koh, C.-G. and Kelly, J.M., November 1987.
- UCB/EERC-87/01 "The FPS Earthquake Resisting System: Experimental Report," by Zayas, V.A., Low, S.S. and Mahin, S.A., June 1987, (PB88 170 287)A06.
- UCB/EERC-87/02 "Earthquake Simulator Tests and Associated Studies of a 0.3-Scale Model of a Six-Story Eccentrically Braced Steel Structure," by Whitaker, A., Uang, C.-M. and Bertero, V.V., July 1987, (PB88 166 707/AS)A18.

- UCB/EERC-87/03 "A Displacement Control and Uplift Restraint Device for Base-Isolated Structures," by Kelly, J.M., Griffith, M.C. and Aiken, I.D., April 1987, (PB88 169 933)A04.
- UCB/EERC-87/04 "Earthquake Simulator Testing of a Combined Sliding Bearing and Rubber Bearing Isolation System," by Kelly, J.M. and Chalhoub, M.S., December 1990.
- UCB/EERC-87/05 "Three-Dimensional Inelastic Analysis of Reinforced Concrete Frame-Wall Structures," by Moazzami, S. and Bertero, V.V., May 1987, (PB88 169 586/AS)A08.
- UCB/EERC-87/06 "Experiments on Eccentrically Braced Frames with Composite Floors," by Ricles, J. and Popov, E., June 1987, (PB88 173 067/AS)A14.
- UCB/EERC-87/07 "Dynamic Analysis of Seismically Resistant Eccentrically Braced Frames," by Ricles, J. and Popov, E., June 1987, (PB88 173 075/AS)A16.
- UCB/EERC-87/08 "Undrained Cyclic Triaxial Testing of Gravels-The Effect of Membrane Compliance," by Evans, M.D. and Seed, H.B., July 1987, (PB88 173 257)A19.
- UCB/EERC-87/09 "Hybrid Solution Techniques for Generalized Pseudo-Dynamic Testing," by Thewalt, C. and Mahin, S.A., July 1987, (PB 88 179 007)A07.
- UCB/EERC-87/10 "Ultimate Behavior of Butt Welded Splices in Heavy Rolled Steel Sections," by Bruneau, M., Mahin, S.A. and Popov, E.P., September 1987, (PB90 254 285)A07.
- UCB/EERC-87/11 "Residual Strength of Sand from Dam Failures in the Chilean Earthquake of March 3, 1985," by De Alba, P., Seed, H.B., Retamal, E. and Seed, R.B., September 1987, (PB88 174 321/AS)A03.
- UCB/EERC-87/12 "Inelastic Seismic Response of Structures with Mass or Stiffness Eccentricities in Plan," by Bruneau, M. and Mahin, S.A., September 1987, (PB90 262 650/AS)A14.
- UCB/EERC-87/13 "CSTRUCT: An Interactive Computer Environment for the Design and Analysis of Earthquake Resistant Steel Structures," by Austin, M.A., Mahin, S.A. and Pister, K.S., September 1987, (PB88 173 339/AS)A06.
- UCB/EERC-87/14 "Experimental Study of Reinforced Concrete Columns Subjected to Multi-Axial Loading," by Low, S.S. and Moehle, J.P., September 1987, (PB88 174 347/AS)A07.
- UCB/EERC-87/15 "Relationships between Soil Conditions and Earthquake Ground Motions in Mexico City in the Earthquake of Sept. 19, 1985," by Seed, H.B., Romo, M.P., Sun, J., Jaime, A. and Lysmer, J., October 1987, (PB88 178 991)A06.
- UCB/EERC-87/16 "Experimental Study of Seismic Response of R. C. Setback Buildings," by Shahrooz, B.M. and Moehle, J.P., October 1987, (PB88 176 359)A16.
- UCB/EERC-87/17 "The Effect of Slabs on the Flexural Behavior of Beams," by Pantazopoulou, S.J. and Moehle, J.P., October 1987, (PB90 262 700)A07.
- UCB/EERC-87/18 "Design Procedure for R-FBI Bearings," by Mostaghel, N. and Kelly, J.M., November 1987, (PB90 262 718)A04.
- UCB/EERC-87/19 "Analytical Models for Predicting the Lateral Response of R C Shear Walls: Evaluation of their Reliability," by Vulcano, A. and Bertero, V.V., November 1987, (PB88 178 983)A05.
- UCB/EERC-87/20 "Earthquake Response of Torsionally-Coupled Buildings," by Hejal, R. and Chopra, A.K., December 1987.
- UCB/EERC-87/21 "Dynamic Reservoir Interaction with Monticello Dam," by Clough, R.W., Ghanaat, Y. and Qiu, X-F., December 1987, (PB88 179 023)A07.
- UCB/EERC-87/22 "Strength Evaluation of Coarse-Grained Soils," by Siddiqi, F.H., Seed, R.B., Chan, C.K., Seed, H.B. and Pyke, R.M., December 1987, (PB88 179 031)A04.
- UCB/EERC-88/01 "Seismic Behavior of Concentrically Braced Steel Frames," by Khatib, I., Mahin, S.A. and Pister, K.S., January 1988, (PB91 210 898/AS)A11.
- UCB/EERC-88/02 "Experimental Evaluation of Seismic Isolation of Medium-Rise Structures Subject to Uplift," by Griffith, M.C., Kelly, J.M., Coveney, V.A. and Koh, C.G., January 1988, (PB91 217 950/AS)A09.
- UCB/EERC-88/03 "Cyclic Behavior of Steel Double Angle Connections," by Astaneh-Asl, A. and Nader, M.N., January 1988, (PB91 210 872)A05.
- UCB/EERC-88/04 "Re-evaluation of the Slide in the Lower San Fernando Dam in the Earthquake of Feb. 9, 1971," by Seed, H.B., Seed, R.B., Harder, L.F. and Jong, H.-L., April 1988, (PB91 212 456/AS)A07.
- UCB/EERC-88/05 "Experimental Evaluation of Seismic Isolation of a Nine-Story Braced Steel Frame Subject to Uplift," by Griffith, M.C., Kelly, J.M. and Aiken, I.D., May 1988, (PB91 217 968/AS)A07.
- UCB/EERC-88/06 "DRAIN-2DX User Guide," by Allahabadi, R. and Powell, G.H., March 1988, (PB91 212 530)A12.
- UCB/EERC-88/07 "Theoretical and Experimental Studies of Cylindrical Water Tanks in Base-Isolated Structures," by Chalhoub, M.S. and Kelly, J.M., April 1988, (PB91 217 976/AS)A05.
- UCB/EERC-88/08 "Analysis of Near-Source Waves: Separation of Wave Types Using Strong Motion Array Recording," by Darragh, R.B., June 1988, (PB91 212 621)A08.
- UCB/EERC-88/09 "Alternatives to Standard Mode Superposition for Analysis of Non-Classically Damped Systems," by Kusainov, A.A. and Clough, R.W., June 1988, (PB91 217 992/AS)A04.
- UCB/EERC-88/10 "The Landslide at the Port of Nice on October 16, 1979," by Seed, H.B., Seed, R.B., Schlosser, F., Blondeau, F. and Juran, I., June 1988, (PB91 210 914)A05.
- UCB/EERC-88/11 "Liquefaction Potential of Sand Deposits Under Low Levels of Excitation," by Carter, D.P. and Seed, H.B., August 1988, (PB91 210 880)A15.
- UCB/EERC-88/12 "Nonlinear Analysis of Reinforced Concrete Frames Under Cyclic Load Reversals," by Filippou, F.C. and Issa, A., September 1988, (PB91 212 589)A07.
- UCB/EERC-88/13 "Implications of Recorded Earthquake Ground Motions on Seismic Design of Building Structures," by Uang, C.-M. and Bertero, V.V., November 1988, (PB91 212 548)A06.

- UCB/EERC-88/14 "An Experimental Study of the Behavior of Dual Steel Systems," by Whittaker, A.S., Uang, C.-M. and Bertero, V.V., September 1988, (PB91 212 712)A16.
- UCB/EERC-88/15 "Dynamic Moduli and Damping Ratios for Cohesive Soils," by Sun, J.I., Goleorkhi, R. and Seed, H.B., August 1988, (PB91 210 922)A04.
- UCB/EERC-88/16 "Reinforced Concrete Flat Plates Under Lateral Load: An Experimental Study Including Biaxial Effects," by Pan, A. and Moehle, J.P., October 1988, (PB91 210 856)A13.
- UCB/EERC-88/17 "Earthquake Engineering Research at Berkeley - 1988," by EERC, November 1988, (PB91 210 864)A10.
- UCB/EERC-88/18 "Use of Energy as a Design Criterion in Earthquake-Resistant Design," by Uang, C.-M. and Bertero, V.V., November 1988, (PB91 210 906/AS)A04.
- UCB/EERC-88/19 "Steel Beam-Column Joints in Seismic Moment Resisting Frames," by Tsai, K.-C. and Popov, E.P., November 1988, (PB91 217 984/AS)A20.
- UCB/EERC-88/20 "Base Isolation in Japan, 1988," by Kelly, J.M., December 1988, (PB91 212 449)A05.
- UCB/EERC-89/01 "Behavior of Long Links in Eccentrically Braced Frames," by Engelhardt, M.D. and Popov, E.P., January 1989, (PB92 143 056)A18.
- UCB/EERC-89/02 "Earthquake Simulator Testing of Steel Plate Added Damping and Stiffness Elements," by Whittaker, A., Bertero, V.V., Alonso, J. and Thompson, C., January 1989, (PB91 229 252/AS)A10.
- UCB/EERC-89/03 "Implications of Site Effects in the Mexico City Earthquake of Sept. 19, 1985 for Earthquake-Resistant Design Criteria in the San Francisco Bay Area of California," by Seed, H.B. and Sun, J.I., March 1989, (PB91 229 369/AS)A07.
- UCB/EERC-89/04 "Earthquake Analysis and Response of Intake-Outlet Towers," by Goyal, A. and Chopra, A.K., July 1989, (PB91 229 286/AS)A19.
- UCB/EERC-89/05 "The 1985 Chile Earthquake: An Evaluation of Structural Requirements for Bearing Wall Buildings," by Wallace, J.W. and Moehle, J.P., July 1989, (PB91 218 008/AS)A13.
- UCB/EERC-89/06 "Effects of Spatial Variation of Ground Motions on Large Multiply-Supported Structures," by Hao, H., July 1989, (PB91 229 161/AS)A08.
- UCB/EERC-89/07 "EADAP - Enhanced Arch Dam Analysis Program: Users's Manual," by Ghanaat, Y. and Clough, R.W., August 1989, (PB91 212 522)A06.
- UCB/EERC-89/08 "Seismic Performance of Steel Moment Frames Plastically Designed by Least Squares Stress Fields," by Ohi, K. and Mahin, S.A., August 1989, (PB91 212 597)A05.
- UCB/EERC-89/09 "Feasibility and Performance Studies on Improving the Earthquake Resistance of New and Existing Buildings Using the Friction Pendulum System," by Zayas, V., Low, S., Mahin, S.A. and Bozzo, L., July 1989, (PB92 143 064)A14.
- UCB/EERC-89/10 "Measurement and Elimination of Membrane Compliance Effects in Undrained Triaxial Testing," by Nicholson, P.G., Seed, R.B. and Anwar, H., September 1989, (PB92 139 641/AS)A13.
- UCB/EERC-89/11 "Static Tilt Behavior of Unanchored Cylindrical Tanks," by Lau, D.T. and Clough, R.W., September 1989, (PB92 143 049)A10.
- UCB/EERC-89/12 "ADAP-88: A Computer Program for Nonlinear Earthquake Analysis of Concrete Arch Dams," by Fenves, G.L., Mojtahedi, S. and Reimer, R.B., September 1989, (PB92 139 674/AS)A07.
- UCB/EERC-89/13 "Mechanics of Low Shape Factor Elastomeric Seismic Isolation Bearings," by Aiken, I.D., Kelly, J.M. and Tajirian, F.F., November 1989, (PB92 139 732/AS)A09.
- UCB/EERC-89/14 "Preliminary Report on the Seismological and Engineering Aspects of the October 17, 1989 Santa Cruz (Loma Prieta) Earthquake," by EERC, October 1989, (PB92 139 682/AS)A04.
- UCB/EERC-89/15 "Experimental Studies of a Single Story Steel Structure Tested with Fixed, Semi-Rigid and Flexible Connections," by Nader, M.N. and Astaneh-Asl, A., August 1989, (PB91 229 211/AS)A10.
- UCB/EERC-89/16 "Collapse of the Cypress Street Viaduct as a Result of the Loma Prieta Earthquake," by Nims, D.K., Miranda, E., Aiken, I.D., Whittaker, A.S. and Bertero, V.V., November 1989, (PB91 217 935/AS)A05.
- UCB/EERC-90/01 "Mechanics of High-Shape Factor Elastomeric Seismic Isolation Bearings," by Kelly, J.M., Aiken, I.D. and Tajirian, F.F., March 1990.
- UCB/EERC-90/02 "Javid's Paradox: The Influence of Preform on the Modes of Vibrating Beams," by Kelly, J.M., Sackman, J.L. and Javid, A., May 1990, (PB91 217 943/AS)A03.
- UCB/EERC-90/03 "Earthquake Simulator Testing and Analytical Studies of Two Energy-Absorbing Systems for Multistory Structures," by Aiken, I.D. and Kelly, J.M., October 1990, (PB92 192 988)A13.
- UCB/EERC-90/04 "Damage to the San Francisco-Oakland Bay Bridge During the October 17, 1989 Earthquake," by Astaneh-Asl, A., June 1990.
- UCB/EERC-90/05 "Preliminary Report on the Principal Geotechnical Aspects of the October 17, 1989 Loma Prieta Earthquake," by Seed, R.B., Dickenson, S.E., Riemer, M.F., Bray, J.D., Sitar, N., Mitchell, J.K., Idriss, I.M., Kayen, R.E., Kropp, A., Harder, L.F., Jr. and Power, M.S., April 1990, (PB 192 970)A08.
- UCB/EERC-90/06 "Models of Critical Regions in Reinforced Concrete Frames Under Seismic Excitations," by Zulfqar, N. and Filippou, F.C., May 1990.
- UCB/EERC-90/07 "A Unified Earthquake-Resistant Design Method for Steel Frames Using ARMA Models," by Takewaki, I., Conte, J.P., Mahin, S.A. and Pister, K.S., June 1990.
- UCB/EERC-90/08 "Soil Conditions and Earthquake Hazard Mitigation in the Marina District of San Francisco," by Mitchell, J.K., Masood, T., Kayen, R.E. and Seed, R.B., May 1990, (PB 193 267/AS)A04.
- UCB/EERC-90/09 "Influence of the Earthquake Ground Motion Process and Structural Properties on Response Characteristics of Simple Structures," by Conte, J.P., Pister, K.S. and Mahin, S.A., July 1990, (PB92 143 064)A15.
- UCB/EERC-90/10 "Experimental Testing of the Resilient-Friction Base Isolation System," by Clark, P.W. and Kelly, J.M., July 1990, (PB92 143 072)A08.
- UCB/EERC-90/11 "Seismic Hazard Analysis: Improved Models, Uncertainties and Sensitivities," by Araya, R. and Der Kiureghian, A., March 1988.
- UCB/EERC-90/12 "Effects of Torsion on the Linear and Nonlinear Seismic Response of Structures," by Sedarat, H. and Bertero, V.V., September 1989, (PB92 193 002/AS)A15.

- UCB/EERC-90/13 "The Effects of Tectonic Movements on Stresses and Deformations in Earth Embankments," by Bray, J. D., Seed, R. B. and Seed, H. B., September 1989.
- UCB/EERC-90/14 "Inelastic Seismic Response of One-Story, Asymmetric-Plan Systems," by Goel, R.K. and Chopra, A.K., October 1990.
- UCB/EERC-90/15 "Dynamic Crack Propagation: A Model for Near-Field Ground Motion.," by Seyyedian, H. and Kelly, J.M., 1990.
- UCB/EERC-90/16 "Sensitivity of Long-Period Response Spectra to System Initial Conditions," by Blasquez, R., Ventura, C. and Kelly, J.M., 1990.
- UCB/EERC-90/17 "Behavior of Peak Values and Spectral Ordinates of Near-Source Strong Ground-Motion over a Dense Array," by Niazi, M., June 1990.
- UCB/EERC-90/18 "Material Characterization of Elastomers used in Earthquake Base Isolation," by Papoulia, K.D. and Kelly, J.M., 1990.
- UCB/EERC-90/19 "Cyclic Behavior of Steel Top-and-Bottom Plate Moment Connections," by Harriott, J.D. and Astaneh-Asl, A., August 1990, (PB91 229 260/AS)A05.
- UCB/EERC-90/20 "Seismic Response Evaluation of an Instrumented Six Story Steel Building," by Shen, J.-H. and Astaneh-Asl, A., December 1990, (PB91 229 294/AS)A04.
- UCB/EERC-90/21 "Observations and Implications of Tests on the Cypress Street Viaduct Test Structure," by Bollo, M., Mahin, S.A., Moehle, J.P., Stephen, R.M. and Qi, X., December 1990.
- UCB/EERC-91/01 "Experimental Evaluation of Nitinol for Energy Dissipation in Structures," by Nims, D.K., Sasaki, K.K. and Kelly, J.M., 1991.
- UCB/EERC-91/02 "Displacement Design Approach for Reinforced Concrete Structures Subjected to Earthquakes," by Qi, X. and Moehle, J.P., January 1991, (PB93 114 569/AS)A09.
- UCB/EERC-91/03 "A Long-Period Isolation System Using Low-Modulus High-Damping Isolators for Nuclear Facilities at Soft-Soil Sites," by Kelly, J.M., March 1991, (PB93 114 577/AS)A10.
- UCB/EERC-91/04 "Dynamic and Failure Characteristics of Bridgestone Isolation Bearings," by Kelly, J.M., April 1991, (PB93 114 528)A05.
- UCB/EERC-91/05 "Base Sliding Response of Concrete Gravity Dams to Earthquakes," by Chopra, A.K. and Zhang, L., May 1991, (PB93 114 544/AS)A05.
- UCB/EERC-91/06 "Computation of Spatially Varying Ground Motion and Foundation-Rock Impedance Matrices for Seismic Analysis of Arch Dams," by Zhang, L. and Chopra, A.K., May 1991, (PB93 114 825)A07.
- UCB/EERC-91/07 "Estimation of Seismic Source Processes Using Strong Motion Array Data," by Chiou, S.-J., July 1991, (PB93 114 551/AS)A08.
- UCB/EERC-91/08 "A Response Spectrum Method for Multiple-Support Seismic Excitations," by Der Kiureghian, A. and Neuenhofer, A., August 1991, (PB93 114 536)A04.
- UCB/EERC-91/09 "A Preliminary Study on Energy Dissipating Cladding-to-Frame Connection," by Cohen, J.M. and Powell, G.H., September 1991, (PB93 114 510)A05.
- UCB/EERC-91/10 "Evaluation of Seismic Performance of a Ten-Story RC Building During the Whittier Narrows Earthquake," by Miranda, E. and Bertero, V.V., October 1991, + (PB93 114 783)A06.
- UCB/EERC-91/11 "Seismic Performance of an Instrumented Six Story Steel Building," by Anderson, J.C. and Bertero, V.V., November 1991.
- UCB/EERC-91/12 "Performance of Improved Ground During the Loma Prieta Earthquake," by Mitchell, J.K. and Wentz, Jr., F.J., October 1991, (PB93 114 791)A06.
- UCB/EERC-91/13 "Shaking Table - Structure Interaction," by Rinawi, A.M. and Clough, R.W., October 1991, (PB93 114 917)A13.
- UCB/EERC-91/14 "Cyclic Response of RC Beam-Column Knee Joints: Test and Retrofit," by Mazzoni, S., Moehle, J.P. and Thewalt, C.R., October 1991, (PB93 120 277)A03.
- UCB/EERC-91/15 "Design Guidelines for Ductility and Drift Limits: Review of State-of-the-Practice and State-of-the-Art in Ductility and Drift-Based Earthquake-Resistant Design of Buildings," by Bertero, V.V., Anderson, J.C., Krawinkler, H., Miranda, E. and The CUREe and The Kajima Research Teams, July 1991, (PB93 120 269)A08.
- UCB/EERC-91/16 "Evaluation of the Seismic Performance of a Thirty-Story RC Building," by Anderson, J.C., Miranda, E., Bertero, V.V. and The Kajima Project Research Team, July 1991, (PB93 114 841)A12.
- UCB/EERC-91/17 "A Fiber Beam-Column Element for Seismic Response Analysis of Reinforced Concrete Structures," by Taucer, F., Spacone, E. and Filippou, F.C., December 1991.
- UCB/EERC-91/18 "Investigation of the Seismic Response of a Lightly-Damped Torsionally-Coupled Building," by Boroschek, R. and Mahin, S.A., December 1991, (PB93 120 335)A13.
- UCB/EERC-92/01 "Studies of a 49-Story Instrumented Steel Structure Shaken During the Loma Prieta Earthquake," by Chen, C.-C., Bonowitz, D. and Astaneh-Asl, A., February 1992.
- UCB/EERC-92/02 "Response of the Dumbarton Bridge in the Loma Prieta Earthquake," by Fenves, G.L., Filippou, F.C. and Sze, D.T., January 1992, (PB93 120 319)A09.
- UCB/EERC-92/03 "Models for Nonlinear Earthquake Analysis of Brick Masonry Buildings," by Mengi, Y., McNiven, H.D. and Tanrikulu, A.K., March 1992, (PB93 120 293)A08.
- UCB/EERC-92/04 "Shear Strength and Deformability of RC Bridge Columns Subjected to Inelastic Cyclic Displacements," by Aschheim, M. and Moehle, J.P., March 1992, (PB93 120 327)A06.
- UCB/EERC-92/05 "Parameter Study of Joint Opening Effects on Earthquake Response of Arch Dams," by Fenves, G.L., Mojtahedi, S. and Reimer, R.B., April 1992, (PB93 120 301)A04.
- UCB/EERC-92/06 "Seismic Behavior and Design of Semi-Rigid Steel Frames," by Nader, M.N. and Astaneh-Asl, A., May 1992.
- UCB/EERC-92/07 "A Beam Element for Seismic Damage Analysis," by Spacone, E., Ciampi, V. and Filippou, F.C., August 1992.
- UCB/EERC-92/08 "Nonlinear Static and Dynamic Analysis of Reinforced Concrete Subassemblages," by Filippou, F.C., D'Ambrisi, A. and Issa, A., August 1992.

- UCB/EERC-92/09 "Evaluation of Code Accidental-Torsion Provisions Using Earthquake Records from Three Nominally Symmetric-Plan Buildings," by De la Llera, J.C. and Chopra, A.K., September 1992.
- UCB/EERC-92/10 "Slotted Bolted Connection Energy Dissipators," by Grigorian, C.E., Yang, T.-S. and Popov, E.P., July 1992.
- UCB/EERC-92/11 "Mechanical Characteristics of Neoprene Isolation Bearings," by Kelly, J.M. and Quiroz, E., August 1992.
- UCB/EERC-92/12 "Application of a Mass Damping System to Bridge Structures," by Hasegawa, K. and Kelly, J.M., August 1992.
- UCB/EERC-92/13 "Earthquake Engineering Research at Berkeley - 1992," October 1992.
- UCB/EERC-92/14 "Earthquake Risk and Insurance," by Brillinger, D.R., October 1992.
- UCB/EERC-92/15 "A Friction Mass Damper for Vibration Control," by Inaudi, J.A. and Kelly, J.M., October 1992.
- UCB/EERC-92/16 "Tall Reinforced Concrete Buildings: Conceptual Earthquake-Resistant Design Methodology," by Bertero, R.D. and Bertero, V.V., December 1992.
- UCB/EERC-92/17 "Performance of Tall Buildings during the 1985 Mexico Earthquakes," by Terán-Gilmore, A. and Bertero, V.V., December 1992.
- UCB/EERC-92/18 "Dynamic Analysis of Nonlinear Structures using State-Space Formulation and Partitioned Integration Schemes," by Inaudi, J.A. and De la Llera, J.C., December 1992.
- UCB/EERC-93/01 "Seismic Performance of an Instrumented Six-Story Reinforced-Concrete Building," by Anderson, J.C. and Bertero, V.V., 1993.
- UCB/EERC-93/02 "Evaluation of an Active Variable-Damping-Structure," by Polak, E., Meeker, G., Yamada, K. and Kurata, N., February 1993.



NTIS does not permit return of items for credit or refund. A replacement will be provided if an error is made in filling your order, if the item was received in damaged condition, or if the item is defective.

Reproduced by NTIS

National Technical Information Service
Springfield, VA 22161

***This report was printed specifically for your order
from nearly 3 million titles available in our collection.***

For economy and efficiency, NTIS does not maintain stock of its vast collection of technical reports. Rather, most documents are printed for each order. Documents that are not in electronic format are reproduced from master archival copies and are the best possible reproductions available. If you have any questions concerning this document or any order you have placed with NTIS, please call our Customer Service Department at (703) 487-4660.

About NTIS

NTIS collects scientific, technical, engineering, and business related information — then organizes, maintains, and disseminates that information in a variety of formats — from microfiche to online services. The NTIS collection of nearly 3 million titles includes reports describing research conducted or sponsored by federal agencies and their contractors; statistical and business information; U.S. military publications; audiovisual products; computer software and electronic databases developed by federal agencies; training tools; and technical reports prepared by research organizations worldwide. Approximately 100,000 *new* titles are added and indexed into the NTIS collection annually.

For more information about NTIS products and services, call NTIS at (703) 487-4650 and request the free *NTIS Catalog of Products and Services*, PR-827LPG, or visit the NTIS Web site
<http://www.ntis.gov>.

NTIS

***Your indispensable resource for government-sponsored
information—U.S. and worldwide***





U.S. DEPARTMENT OF COMMERCE
Technology Administration
National Technical Information Service
Springfield, VA 22161 (703) 487-4650
